Carbons and Electrolytes for Advanced Supercapacitors

By *F. Béguin, V. Presser, A. Balducci, and E. Frackowiak**

Prof. F. Béguin, Prof. E. Frackowiak
Institute of Chemistry and Technical Electrochemistry
Poznan University of Technology
Piotrowo 3, 60-965 Poznan, Poland
E-mail: francois.beguin@put.poznan.pl; elzbieta.frackowiak@put.poznan.pl

Prof. V. Presser
INM - Leibniz Institute for New Materials & Saarland University
Campus D2 2, 66123 Saarbrücken, Germany
E-mail: volker.presser@inm-gmbh.de

Dr. A. Balducci
Westfälische Wilhelms Universität
Institut für Physikalische Chemie – MEET Battery Research Center
Corrensstr. 28/30, 48149 Münster, Germany
E-mail: andrea.balducci@uni-muenster.de

Abstract

Electrical energy storage (EES) is one of the most critical areas of technological research around the world. Storing and efficiently using electricity generated by intermittent sources, and the transition of our transportation fleet to electric drive, depend fundamentally on the development of EES systems with high energy and power densities. Supercapacitors are promising devices for highly efficient energy storage and power management, yet they still suffer from moderate energy densities compared to batteries. To establish a detailed understanding of science and technology of carbon/carbon supercapacitors, this review first discusses the basic principles of the electrical double-layer (EDL), especially regarding the correlation between ion size / ion solvation and the pore size of porous carbon electrodes. We summarize the key aspects of various carbon materials synthesized for use in supercapacitors. With the objective of improving the energy density, the last two sections are dedicated to increasing the capacitance by either introducing pseudocapacitive materials or by using novel electrolytes that allow to increasing the cell voltage. In particular, advances in ionic liquids, but also in the field of organic electrolytes, are discussed and electrode mass balancing is expanded because of its importance to create higher performance asymmetric electrochemical capacitors.
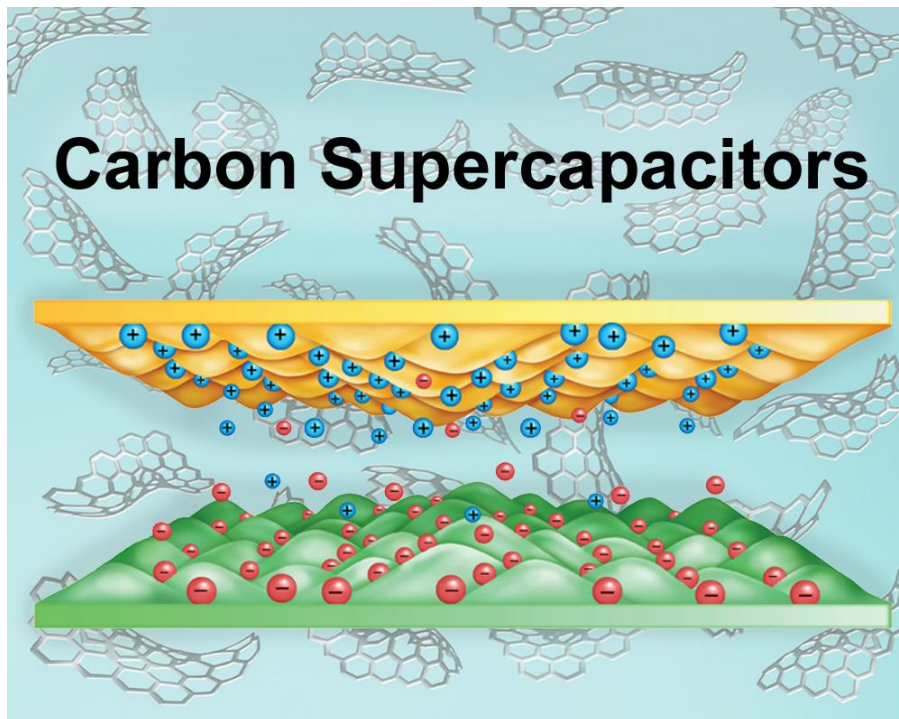
1. Introduction

Reducing fossil fuel consumption and greenhouse gas emissions has become a global objective and is recognized as an imperative for the sustainable development of economy and society. Electricity production from renewable energy sources and further improvement of energy efficiency are the most promising solutions for reaching these objectives. Most nations or multinational associations have devised plans to achieve this challenging goal; for example, the European Union has set a goal by 2020 to reduce greenhouse gas emissions by 20%, drawing 20% of energy from renewable sources, and cutting the EU-wide energy use by 20%. Implementation of renewable energy sources, such as solar or wind energy, however, causes paramount challenges to power grid management and grid stability because of the large fluctuations in electricity generation that are completely decoupled from the actual energy demand. Various technologies exist or are being developed to achieve this task, ranging from mechanical, physical, thermal, chemical and electrochemical energy storage systems. Considering a reliable, stable, and sustainable large-scale use of renewable energy, batteries and/or supercapacitors play a key role for advanced and highly efficient energy storage and management. In general, lithium-ion and Ni/MH batteries are used for their relatively high energy density, while supercapacitors are applied for their high power density, this means the two devices might play complementary functions when they are hybridized.

Currently both technologies require further optimization – with regards to employing environmentally safe and much more cost effective materials. Specifically research and industrial developments for supercapacitors are essentially oriented to improving the device's energy density through the design of new electrode materials, new electrolytes, and new electrochemical concepts. As far as power is concerned, intelligent engineering of electrodes and whole device is most often more effective than designing complicated nanostructured materials.

Microporous carbons are the primary materials used to make supercapacitor electrodes. They have relatively high electrical conductivity, essential for power applications, and large specific surface area (SSA), necessary for enhancing the capacitance. They are mostly derived from sustainable, natural, abundant, low to moderate cost resources, an important factor for industrial applications. In addition, they are available in a wide variety of forms such as: powders, fibers, cloths, monoliths, nanotubes, nanospheres and so on. Carbon's versatility allows the engineer to match the material characteristics exactly to a given application (*e.g.*, flexible devices or large scale stationary systems). Carbons' most attractive properties are their diversity of textures/structures and surface chemistries. By adjusting these parameters, altering the electrochemical performance of the materials and adapting them to various kinds of electrolytic media and system configurations is possible.

This review describes the design of carbons and electrochemical capacitor systems based on carbon electrodes, with the objective to enhance the capacitance or/and voltage to improve the energy density of the device. First, the general properties of electrical double-layer capacitors, the optimization of capacitance and charge propagation will be introduced. The impact of carbon porosity and pore architecture will be discussed in detail and design strategies will be outlined. Then the different possibilities for enhancing capacitance, through fast redox reactions in protic electrolytes, are explained. In particular, it will be shown that new forms of carbons, such as nanotubes or graphene, are an excellent support for pseudocapacitive materials such as transition metal oxides and electrically conducting polymers. Finally, the possibilities of enhancing the voltage through the use of advanced electrolytes or hybrid system designs will be discussed. In all examples of supercapacitor systems, the material - electrolyte couple will be at the centre of discussion.

2. Electrical Double-Layer Capacitors (EDLCs)

2.1 Introduction

The main energy storage mechanism in supercapacitors arises from the reversible electrostatic accumulation of ions on the surface of porous carbon. The Helmholtz model (Ref. [1]) describes the charge separation at the electrode/electrolyte interface when an electrode of surface area S (m^2) is polarized. Under this condition, ions of opposite sign diffuse through the electrolyte to form a condensed layer a few nanometers thick in a plane parallel to the electrode surface ensuring charge neutrality. This accumulation of charges is called electrical double-layer (EDL). The potential in the vicinity of the electrode then decreases when the distance d (m) between the ions and the electrode increases (**Fig. 1a**). This simplified Helmholtz double-layer (DL) can be regarded as an electrical capacitor of capacitance C defined by **Eq. (1)**:

$$C_H = \varepsilon_0 \cdot \varepsilon_r \cdot \frac{S}{d} \qquad\qquad (1)$$

where ε_0 is the vacuum permittivity (ε_0 = 8.854·10^{-12} F/m), ε_r the relative permittivity of the dielectric electrolyte, and d is the effective thickness of the DL, often approximated as the Debye length. Considering the very large SSA of porous carbon electrodes (up to 3000 m^2/g) and a Debye length in the range of <1 nm, the resulting capacitance of DL's will be much higher than for flat plate capacitors.

Since the Helmholtz model does not take into account several factors such as the diffusion of ions in the solution and the interaction between the dipole moment of the solvent and the electrode, Gouy and Chapman proposed a diffuse model of the EDL in which the potential decreases exponentially from the electrode surface to the fluid bulk (**Fig. 1a**).[2] However, the Gouy-Chapman model is insufficient for highly charged double-layers, and in 1924, Stern (Ref. [3]) suggested a model combining the Helmholtz and Gouy-Chapman models by accounting for the

hydrodynamic motion of the ionic species in the diffuse layer and the accumulation of ions close to the electrode surface (**Fig. 1c**). These two layers are equivalent to two capacitors in series, C_H (Helmholtz layer) and C_D (diffuse layer), and the total capacitance of the electrode (C_{DL}) is given by *Eq. (2)*:

$$\frac{1}{C_{DL}} = \frac{1}{C_H} + \frac{1}{C_D} \tag{2}$$

An electrical double-layer capacitor (EDLC) consists of two porous carbon, generally activated carbon (AC), electrodes in direct contact with the current collector and separated by a porous film impregnated with an electrolyte solution (**Fig. 2**). When an electric potential difference is applied between the electrodes, the negative charge carriers, electrons, in the negatively polarized electrode are balanced by an equal number of positive cations at the electrode/electrolyte interface, while the holes stored at the positively polarized electrode are electrically balanced by anions. Hence, a supercapacitor consisting of two electrodes is equivalent to two capacitors in series and the resulting capacitance (C) can then be expressed according to *Eq. (3)*:

$$\frac{1}{C} = \frac{1}{C_+} + \frac{1}{C_-} \tag{3}$$

where C_+, C_-, and C are the capacitance (Farad = Coulomb/Volt) of the positive electrode, the negative electrode, and of the resulting device, respectively.

To provide a basis for comparison between different electrode materials, it has become common practice to provide a specific (gravimetric) capacitance, which is related to the capacitance of one single electrode, C_{SP} (F/g). In case of a symmetric system, where both electrodes are equal in mass, thickness, size, and material, the *Eq. 4* can be used:

$$C_{SP} = 4 \cdot \frac{C}{m_{AM}} \tag{4}$$

where m_{AM} is the total mass of active material. While some authors subtract the amount of binder or other additives, it is more accurate to use the total mass of both dry electrodes. The factor 4 is related to normalization to the mass of one electrode for the two identical capacitors in series. The stored specific energy E (Wh/kg), also called energy density, in a supercapacitor is given by *Eq. (5)*:

$$E = \frac{C \cdot U_{max}^2}{2 \cdot m \cdot 3600} \tag{5}$$

where m (kg) is the mass of the supercapacitor and U_{max} (V) the maximum region of electrochemical stability. The normalization to the supercapacitor weight provides a basis for comparison with other devices, especially from an application point of view.

The maximum specific power (W/kg) also depends on the maximal applicable voltage and is given by *Eq. (6)*:

$$P = \frac{U_{max}^2}{4 \cdot ESR \cdot m} \tag{6}$$

where ESR (Ω) is the equivalent series resistance of the system. The ESR corresponds to the sum of the resistances related to the ionic resistance of the electrolyte impregnated in the separator, the electronic resistance of electrodes, and interface resistances between electrodes and current collectors. Alternatively, the normalization can also be carried out by the device volume v (m^3) rather than the mass m (kg), to provide a comparison for the compactness of energy and power devices.

Due the purely physical formation of the EDL without electrochemical reactions, the charging of EDL capacitors (EDLCs) is very rapid. This fundamentally differs from batteries, where energy is stored through redox processes. In other words, EDLCs can deliver very high power densities (~15 kW/kg) compared to, for example, Li-ion batteries (up to about 2 kW/kg).[4] However, the specific energy of EDLCs is much lower (5-8 Wh/kg) than that of Li-ion batteries (up to 180

Wh/kg for commercial products).[5] Therefore, a lot of research effort is devoted to increasing the energy density of supercapacitors through an optimization of capacitance and/or voltage, following **Eq. (5)**.

2.2 General Properties of Electrolytes for EDLCs

Electrolytes used in supercapacitors are aqueous, organic, or liquid salts (commonly known as ionic liquids). The two main criteria for selection of an electrolyte are the electrochemical stability window and the ionic conductivity. The first is important to maximize the specific energy values (**Eq. (5)**), while the second has a major influence on the values of power (**Eq. (6)**). Acid-based (H_2SO_4) and alkali (KOH) aqueous electrolytes have a higher conductivity (up to ~1 S/cm) compared to organic electrolytes (based on acetonitrile or propylene carbonate), giving the system a higher power performance. However, due to the narrow electrochemical stability window (1.23 V) of water, the operating voltage is relatively low (~1 V)[6] and consequently, the energy that can be stored in the device is limited. Khomenko *et al*. [7] demonstrated it is possible to increase the operating voltage of carbon based supercapacitors in aqueous H_2SO_4 up to 1.6 V by using different optimized carbons as positive and negative electrodes and/or by balancing the mass of electrodes. It is important to note that, depending on the used carbon, the over-potential for electrolyte decomposition varies and temperature plays an important role in the degradation mechanism. To mitigate the corrosive character of the acid media, electrolytes with neutral pH have been investigated, and voltage values up to 2 V, with good charge/discharge cycle life, have been observed for symmetric AC cells in Na_2SO_4 and Li_2SO_4.[8, 9] Neutral pH electrolytes have been also implemented in asymmetric capacitors with an AC negative electrode and a positive electrode from transition metal oxide, for example MnO_2.[10]

Electrolytes composed of a salt dissolved in an organic solvent provide a wider electrochemical stability window in the range of 2.7 - 2.8 V compared to aqueous solutions. However, their ionic conductivity and the specific capacitance (100 - 150 F/g) are lower than for aqueous electrolytes.[11, 12] The high cell voltage allows supercapacitors using organic electrolytes to deliver a higher specific energy than aqueous systems and for this reason the majority of industrial systems are currently produced with organic electrolytes. Propylene carbonate (PC) and acetonitrile (AN) are the most commonly used solvents in supercapacitors. Ue *et al.* [13] reported using PC as a solvent because of its wide electrochemical window and its resistance against hydrolysis; however, due to its high viscosity, the performance of supercapacitors prepared with PC is more sensitive to temperature variations compared to AN.[14] Salts commonly applied in organic electrolytes are quaternary ammonium salts out of which tetraethylammonium tetrafluoroborate (TEA-BF$_4$) is the most widely used for commercial supercapacitors. It is necessary to optimize the conductivity of the electrolyte by selecting the appropriate salt.[15]

The graph in **Fig. 3** illustrates how the electrolyte conductivity increases with increasing salt concentration up to a maximum.[16] Beyond the maximum conductivity point, additional salt ions do not contribute to the conductivity of the electrolyte. Note that at 25 °C, TEA-BF$_4$ shows a maximum conductivity in PC at a concentration of 1 M, while the other salts have higher conductivities for higher concentrations. Due to high costs, salts like EMI-BF$_4$ (1-ethyl-3-methylimidazolium tetrafluoroborate) or MEPY-BF$_4$ (1-ethyl-1-methylpyrrolidinium tetrafluoroborate) are currently unsuitable for industrial applications. Instead, it is possible to use TEMA-BF$_4$ (triethylmethylammonium tetrafluoroborate) at higher concentrations (2 M) yielding higher ionic conductivities and avoiding ion depletion during charging of large cells at high power.[17] Another salt, TMPY-BF$_4$ (tetramethylene-pyrrolidinium tetrafluoroborate), shows even

higher solubility in propylene carbonate which translates to a higher ionic conductivity, and it is already introduced to commercial applications.[18]

Room temperature ionic liquids (RTILs) are molten salts that have been considered recently as a promising class of electrolytes in supercapacitors.[19] Since no solvent is required, these electrolytes have a very low vapor pressure, limiting environmental exposure and preventing the risk of explosion. Other attractive properties are their stability at increased temperatures extending well beyond the ~80 °C limit of organic electrolytes and a broad electrochemical stability which appears superior to that of organic solvents.[20] However, the ionic conductivity of RTILs, especially at room temperature, is generally lower than that of organic electrolytes,[21] reducing the power performance of supercapacitors.

2.3 General Properties of Carbon Materials for EDLCs

Carbon is one of the most abundantly available and structurally diverse materials, and most present-day EDLCs employ porous carbons as the active material. Abundantly available organic materials, including food waste[22], are a particularly attractive natural resource for the production of carbon materials. ACs, such as those derived from coconut shells or charcoal, are the most common commercially used porous carbons.

There is a general trend of increased capacitance with increased SSA, however the carbon structure including pore shape, surface functional groups, conductivity has to be considered as well. Activation of porous carbons, using CO_2 or KOH treatment, improves the capacitance by increasing the surface area by opening pores that are closed, clogged, or obstructed.[12] This has been shown for ACs,[23] hydrothermally-derived hydrochars,[24] carbide derived carbons(CDCs),[25] and multi-wall carbon nanotubes (CNTs)[26] , among others (see Ref. [27] for a more detailed review of this topic). In particular, S_{BET} values of more than 3000 m^2/g and pore

volumes in excess of 1.6 cm^3/g are reported for coal and semi-coke activated in KOH for 5 h at 800 °C.[23] Similarly, hydrothermal treatment of eucalyptus wood sawdust and subsequent KOH activation at 800°C yielded up to 2967 m^2/g S_{BET} and a pore volume of 1.2 cm^3/g.[24] Activation with KOH of low-temperature chlorine treated carbide derived carbons, exhibiting comparatively small pores with pore walls consisting of disordered carbon, almost doubled the S_{BET} from ~1100 m^2/g to ~2100 m^2/g, while the capacitance increased by 15%.[25] There are disadvantages to introducing too much porosity. In fact, a high surface area or large pore volume limits high power or energy density, and a very large porosity directly translates to low volumetric density resulting in moderate to low volumetric power and energy performance[28].

The International Union of Pure and Applied Chemistry (IUPAC) defines pores strictly according to their size as follows (Ref. [29]):

- Macropores: larger than 50 nm

- Mesopores: between 2 and 50 nm

- Micropores: smaller than 2 nm

Since the term micropores may be associated with micrometer-sized pores, some authors have preferred the term "nanopores" for pore diameters smaller than 2 nm; we, however, prefer to the IUPAC definition and adhere to it throughout the paper.

All porous carbons display pore size dispersion, not just "one" pore size, which is characterized with an average pore size (d_{50}, sometimes also called L_0; defined as the pore size up to which 50% of the pore volume is represented in a cumulative pore size distribution [PSD] plot). There are several chemical and physical processes used to tailor and optimize pore characteristics, especially for ACs.[30] Considering the significant influence of the pore size on the capacitance, it is critical to understand the PSD of porous carbons and the techniques by which they have been measured. For example, PSDs can be determined from X-ray or Neutron scattering and gas

adsorption; the latter usually involves deconvolution of the adsorption isotherms with DFT using either non-local (NLDFT) or quenched-solid (QSDFT)[31] or grand canonical Monte Carlo simulations.[32] The DFT-based deconvolution of adsorption data is widely used; however, such calculations are complicated because:

i.   knowledge of the pore geometry (*e.g.*, slit-shape, cylindrical, spherical) is required for the model-dependent calculations;

ii.   the heat of adsorption is often used as a fixed parameter rather than being determined independently for an actual sample.

From studies on CDCs, it has been shown that the pore shape[33] and heat of adsorption[34] varies as a function of the synthesis temperature, therefore functions describing these variations have to be incorporated in the DFT calculations. In this context, the term "average pore size" might be misleading for porous carbons because it does not reflect (i) the magnitude, and (ii) the modality of the pore size dispersion, for example, the width of the PSD and the number of distribution maxima. Only carbons with a narrow PSD, such as CNTs, many CDCs, and some ACs, exhibit a meaningful "average" pore size (d_{50}), while most porous carbons exhibit a much more random distribution.

2.4 Effect of Carbon Structure and Porous Texture on EDLC Performance

2.4.1 Introduction

In *Section 2.3*, carbons were introduced as the material traditionally used in EDLCs and AC is ubiquitous in commercial devices. The porous texture of carbon materials, described by the SSA, PSD, and pore volume, as well as the presence of heteroatoms, confers a diverse range of material properties. It is important for device design to understand the effect the porous texture has on EDLC performance. To get an idea of how ions are adsorbed on the surface of AC, it is

necessary to conceptualize a structural and textural model. Early studies on carbons from R. Franklin in 1951, using X-ray diffraction data, proposed to distinguish two classes: non-graphitizable and graphitizable carbons.[35] ACs are part of the first class because they are unable to form a repetitive stack of graphene sheets even after treatment at 3000°C. The first transmission electron microscopy imaging of a non-graphitizable carbon prepared from polyvinylidene chloride (PVDC) by Ban *et al.* [36] in the 1970s suggested a ribbon type structure/texture as illustrated in **Fig. 4a**.

To explain the textural entanglement of non-graphitizable carbons, it has been proposed that some carbon atoms in the graphene structure are actually sp^3-hybridized.[37] Harris *et al.* suggested that ACs have structural fragments resembling fullerenes, that is, the graphene structure includes pentagons and/or other non-hexagonal rings,[38, 39] giving rise to curvatures as shown in **Fig. 4b**. The presence of pentagonal rings was confirmed by transmission electron microscopy (TEM) on the commercial AC "Norit GSX" post-treated at 2000°C[40] and it has been suggested that these rings were already present in the original AC because the heat treatment is more favorable to the development of aromatic rings. This work can be correlated with the Monte-Carlo modeling of the porosity of microporous carbons, where the presence of pentagonal and heptagonal rings helping for the curvature of the graphene sheets was demonstrated.[41]

Early studies trying to correlate the EDLC performance with the porous texture suggested a linear dependence between the specific capacitance and the SSA[42] calculated from the Brunauer-Emmett-Teller (BET) method.[43] It was assumed that the S_{BET} is the same as the surface area of the electrode/electrolyte interface in Eq. (1). Typically, there is a general correlation for small S_{BET} values, but the capacitance becomes almost constant for values higher than 1200 - 1500 m^2/g. The BET method often overestimates the SSA for carbons therefore, Barbieri *et al.* applied the density functional theory (DFT) method to estimating SSA and showed a slightly better

correlation, but there is still a plateau for values higher than 1500 m^2/g.[44] To understand this trend, it was suggested that for carbons with high SSA the pore walls may become too thin to provide complete charge screening of ions in adjacent pores, in contrast to the low porosity carbons which have thicker walls. A similar observation was made for single graphene sheets suspended in an electrolyte, where the capacitance per unit area (F/cm²) decreased when the electrolyte had access to both faces of the graphene sheets; correspondingly, the areal capacitance was higher when only one side of graphene was exposed to the electrolyte. [45]

To get a more complete understanding of the capacitance properties and the correlation between the SSA and capacitance, other porous texture parameters must be explored. The respective sizes of ions and pores and the way the pores are connected may strongly influence the values of capacitance, particularly under high operating current densities found in supercapacitors. Moreover, the size of the solvated or partially desolvated ions under polarization differs from the molecular probes (N_2, CO_2) commonly used for characterizing the porosity *via* gas adsorption. Thus, the calculated S_{BET} may not sufficiently reflect the "effective" surface area and porous characteristics for carbon materials.

2.4.2 Ion Sieving

New aspects have to be considered when decreasing the pore size of the carbon materials to the range of the ion sizes present in the system. Using carbons with an average pore size approaching the size of hydrated ions, Aurbach *et al.* demonstrated it was possible to selectively electrosorb ions based on size.[46-48] They defined this as ion sieving. In the three-electrode cyclic voltammograms (CVs),[49] where the potential of the working electrode is controlled versus a reference electrode, three situations (**Fig. 5**) can be differentiated:

14

i. A typical capacitive rectangular-shape of CV with $MgSO_4$ electrolyte when the average pore size (0.58 nm) of the carbon material is significantly larger than the size of ions.

ii. For a smaller pore size carbon (0.51 nm), the current is negligible in all the potential range, because both Mg^{2+} and SO_4^{2-} ions are larger than 0.51 nm.

iii. When the size of one of the electrolyte ions is larger than the average pore size, the capacitive current is negligible in the corresponding part of the voltammogram, while it becomes important for the other part associated with the counter ion smaller than the pores. This is the case for Li_2SO_4 and $MgCl_2$ aqueous electrolytes with the carbon of average pore size 0.51 nm. The triangular shape and the narrowing of the two voltammetry curves confirms the adsorption of the small ions (Li^+ or Cl^-) into the pores and the absence of adsorption of the larger ions (SO_4^{2-} or Mg^{2+}, respectively) on the other side of the point of zero charge.

The electrosorption and insertion of a certain ion in pores of different sizes does not necessarily lead to the same capacitance, even not for materials of comparable S_{BET} values. In fact, the capacitance will be controlled by the relationship between the average pore size and the effective size of ions. Such processes can be studied by means of cyclic voltammetry and in the case where the average pore size is slightly smaller than the size of the ions, it is possible to force their insertion into the pores by slowing down the scan rate applied. In this case, ion sieving also results in increased, yet reversible swelling of the pore network, as shown by electrochemical dilatometry[50] and electrochemical atomic force microscopy.[51] However, if the average pore size is substantially less than the size of the ions of the electrolyte, a decrease or even disappearance of the capacitive current is observed on the cyclic voltammograms.

Using carbons with pores of size less than 0.7 nm, Noked *et al.* have demonstrated that the geometry of ions from aqueous solutions has an impact on their electrosorption.[48] Planar solvated ions, like NO_3^-, are adsorbed in slit-shaped pores, while spherical solvated ions, such as Cl^-, are excluded. A similar study was carried out with Na^+, Ca^{2+}, and Mg^{2+} which showed that electrosorption of hydrated monovalent sodium ions in micropores is preferred while the hydrated bivalent cations are excluded.[46]

The sieving effect was also evidenced by studying the capacitance of an AC in a series of solvent-free ionic liquids (ILs) of increasing cation size.[52] Unlike for organic or aqueous electrolytes, ions in ILs are not solvated enabling a more direct approach to interpret the capacitance properties by comparing the size of pores and ions calculated by molecular modeling. It was found that the overall porosity of the carbon is noticeably underused, because an important fraction of the pores are smaller than the effective size of the cations. Hence, the dimensions of pores and ions must match to each other.[52]

Comparable results were obtained when keeping the same ionic liquid (1-ethyl-3-methylimidazolium-bis(trifluoromethylsulfonyl)imide, EMI-TFSI) and using a series of microporous carbons with average pore width in the range of 0.65 to 1.1 nm.[53] The ion sizes, calculated along the longest expansion, are 0.79 and 0.76 nm for $TFSI^-$ and EMI^+, respectively. The plot of normalized capacitance *versus* average pore size in **Fig. 6** shows a capacitance increase when the average pore size decreases from 1.1 to 0.7 nm, and a decrease of capacitance below ~0.7 nm, that is when the pore size becomes smaller than the longest dimension of both types of ions. It must also be noticed that the results reported in Ref. [52, 53] are consistent with the assumption that the IL cations are vertically aligned, that is, with their largest dimension perpendicular to the pore walls. In this orientation, more ions can occupy the available active surface of the pores, i.e. the electrosorbed charge carriers are more closely packed.

2.4.3 Ion Desolvation

In the case of solvent based aqueous or organic electrolytes, the effective ion size is larger due to the solvation shell as compared to the ion itself. Pores too small for ions to enter are to be avoided for the rational design of porous carbon electrodes in EDLCs. However, the optimum pore size yielding the best EDLC performance is more difficult to identify. For templated carbons, Vix-Guterl *et al.* [54] showed that the capacitance is proportional to the ultra-micropore volume (pores smaller than 0.7 - 0.8 nm) measured by CO_2 gas sorption, in both aqueous and organic media (**Fig. 7**). Taking into account the size of solvated and desolvated tetraethylammonium (TEA$^+$) and tetrafluoroborate (BF$_4^-$) ions in AN, listed in **Table 1**, it was demonstrated for a two-electrode set-up that at least partial desolvation of ions is necessary to enable their access into the pores. The sieving effect is more important for the negative electrode, where the cations are trapped, than for the positive one meaning that the cell capacitance is essentially controlled by the negative electrode according to *Eq. (3)*.

Desolvation has been confirmed with ACs or CDCs homologous series of varying average pore size in organic (TEA-BF$_4$ in AN) and aqueous (KOH and H$_2$SO$_4$) electrolytes. The capacitance, normalized to S_{BET} (m^2/g)[55],[56], increases when the average pore size decreases as seen in **Fig. 8**. In organic electrolyte, it reaches its highest value for average pore size around 0.7 -0.8 nm, which corresponds approximately to the size of the desolvated TEA$^+$ ion (0.67 nm). The sharper increase with CDCs as compared to ACs could be attributed to the generally claimed narrower PSD of CDCs.[57] Initially, ion desolvation in confinement of small micropores had been proposed based on electrochemical measurements; however, recently published data based on nuclear magnetic resonance (NMR) also clearly confirm the occurrence and importance of ion desolvation for the system of 1 M TEA-BF$_4$ in AN.[58] We note that the correlation between pore

size and capacitance is still under investigation with disagreeing research findings and interpretations.[59]

The specific capacitance has been further determined in a two-electrode cell with a silver reference electrode using TEA-BF$_4$ in AN as a function of the average pore size.[60] The specific capacitance of the system (C$_{total}$) shows a maximum around 0.7 nm (**Fig. 9**), leading the authors to confirm a partial desolvation of TEA$^+$ and BF$_4^-$ ions. The maximum capacitance of the positive electrode (C$_-$, attracting anions) is at a pore size value greater than that observed for the negative electrode (C$_+$, attracting the cations) (**Fig. 9**), because the anions are less bulky than the cations. Hence, removal of the solvent from the solvation sphere plays an important role in the mechanism of energy storage. The drop in capacitance for carbons which average pore size is less than 0.7 nm (**Fig. 9**) is explained by the sieving effect when pores become smaller than the size of desolvated ions.

The capacitive behavior of microporous carbons with a very narrow PSD (carbide-derived carbons - CDC, especially TiC-CDC; Ref. [61]) and with an average pore size (d$_{50}$) ranging from 0.68 to 1.0 nm has been studied using a cavity microelectrode in a three-electrode set up with TEA-BF$_4$ dissolved in either AN or PC.[62] It was found that the size of the electrosorbed cations and anions is larger in PC than in AN. The comparison of the size of the adsorbed ions deduced from these measurements to the solvated ion size demonstrates that, in both solvents, ions have to be at least partially desolvated to enter the pores. This correlation, along with a maximum capacitance for an average pore size of 0.75 nm was corroborated by modeling using classical DFT calculations.[63] It is also important to consider the pore wall / solvent interactions. As one example, Boukhalfa et al. have shown that the accessibility for small micropores varies greatly in 1M aqueous sulfuric acid, as a result of different solvent / carbon wall interactions and solvation behavior, when substituting H$_2$O with D$_2$O.[64]

19

Apart from capacitance limitations, too narrow pores may also contribute to an increased ESR, and consequently a decrease of power; especially if the carbon is exclusively microporous, the equivalent resistance is rather high.[65] For a series of carbons with average pore size less than 1 nm in 1.5 M TEA-BF$_4$ dissolved in AN, the diffusion resistance of the BF$_4^-$ ion is the same for all carbons.[66] In contrast, the diffusion resistance of the larger TEA$^+$ ions increases as the pore size decreases. Hence, carbons with subnanometer-sized pores are recommended for enhancing ions trapping, but a small proportion of mesopores (*i.e.*, pores between 2 and 50 nm) is necessary to reduce the diffusion resistance. This is reflected in the high power handling ability of templated CDCs which combine a large volume of micropores with the presence of ordered mesopores.[67] Optimized pore architecture of templated carbons has shown to be a critical factor to enable application at very low temperatures where limited ion mobility is a major limitation to the energy storage mechanism.[68]

The capacitance increase which occurs when the pore size decreases (**Fig. 8**)[55] cannot be simply modeled by the Helmholtz model (**Eq. (1)**). Therefore, Huang *et al.* have proposed models where the ionic species enter the pores partially desolvated and arrange in lines within the entire pore length.[69] In the mesopores (2 to 50 nm), solvated ions approach the pores wall and form an electrical double-cylinder capacitor (EDCC) of capacitance given in **Eq. (7a)** and **Eq. (7b)**:

$$C = \frac{2 \cdot \varepsilon_0 \cdot \varepsilon_r \cdot L}{\ln\left(b/a\right)} \tag{7a}$$

$$\frac{C}{S} = \frac{\varepsilon_0 \cdot \varepsilon_r}{b \cdot \ln\left(b/b-d\right)} \tag{7b}$$

where *L* is the pore length and *b* and *a* are the radii of the outer and inner cylinders, respectively (**Fig. 10**). In such case, the effect of pore size and pore curvature becomes prominent as compared to the distance *d* between ions and pore wall.

In the case of micropores, desolvated or partially desolvated counter ions line-up to form an electrical wire-in-cylinder capacitor (EWCC), which capacitance is given by *Eq. (8)*:

$$\frac{C}{S} = \frac{\varepsilon_0 \cdot \varepsilon_r}{b \cdot \ln\left(b \middle/ a_0 \right)} \qquad (8)$$

where a_0 is the radius of the inner cylinder (effective size of counter ions) and b the micropore radius.

In the case of macropores (>50 nm), the pore diameters are large enough so that pore curvature is no longer significant; the classical Eq. (1) can be applied. The increase of normalized capacitance observed in Ref. [55, 56] for pores smaller than 1 nm can be fitted by the application of equations (7b) and (8).

2.4.4 Pore Saturation

When designing carbons with subnanometer-sized pores, it was demonstrated that the porosity of carbon could be saturated with electrolyte ions for high voltage values in 1.5 M TEA-BF$_4$/AN electrolyte.[70] **Fig. 11a** shows the cyclic voltammograms of two-electrode cells built from two ACs, namely APC (S_{DFT} = 1434 m^2/g; average pore size: 0.7 nm) and AVC (S_{DFT} = 2160 m^2/g; average pore size: 1.4 nm). Whereas AVC shows a typical rectangular voltammogram in the whole voltage range, for APC the capacitive current dramatically decreases at voltage higher than 1.5 V, although most pores of the later carbon have presumably an optimal size.[56] For the APC carbon, the charge determined by integration of the voltammogram is approximately equal to the theoretical maximum charge storable in the pores larger than the desolvated cations, leading the authors to propose that the reduction of the capacitive current is due to the saturation of the pore volume accessible to ions.[70] By contrast, in the case of AVC, the theoretical value of charge is larger than the experimental one, demonstrating that for this carbon the porosity is not saturated,

21

at least for the maximum voltage value reached in this experiment. During galvanostatic cycling at 960 mA/g, the porosity saturation is reflected for APC by the non-linear shape of the "voltage-time" curve, whatever the current density (**Fig. 11b**).

In order to confirm this interpretation, the microporous carbon AVC has been used with 0.5 M solutions of symmetrical quaternary ammonium bis(trifluoromethylsulfonyl)imides in AN - denoted as $[R_4N]^+[Tf_2N]^-$ - where R is $n-C_2H_5$, $n-C_3H_7$, $n-C_4H_9$, $n-C_5H_{11}$ substituents of increasing size.[71] The voltammograms of two electrode cells showed that the capacitive current normalized by the mass of one electrode is the same for all ions up to a voltage of 1 V. While the voltammograms did not show any decrease in capacitive current at high voltage for the tetraethylammonium-based salt, a current decrease could be distinguished for the tetrapropyl-, tetrabutyl-, and tetrapentylammonium-based salts as the charging progresses, and this decay is more pronounced for the gradually bulkier cations. It has also been shown that the galvanostatic characteristics deviate from linearity at progressively lower voltage and to a higher extent as the size of the cation's alkyl substituent increases.[71] Such behavior of AVC carbon with $[R_4N]^+[Tf_2N]^-$ solutions in AN can be as-well interpreted as porosity saturation, similarly to the above case of tetraethylammonium tetrafluoroborate and APC carbon.

These results demonstrate that if the pore size is adjusted to the size of ions, the pore volume may become saturated by electrolyte species, limiting the maximum operating voltage and the energy stored in the supercapacitor. Therefore, it is not enough to design carbons with the pore size compatible with that of ions, but it is also necessary that the porosity be sufficiently developed to accommodate a maximum number of ions. These two constraints are partly antagonistic, because the development of porosity generally results in an enlargement of pores or a broadened PSD. The latter has been shown to be detrimental to achieve high energy density values.

2.4.5 Distortion, Insertion/Intercalation, and Trapping of Ions

Besides desolvation, other effects might occur when the pore size of carbons approaches or is even lower than the size of desolvated ions. For example, an unexpectedly high capacitance of 92 F/g has been observed in TEA-BF$_4$/AN electrolyte using a microporous carbon with average pore size centered at 0.58 nm and with 63% of its pores smaller than the size of the desolvated TEA$^+$ ion (0.68 nm).[72] To explain this behavior, it was suggested that distorted cations penetrate in the pores under the effect of the electric field, showing slightly smaller dimensions that their computed rigid size. For some TEA$^+$ conformations, a size smaller than the average pore size of the carbon has been computed.[72]

Through electrochemical dilatometry measurements with a three-electrode configuration in TEA-BF$_4$/AN, Hahn *et al.* observed variations in size of the AC working electrode (**Fig. 12**). The expansion is larger at negative polarization, with for example 0.6 % at -1.35 V *versus* immersion potential (ip), while it is less than 0.2 % for a positive polarization of 1.15 V *versus* ip. When the potential is swept from -2 to 2 V *versus* ip, the expansion is greatly amplified, and reaches 3% and 2% for the negative and positive polarization, respectively.[73] Considering that TEA$^+$ cations are larger than the BF$_4^-$ anions, the differences of expansion observed between the two polarities are related with the insertion of ions in the electrode material. Taking into account the relatively low value of expansion, it might be anticipated that both distortion [72] and intercalation/insertion [73] of ions can occur in ACs.

With supercapacitors made from microporous carbon electrodes in TEA-BF$_4$/PC electrolyte, Aurbach *et al.* showed that the cations of the electrolyte could be trapped irreversibly in the pores after charging to 2.3 V and then keeping the system at this voltage for 1000 h (*i.e.*, floating) at 50 °C.[74] After the floating period, each of the electrodes was tested separately in a three-electrode cell. The voltammogram of the negative electrode in its operating range shows a loss of

capacitive current, C_-, while the capacitive current of the positive electrode is the same before and after floating (**Fig. 13**). However, if the negative electrode is polarized to about 4.2 V *versus* Li, there is an intense anodic peak attributed to desorption of TEA^+ ions trapped in the porosity during floating. The lower capacitance of the negative electrode after floating could be related either to the adsorption of TEA^+ ions in narrow micropores or their intercalation in disordered graphene clusters.[75] The floating parameters such as temperature and voltage can also affect the capacitance of the system and/or an electrode depending on the solvent used.[76] Similarly, the formation of decomposition products, which could be accumulated in the pores, may play a role.[76-78]

A similar effect has been observed with CDC with an average pore size of 0.68 nm, using a cavity microelectrode as working electrode in a three-electrode set-up with a 2 M EMI-TFSI/AN solution.[79] When the scan is limited to the EMI^+ electrosorption potential range (blue plot in **Fig. 14**), the cyclic voltammogram displays a rectangular shape typical for DL behavior. However, at potential higher than 0.7 V *versus* reference, the current dramatically drops down on the positive scan, demonstrating that the accessible pores are saturated with the $TFSI^-$ ions (red plot in **Fig. 14**). On the reverse scan, a cathodic peak appears at 0.25 V *versus* reference and is attributed to the electrostatic repulsion of the $TFSI^-$ anions which were forced to enter the small pores during the positive potential scan. This trapping is related to the form factor (length/thickness ratio) of the $TFSI^-$ ions that forces them to orient and align in order to penetrate into the porous network.

In conclusion, the desolvation, distortion, intercalation/insertion and trapping of ions all simultaneously occur during/charging supercapacitors in organic electrolyte. These effects added to the operating conditions of supercapacitors may reduce the voltage window, due to porosity saturation, or accelerate aging. Therefore, the study of the relationship between supercapacitor

performance and the texture/structure of carbons in the electrodes remains a research topic relevant for the optimization of these systems. Studies with single wall carbon nanotubes and ACs in organic medium by Kimizuka *et al.*[80] and Ruch *et al*. [81] have shown that the porous texture of carbons is not solely responsible for their electrochemical properties. The increase of capacitance and decrease of electrical resistance observed under high polarization of single wall carbon nanotubes could be related to electrochemical doping resulting in a shift of the Fermi level toward the valence band or the conduction band of the graphene layers during charging; this explains the "butterfly" shape of three-electrode cell voltammograms. As this behavior is also observed in the case of ACs,[81] the single-layer modeling proposed by Harris *et al.*[38] is fully relevant (**Fig. 4b**). The electrochemical doping is dependent on the carbon structure, which makes interpreting the distribution of ions in the micropores during charging of supercapacitors much more difficult.

3 Design of Carbon-based EDLC Electrodes

3.1 Tailoring Pore Characteristics and Particle Size

From the foregoing, the control of the pore characteristics of electrode materials for EDLCs is a key performance parameter. Therefore, variations in the synthesis routes of porous carbons have been established to leverage new insights into ion transport behavior and to optimize the device performance. As one example, the major advantage of some CDCs, such as TiC-CDC or SiC-CDC, compared to many other porous carbons, is the high level of control over a narrowly distributed PSD and d_{50} as a function of the precursor and synthesis temperature - especially in the critical pore size range between 0.5 and 1.0 nm.[61] As a result, the maximum specific

capacitance of CDC supercapacitors is rather large (*e.g.*, 140 F/g for TiC-CDC in 1 M TEA-BF$_4$ in AN).[24, 82]

Another group of tunable materials are templated carbons[83] which usually employ zeolites (ZTC, **Fig. 15**)[84] or silica[83, 84] as sacrificial scaffold. Work by Matsuoka *et al.* [85] illustrates that very high S_{BET} values (3360 m^2/g) can be achieved, with the majority of the pores ranging between 1 and 2 nm. Zeolite templated carbons have been used successfully as a model system for the study of EDLC performance.[86] This "hard" templating involves a number of synthesis steps, which can be broken down in (i) synthesis of the template itself, (ii) infiltration with carbon or a carbon-containing precursor, and, finally, (iii) removal of the skeletal template (**Fig. 15a**). Typical zeolites used for carbon templating are zeolite Y or X; also, SBA-15 and MCM41 are often employed for silica templating yielding ordered mesopores. The ordered pore structure of ZTCs and silica templated carbons are in contrast to the largely disordered pore networks of ACs or CDCs. In particular, silica templating (*i.e.*, hard templating) has attracted attention as a way to obtained mesoporous CDC with an ordered pore structure.[87] The reported specific capacitance of templated carbons varies and typical values range between 100 and 190 F/g.[88]

Compared to the synthesis of CDCs or CNTs, and in particular ACs, templating is rather elaborate, resulting usually in lower carbon yields and inherently higher costs. An alternative templating method to hard templating is soft templating[89] using resorcinol formaldehyde as the carbon source and self-assembly of block copolymers (BCPs; especially triblock copolymers) as the template.[90] As shown in **Fig. 15b**, after a film of polystyrene-b-poly(4-vinylpyridine) (PS-P4VP) and resorcinol-formaldehyde has been cast on a substrate (step 1), phase separation is initiated by annealing at 80°C in a DMF/benzene atmosphere (step 2). After polymerization and cross-linking in formaldehyde gas (step 3), the material is then pyrolysed under nitrogen flow so that a film of ordered hexagonal carbon channels can be obtained after the block copolymer has

fully decomposed (step 4). Adjusting the pyrolysis temperature from 400 to 800°C yielded a SSA ranging from 624 to 1354 m^2/g and an average pore size ranging from 7.4 to 5.9 nm; also, samples pyrolyzed at 800 °C still showed a high oxygen content (17.4 wt.%).[90] This high level of control of the pore size and pore alignment is useful to provide optimized transport pathways for ion transport and to optimize the EDLC device performance.

As we have seen, ion transport is a limiting parameter for high charge/discharge rates in EDLC devices. While low ionic conductivity can be a feature of the electrolyte,[19] effective ionic transport is closely related to transport limitations within porous carbon particles.[91, 92] Thus, while using the same electrolyte, the ion transport can be facilitated by either using very small particles (nanoparticles or thin films) to decrease the diffusion length, or utilizing hierarchical porosity.

Different studies [67, 93] have demonstrated that the EDLCs performance of CDCs depends not only on the PSD but also on the particle size. Nanoparticulate CDCs (20 - 30 nm) exhibit easier ion transport through the porous particle compared to CDCs with average particle size of 6 - 20 μm, and a clear trend of increased power (and energy) density with decreased particle size was established.[93, 94]

Transport-optimized 3D pore networks have been already the focus of research activities; for example, Keil and Rieckmann calculated an optimized porous material for catalysis applications.[95] Hierarchical pore networks decrease transport limitations, resulting in an improved performance beyond the field of catalysis and into applications such as high-performance liquid chromatography (HPLC) separation.[96] Hierarchical meso- and microporous carbons have been created by using templated mesoporous carbides to obtain CDCs that exhibit both, ordered mesopores for improved ion transport and, through chemical etching, micropores for improved ion storage (**Fig. 16a**). As a first step, ordered mesoporous (OM) carbides, such as

27

SiC[97] and WC/C composites,[98] were obtained by SBA-15 templating, known as nanocasting. In the second step, OM carbides are transformed into porous carbons *via* thermal halogenation (*i.e.*, chemical etching).[87] Ordered mesoporous CDCs maintain the ordered nature of the mesopores from the carbide precursors (**Fig. 16b**) while introducing a large micropore volume to the total porosity (**Fig. 16c**); such OM CDCs exceed conventional CDCs in power handling ability and measured capacitance (**Fig. 16d**). Compared to the performance of ~170 F/g at ~1 A/g, ordered mesoporous SiC-CDCs synthesized at 700 °C exhibit only a 15 % reduction in the capacitance in a full cell experiment at a current density of 18 A/g in 1 M TEA-BF$_4$ in AN.[67]

Another kind of hierarchical porous carbon has been reported by Wang *et al.*[99]: hierarchical porous graphitic carbon (HPGC). After mixing Ni(OH)$_2$ with phenolic resin, followed by carbonization at 600°C and removal of the metal oxide scaffold with 3 M HCl solution, porous carbons can be obtained. While 43% of the pore volume is associated with micropores, there are two more maxima in the PSD at approximately 20 and 60 nm, indicating there is a hierarchy of pores in the system. The capacitance of the HPGC is 270 F/g in 6 M KOH and is likely the product of EDL and pseudocapacitance, as it cannot be accounted solely by the moderate SSA of 970 m^2/g. Nevertheless, compared to conventional ACs, these materials display high capacitance at high current densities, up to 50 A/g, and scan rates up to 100 mV/s.

Porous carbon fibers represent a special class of hierarchical porosity containing interfiber and intrafiber pores. For example, activated carbon fibers (ACF) derived from polyacrylonitrile (PAN), phenolic-resin, or pitch-based carbon fibers, have been investigated as supercapacitor electrode materials. Yoshida *et al.*[100] established the feasibility of using high surface area phenolic-resin based fibers with SSA up to ~2500 m^2/g as active electrode materials in coin cells with a capacitance of up to 119 F/g in TEA-BF$_4$/AN.[101] Even higher values for S_{BET} (2832 m^2/g) were reported for ACFs by Leitner *et al*. and, using a three electrode setup, a maximum

capacitance of 175 F/g was measured in 5.25 M H_2SO_4.[102] An upper limit to carbon fiber activation was discussed by Yoon *et al*., where over-activation in KOH at 1000°C leads to fiber structural collapse which was associated with decreased electrochemical performance.[103] Electrospinning of a spin dope containing n-butoxide (TiBO) and furfuryl alcohol combined with pyrolysis under neutral atmosphere (producing TiC/C composite fibers) and subsequent chlorine treatment yields mechanically stable and flexible ultrathin TiC-CDC fibers mats[28] which exhibit micro- and mesopores.[104] Such CDC fiber mats showed a beneficial power handling ability in a two electrode setup: starting with 135 F/g in aqueous and 120 F/g in 1 M TEA-BF$_4$/AN at low scan rates, there was a fade in capacitance of approximately 50% at 5 V/s. However, such fiber-electrodes show usually a moderate or low volumetric capacitance, such as only 19 F/cm^3 in the case of CDC fiber mats because of the low density of the electrode ($\sim$ 0.14 g/cm^3).

3.4 Exohedral Carbon EDLC Electrodes

Another strategy for high power EDLC electrodes is the use of dense nanoparticles with only an external surface area and positive surface curvature, such as capped CNT or onion-like carbon (OLC, also known as carbon onions), which provide abundant interparticle pores. In such systems, the SSA remains significantly smaller compared to porous carbons and limited by the particle size. Typically, these exohedral carbons exhibit S_{BET} of only 300-500 m^2/g, and correspondingly, they show usually a moderate capacitance of only 20 - 100 F/g. Yet, the highly graphitic nature and external surface area makes these materials suitable for fast charge and discharge applications.[105-107]

In general, exohedral carbons have the intrinsic ability to enable high power density and normalized capacitance. The positive curvature of tubes or spheres of the exohedral carbon family (carbon onions and CNTs) facilitates DL formation, and the reduced electrical field near

spherical or cylindrical surfaces (**Fig. 17b**) decreases the driving force for counter-ion adsorption and co-ion desorption.[108, 109] This effect is more pronounced for spheres compared to tubes, and increases as the curvature increases (**Fig. 17a**).[108]

As seen, curvature or, when considering surfaces in general, nanotexture, is a parameter of particular importance for the resulting energy density. It has been shown for different carbon surface structures in carbon nanofibers that layers of graphitic carbon oriented parallel to the surface show a lower specific capacitance compared fibers with a roughened surface with tubular- or herringbone-like structures on the surface.[110] These findings, derived from experiments carried out in 0.5 M H_2SO_4, are qualitatively well in agreement with simulation results of nanopatterened carbon electrode surfaces; for the latter, N-methyl-N-propylpyrrolidinium bis(fluorosulfonyl)imide was used and, compared to the flat surface, the roughened electrode showed a significantly higher normalized capacitance (F/m^2), that is, even when the larger total surface area was considered.[111]

Capped CNTs are the most commonly known and widely investigated exohedral carbon material and can be envisioned as one-dimensional carbon wires. Oxidized MWCNTs (S_{BET}: 430 m^2/g) in 6 M H_2SO_4 aqueous electrolyte exhibit a capacitance of 102 F/g[112] and later studies show moderate intrinsic capacitance (18-137 F/g) for single-wall and multi-wall CNTs in 6 M KOH aqueous electrolyte.[113] Activation, for example with KOH, increases the capacitance of MWCNTs but it usually comes with the trade-off in power handling ability and power density.[114, 115]

High purity single-wall CNTs were claimed to open a large usable voltage window of 4 V in TEA-BF$_4$/PC with a specific capacitance of ≈160 F/g at current densities up to 20 A/g.[116] These values would correspond to a power density of 210 W/g and an energy density of 0.094 Wh/g, which is significantly larger than AC electrodes tested in the same electrolyte at a smaller

maximum voltage window (60 W/g and 0.033 Wh/g). However, cycling stability has not been demonstrated for such high cell voltages and it is unlikely that long term performance of actual devices is possible under such extreme conditions.

Besides capped CNTs, OLC (**Fig. 17C**) is another group of exohedral nanocarbons used as electrode material for EDLCs.[117] Carbon onions can be envisioned as spherical (quasi zero-dimensional) nanoparticles. There exist a number of ways to synthesize carbon onions, but the most facile technique is to derive OLC from detonation nanodiamond *via* thermal annealing in vacuum.[107] Carbon onions obtained from this process have been studied in the microcavity electrode (MCE) and even though this method does not reflect the performance of macroscopic films or assembled EDLC devices, it still documents the high power handling ability of carbon onions.[118, 119] For thin film systems, OLC EDLC performance has been studied up to 200 V/s, and as documented by MCE testing in 1 M H_2SO_4, the synthesis conditions significantly influence the power and energy density of carbon onions.[118] Low vacuum annealing (1200°C) yields onions that, when tested at a scan rate of 2 V/s, yielded a capacitance of 4.7 F/cm^3; increasing the annealing temperature to 1800°C resulted in a decrease of the capacitance ($\approx$3 F/cm^3). However, the current density and power handling ability increased with higher annealing temperatures because they are related to the intrinsic electrical conductivity of the material.

The moderate intrinsic capacitance of CNTs and OLCs, have motivated the use of these exohedral carbon nanomaterials as an alternative to carbon black (CB) conductivity additive, rather than active electrode materials. As shown in 1 M $LiClO_4$/ethylene carbonate - diethyl carbonate electrolyte, small addition of multi-wall CNTs (3 wt.%) to AC yielded a capacitance and power handling ability comparable to AC mixed with 9 wt.% CB;[120] this effect can be explained by the improved electron transport along the nanotubes, compared to isolated spherical

31

CB particles. A compromise between energy and power density was found by adding 15 wt.% of CNTs to AC electrodes tested in 1 M TEA-BF$_4$/AN;[121] the addition of CNTs lowers the capacitance because of their low SSA, while the ESR decreases as the content of the highly conductive CNTs increases.

OLC as a conductive additive was described in Ref. [122] where soft templated ordered mesoporous carbons were blended with carbon onions, and the electrochemical performance in AN with 1.8 M triethylmethylammonium-tetrafluoroborate evidenced a lower ESR and, hence, an improved power handling ability. In particular, adding 5 wt.% of OLC yielded a lower ESR than when 25 wt.% of CB was added to the mesoporous carbon which may be related to the finer dispersion of the carbon onions in the electrode.[122] In agreement with these results, the addition of 10 wt.% carbon onions to AC supported on a polyester microfiber substrate lowered the device resistance from 9 to 3.5 Ω.[123]

3.5 Carbon Thin Film EDLC Electrodes

EDLC ratings, especially when normalized to the volume and not to the weight, are sensitive to the compactness of the porous carbon electrode. Eliminating interparticle spaces and, at the same time dead weight / dead volume, provides a higher volumetric device performance. While matching pore size to ion size is beneficial for capacitance, this improvement is attenuated as the electrode's thickness increases. As shown by Chmiola *et al.*,[124] varying the film thickness of monolithic TiC-CDC films drastically decreases the volumetric capacitance (**Fig. 18a**). A 5 μm thick film yielded a specific capacitance of ≈160 F/g in 1 M H$_2$SO$_4$ and ≈180 F/g in 1 M TEA-BF$_4$/AN, but these values dropped by approximately 50% for the aqueous and by more than 80% for the organic electrolyte for a 50 μm thick CDC film with the exact same porosity. These examples show that diffusional limitations are more severe for larger ions / more viscous

electrolytes, and films which are monolithic and consisting only of microporous carbons must be very thin to fully benefit from an increased volumetric power and energy density. Similar limitations were observed when increasing the thickness of printed CNT-based electrodes to more than 5 μm when comparing the performance in 1 M H_2SO_4 with a gel electrolyte.[125]

There are two manufacturing approaches to making carbon thin film supercapacitors: top-down and bottom-up. Top-down, involves synthesis of a carbon precursor, such as carbides, and conversion into carbon. This has been shown for CDC derived from monolithic TiC[124] and TiC thin films deposited with magnetron sputtering on glassy carbon, highly-oriented pyrolytic graphite (HOPG), sapphire, or thermally oxidized silicon.[126] Such films can be patterned so that interdigitated electrodes are obtained (**Fig. 18b**) and a gold coating on top of the CDC layer can be utilized as the current collector. A similar approach was recently reported by using low-pressure chemical vapor deposition (CVD) of silicon carbide (SiC) thin films.[127] On-chip integrated devices obtained from partial graphitization (reactive plasma etching) yielded an approximately 1 μm thick SiC-CDC layer on top of SiC exhibiting a very low time constant (τ = 62 ms).[127] The time constant (RC time constant) is defined as the product of resistance and capacitance (τ = R·C) and it is representative of the time required to charge or discharge a capacitor by 63.2 % (*i.e.*, $1 - \frac{1}{e}$),

The bottom-up approach involves the selective deposition of nanoparticulate carbons on a current collector; the latter may be patterned, so that the interdigitated feature described before can be utilized. Printing[125] or electrophoretic deposition[92, 115] have been used to obtain thin film supercapacitor electrodes based on CNTs and OLC. Such patterned thin film electrodes have become known as "micro-supercapacitors" and their manufacturing and performance was documented for OLC and AC[92] thin films (5 - 7 μm thick). While the OLC micro-supercapacitor displayed a very short time constant (26 ms) in combination with a small decrease in the

33

capacitance up to a scan rate of 200 V/s, the AC-based device exhibited a larger time constant (700 ms) and lower power handling ability (up to approximately 20 V/s; tested in 1 M TEA-BF$_4$/PC). We note that 200 V/s is two orders of magnitude higher than the usual limit for conventional AC film electrodes. Also, because of the low surface area of OLC, the AC micro-supercapacitor had an energy density approximately one order of magnitude larger than the OLC-based one ($\approx$0.04 Wh/cm^3 *versus* 0.001 Wh/cm^3); the latter had a significantly larger power density ($\approx$250 W/cm^3 *versus* $\approx$40 W/cm^3).

Cost and production considerations are important also for the advancement and implementation of micro-supercapacitors. Noticeably, a very facile way for mass production of micro-supercapacitors was recently introduced *via* the use of a CO$_2$ laser[128] or a LightScribe DVD burner, where 100 employing laser-scribed graphene (LSG) devices were fabricated in 30 minutes.[129] Such micro-patterned and flexible systems showed a high volumetric capacitance of 3.05 F/cm^3 when using a hydrogel polymer electrolyte (poly(vinyl alcohol-H$_2$SO$_4$) and 2.35 F/cm^3 when employing a fumed silica / IL ionogel (all values for a stack of 16 interdigitated micro-electrodes).[129]

While preferred orientation is not a concern for OLC (as they are spherical particles), this is not the case for CNTs. Electrophoretic deposition, for example, yields randomly oriented CNTs without any periodicity (**Fig. 19a**), while well-oriented patterns of vertically aligned multi-wall CNTs (VA-MWCNTs) can be obtained *via* chemical vapor deposition (CVD, **Fig. 19c**). Laterally, even complex pattern are possible for VA-CNT films, as shown in **Fig. 19b**; such nanotube meshes can be obtained by growing the CNTs in a prefabricated template, such as a glass substrate that was patterned by photolithography to yield a regular array of hexagonal holes.[130] Maintaining a vertical alignment with respect to the substrate, as shown in **Fig. 19c**, enhances electron transport to the current collector, while direct deposition decreases the contact

resistance.[131] As shown in Ref. [132], mostly vertically aligned CNTs can be synthesized on carbon paper (*i.e.*, sheets of carbon fibers with a diameter of 7 μm). Although such films were relatively thick (500 μm), a high power handling ability up to 150 A/g was documented in 1 M H_2SO_4 (~250 F/g @ 2 A/g; ~180 F/g @ 150 A/g = -28%); yet, the power handling ability was significantly lower in an organic electrolyte (1 M TEA-BF_4/AN; ~170 F/g @ 2 A/g; ~124 F/g @ 30 A/g = -27%).

The utilization of thin VA-MWCNTs films (≈20 μm thick) on aluminum in combination with an ionic liquid mixture (1:1 mixture of N-methyl-N-propylpiperidinium bis(fluorosulfonyl)imide, $PIP_{13}FSI$, and N-butyl-N-methylpyrrolidinium bis(fluorosulfonyl)imide, $PYR_{14}FSI$) has been documented up to 20 V/s between 20 and 100 °C, and up to 50 mV/s at -50 °C.[131] Such thin VA-MWCNT films did show a stable capacitance when comparing low (-50 °C) with high temperature performance (+100 °C); in contrast a 200 μm thick OLC film, tested under the same conditions, did show a significant drop in capacitance and increase in series resistance when ionic mobility dropped at low temperatures. Considering the high power handling ability of OLC micro-supercapacitors, this must be related to transport limitations at increased film thickness.

The ultimate carbon thin film system, of course, is monolayer graphene. There has been tremendous excitement stimulated by the promising properties of graphene (high surface area, 2,630 m^2/g, high electron mobility, etc.), and first graphene EDLC electrodes have been reported. Ref. [133] exemplified the utilization of chemically modified graphene (CMG; **Fig. 20a**) yielding 135 F/g in 5.5 M KOH and 99 F/g in 1 M TEA-BF_4/AN (94 F/g in PC). CMG, however, yielded in this early study a relatively low BET SSA (705 m^2/g) with a nitrogen content of 4 at.% and an oxygen content of 8 at.%. A similar performance was reported for graphene films derived by reducing graphene oxide, and the best performance was seen for a thin graphene electrode (25 nm: 135 F/g; 100 nm: 103 F/g in 2 M KCl) deposited on a polyethylene terephtalate (PET)

substrate.[134] High power density (up to $\approx$10 kW/kg at 8 A/g for a 4 V window) was measured for low loading (6.6 mg for a 1.3 cm^2 electrode) of graphene flakes (**Fig. 20b**) in EMIM-BF$_4$.; yet, no cycling stability was documented for such a large operational cell voltage.[135] Miller *et al.*[136] documented a time constant of 200 µs with a 600 nm thin electrode of vertically aligned graphene in KOH (3 F/cm^3), enabling line filtering applications at a 120 Hz frequency (**Fig. 20c**) and approaching the response rate of electrolytic capacitors. High SSA reduced graphitic oxide (S_{BET}: 2687 m^2/g) has recently been reported to yield up to 220 F/g in 1 M TEA-BF$_4$/AN in a three electrode setup.[137]

4. Pseudocapacitance and Carbon Electrodes

4.1 Introduction

Besides tailoring the pore size and total pore volume, the achievable maximum capacitance of conventional EDLCs remains limited, and high energy density supercapacitors require a different technological solution. One strategy to increase the capacitance is related to pseudocapacitive phenomena at the electrode/electrolyte interface. Pseudocapacitance typically originates from materials such as conducting polymers,[138, 139, 140, 141] transition metal oxides,[7, 142-144, 145, 146-148] carbons enriched in heteroatoms (oxygen, nitrogen),[149-152, 153, 154] or microporous carbons with electrosorbed hydrogen.[54, 155, 156, 157, 158, 159, 160, 161, 162] In addition to electrode materials, pseudocapacitance can also originate from redox reactions of the electrolyte species.[163-166, 167] In the following sections, examples of pseudocapacitive materials mainly their composites with carbon and redox species active at carbon/electrolyte interface will be discussed.

4.2 Conducting Polymers / Carbon Composites

Electrically conducting polymers (ECPs) such as polypyrrole (PPy), polyaniline (PANI), polythiophene (PTh), poly[3-methylthiophene] (PMTh), or poly[3,4-ethylenedioxythiophene] (PEDOT) can store and release charges through redox processes associated with the π-conjugated polymer chains.[138, 139, 140, 141] When oxidation (= doping) occurs, ions from the electrolyte are transported to the polymer backbone, and released back into the solution during reduction (= dedoping). The doping/dedoping process, as shown in *Eq. 9* for PPy, involves the entire electrode material, enabling high values of specific capacitance.

$$\left[PPy^+ A^- \right] + e^- \leftrightarrow PPy^+ + A^- \tag{9}$$

The insertion/extraction of counter ions during cycling causes volumetric changes of conducting polymers that may contribute to mechanical degradation (swelling, breaking, shrinkage) of the electrode.[132, 134] Hence, the application of a moderate amount of CB, carbon fibers, CNTs, or graphene to improve the mechanical properties of the electrodes is crucial.[140, 141, 168, 169, 170, 171] Furthermore, they also enhance the electrical conductivity of electrodes. Among these materials, multi-wall or single-wall carbon nanotubes have the advantage of an electrically conducting and flexible network; also, the mesopores (between the nanotubes) facilitate ion diffusion that is critical to the doping process. ECP/CNTs nanocomposites can be obtained by electrochemical or chemical polymerization of monomers. When comparing these two methods, we see that the latter is less expensive and often more convenient.

The applied voltage is the key factor influencing the specific capacitance of supercapacitors based on ECP/CNT nanocomposites.[141] When the same ECP/CNT material is used for both electrodes, it shows a poor cycling stability if the maximum voltage exceeds some limit. Beyond this limit, one electrode reaches a potential at which the ECP is electrochemically unstable and the performance degrades.[141] Taking into account that ECP/carbon composites only operate reversibly in a narrow range of potential, their optimal application requires an asymmetric configuration, realized by selecting different types of ECPs for positive and negative electrodes or combining them with another electrode material such as AC or a metal oxide. This approach extends the operating voltage and consequently, higher energy and power densities can be achieved.[7, 144] [172]

4.3 Metal Oxide / Carbon Composites

Transition metal oxides are also considered as attractive materials to achieve high energy storage in supercapacitors. Among them, ruthenium oxide (RuO_2) exhibits very high capacitance, good electrical conductivity, excellent electrochemical reversibility, high rate capability, and long cycling life. However, the cost, the lack of abundance, and toxicity has made it necessary to find alternative materials, and significant attention has been devoted particularly to manganese oxide (MnO_2) because of its environmentally friendly character and large abundance.[7, 142-144, 145, 146-148]

The electrochemical performance of MnO_2 is strongly affected by its texture, and various methods have been applied to prepare oxide with an optimized architecture. Microporous hydrous MnO_2 has been studied by the organic-aqueous interfacial method,[147] and the SSA and PSD were controlled by adjusting the reaction time and the concentration of surfactant in the aqueous phase. MnO_2 synthesized by this method demonstrated a capacitance of 261 F/g with good cycling; however, the performance was limited to very low charge/discharge rates (0.5 mA/cm^2) because of the low electrical conductivity.

Almost pure manganese oxide (λ-MnO_2) has been obtained through lithium exclusion from the layered structure of spinel-type $LiMn_2O_4$ using 0.5 M aqueous H_2SO_4, and most of the lithium ions could be removed from the tetrahedral sites while preserving the framework of spinel.[148] Even if the final product has a very low SSA ($S_{BET} = 5$ m^2/g), high values of capacitance (300 F/g) were measured, but only at moderate discharge current (100 mA/g). [148]

Another method for preparing MnO_2 is the oxidation of a Mn^{2+} salt by a strong oxidant. In this case, amorphous a-MnO_2 has been precipitated on CNTs by adding $Mn(OAc)_2 \cdot 4H_2O$ to a $KMnO_4$ solution.[146] Scanning electron microscopy (SEM) showed that the CNTs acted as the substrate with an extremely good adhesion of the oxide layer. Such textural characteristics are useful for an

easy access of ions to the bulk of the active material whereas the mechanical properties of CNTs are beneficial for a good resiliency of the composite electrodes and an enhanced electrical conductivity.

Generally, the pseudocapacitive properties of amorphous manganese oxide (a-MnO$_2$·nH$_2$O) are attributed to the redox exchange of protons and/or cations with the electrolyte as shown in **Eq. 10** (Ref. [143]):

$$MnO_x\left(OH\right)_y + nH^+ + ne^- \leftrightarrow MnO_{x-n}\left(OH\right)_{y+n} \tag{10}$$
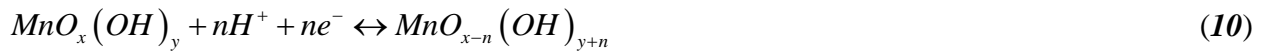
where $MnO_x(OH)_y$ and $MnO_{x-n}(OH)_{y+n}$ indicate interfacial a-MnO$_2$·nH$_2$O in higher and lower oxidation states, respectively. Symmetric two-electrode capacitors built with a-MnO$_2$/CNTs composite electrodes demonstrated a dramatic decrease of cell resistivity from 2000 Ω·cm^2 to 4 Ω·cm^2 and an increase in capacitance from 0.1 F/g to 137 F/g after adding 15 wt.% of CNTs. It has been also shown that 15 wt.% of CNTs is an optimal ratio more beneficial than using CB, with the latter being the commonly used material as conductive additive in electrodes.

A lot of research has been dedicated to optimize the SSA of oxides through a hierarchical structure of the composite. The oxide component was placed on carbon nanotubular support in various exotic forms such as nanorods, nanoflowers, nanoflakes.[91, 171, 173, 174] For instance, flower-like shaped MnO$_x$ has been deposited on a CNT array with a resulting SSA of 236 m^2/g. As an effect of the hierarchical morphology,[148, 204] the high density of this composite (1.5 cm^3/g) allows a great volumetric capacitance of 305 F/cm^3 to be reached and due to such accessible porous morphology of the composite a capacitance of up to 100 F/g has been observed even at a high current load of 77 A/g.

These studies show that only nanostructured carbon/MnO_2 composites with an optimized SSA and good dispersion of oxide yield a high performance. Furthermore, it is important to employ such materials only within the electrochemical stability window, as exemplified by the Pourbaix diagrams for aqueous electrolytes (*i.e.*, potential *versus* pH-value).[175] Commonly, the composites are used as positive electrode in an asymmetric configuration with AC, conducting polymer or another oxide at the negative electrode.

Besides Ru- or Mn-based oxides, the advantages of using CNTs as the substrate for nanocomposite electrodes have also been shown with other pseudocapacitive materials, such as nickel, cobalt, vanadium, and iron oxides.[170, 174] However, achieving high performance and high stability in pseudocapacitors based on transition metal oxides remain a challenge. The surface and bulk redox phenomena involve diffusion processes that preclude high rate performance from these materials. Additionally, the limited electrical conductivity of most oxides is at the origin of further problems that can be mitigated by blending carbon, preferentially CNTs or graphene, to the materials. Some novel advanced composites based on two pseudocapacitive materials, for example, metal oxides and conducting polymers together with CNTs have also been developed.[176] The resulting specific gravimetric capacitance of, for instance, PEDOT/CNT/MnO_2, can reach over 400 F/g especially with functionalized nanotubes and moderate regime whereas 200 F/g was obtained at 3.3 A/g charge/discharge rate with satisfactory charge retention and cycling stability (1000 cycles).[213] For the same ternary composites, a maximum capacitance of 280 F/g at 200 mV/s scan rate was indicated. [211]

In summary, **Fig. 21** shows the advantages of depositing pseudocapacitive materials (ECPs and oxides) on CNTs arrays in order to get a synergy of the two components and superior capacitive

properties. In particular, it illustrates the usefulness of mesoporosity for ions access and resiliency of electrodes.

4.4 Pseudocapacitance of Carbons with Heteroatoms

4.4.1 Introduction

A greatly increased capacitance can also be obtained by using different types of faradaic reactions originating from oxygen and nitrogen heteroatoms in the carbon network.[101, 143- 148, 171-174] Such pseudocapacitive effects additionally accompany the typical electrical double-layer charging and they can be connected with either quick faradaic reactions of functional groups or also with a local modification of the electronic structure of the doped carbon. In this case, the decrease of gap between the conduction and valence bands enhances conductivity, in turn, ions sorption due to an increase of local free electrons.[162] When using carbons enriched in heteroatoms, special attention should be paid to an optimal selection of the doped material depending on the electrode polarity. Some oxygenated functional groups, for example, quinone-hydroquinone redox pairs, play a significant role for the electrode of positive polarity,[105, 177, 178] preferably in acidic media, whereas quaternary nitrogen seems to be an optimal functionality for the negative electrode operating in alkaline medium.[218]

4.4.2 Oxygen-Enriched Carbons

Introducing oxygenated functionalities in the carbon network can greatly enhance the capacitance.[105, 177, 178] A common method to achieve a highly oxygenated carbon is to choose a suitable oxygen rich precursor for carbonization or post-treatment of carbon in strongly oxidative atmosphere.

Carbon materials with a high performance, for example, were obtained by one-step carbonization of a seaweed biopolymer, such as sodium alginate, without further activation.[177] Although sodium alginate has a structure very close to the structure of cellulose, its thermal behavior is different; while the thermal decomposition of cellulose comes to a completion at 400 °C, alginate still shows a significant weight loss associated with CO evolution between 700 and 900 °C. Pyrolysis of sodium alginate at 600 °C under argon flow yielded a slightly microporous (S_{BET} = 273 m^2/g) material which contains a high amount of oxygen (15 at.%) retained in the carbon framework. Despite this low value of S_{BET}, the capacitance in 1 M H_2SO_4 reaches up to 200 F/g - a value comparable to the best available ACs. The contribution of pseudocapacitance was confirmed with cyclic voltammetry by the presence of reversible redox peaks connected with the quinone/hydroquinone pair, and involving a proton-coupled electron transfer of two electrons and two protons.[177] Pyrone-like structures (*i.e.*, the combination of non-neighboring carbonyl and ether-oxygen atoms at the edge of the graphene layers) can also effectively accept two protons and two electrons in the same electrochemical potential range as the quinone/hydroquinone pair.[179] Consequently, in the carbon obtained from sodium alginate, the high value of capacitance is related with charge transfer reactions on the quinone, phenol, and ether groups.[177] The resulting material has also a high density and a good electrical conductivity that yields a volumetric capacitance higher than for highly porous carbons and fast charge/discharge rates without requiring the presence of conductivity additives in the electrodes. Further research has been performed on the carbon from a pure seaweed precursor.[178] Special types of seaweeds (*Lessonia Nigrescens*) rich in alginate (30-40%) after carbonization at 600 °C pointed out interesting capacitance properties because of a well-balanced micro/mesoporosity. The relatively high BET SSA (746 m^2/g) was originated from metallic elements present in precursor being responsible for self-induced activation. The final carbon of higher density than typical ACs

exhibited a great capacitance of 264 F/g in 1 M H_2SO_4 with long durability at 1A/g current load. Additionally, improved power handling was obtained by incorporating CNTs in the seaweeds before the thermal treatment.[180]

4.4.3 Nitrogen-Enriched Carbons

Nitrogen enriched carbons can be obtained by ammoxidation of nanoporous carbons[181] or by carbonization of nitrogen-rich polymers followed by steam activation.[149, 153] However, since one of the reactions involved in these procedures occurs in oxidative conditions, oxygen is also incorporated together with nitrogen in the carbon network and it is difficult to assess completely the measured values of capacitance to the unique contribution of the nitrogenated functionality. Nevertheless, a correlation has been found between capacitance and the nitrogen content for a unique series of nitrogen enriched carbons prepared by carbonization of polyacrylonitrile (PAN) or pitch/PAN and pitch/polyvinylpyridine blends, followed by steam activation (**Fig. 22**). These samples of comparable porosity ($S_{BET} \approx 800$ m^2/g) demonstrate a capacitance proportional to the nitrogen content in aqueous medium, whereas it was almost constant in an organic aprotic electrolyte.[149] This dependence shows the important role of protons for pseudocapacitive effects. The enhancement of capacitance with the nitrogen content in H_2SO_4 medium is interpreted by pseudofaradaic reactions due to the nitrogenated functionality as exemplified in **Fig. 23**.

Another nitrogenated carbon composite has been obtained by one-step carbonization of PAN blended with carbon nanotubes (70/30 wt.%) at 700 °C.[182] The relatively high capacitance of 100 F/g in contrast to a moderate SSA of 220 m^2/g is related to the presence of nitrogen. The beneficial effect of nitrogen in composites with an incorporated nanotubular backbone has clearly been demonstrated using melamine as nitrogen-rich (45 wt.%) carbon precursor.[154] Such carbon

composites have been obtained by polymerization of melamine with formaldehyde without any catalyst in the presence of a controlled amount of multi-wall CNTs. The polymerized blends were carbonized at 750 °C for one hour under nitrogen flow to give composites with various proportions of components (see **Table 2**). The results of elemental analysis showed that the nitrogen content in the final product varies from 7.4 to 21.7 wt.% and the oxygen content varied in all the samples from 5.9 to 7.8 wt%. The porosity characteristics of all the composites are illustrated in **Table 2** and correlated with their capacitance properties. **Fig. 24** shows that the ability for charge accumulation in 1 M H_2SO_4 diminishes with the increase of current density, but the composite from melamine, formaldehyde (proportion 2:1) and carbon nanotubes, i.e., sample Nt+2M+F is still able to supply a capacitance of 60 F/g at a high current density of 50 A/g. The high charge propagation of this composite can be explained by the fast electronic transport along the CNTs which are preserved after the carbonization process. Albeit the positive effects of nitrogen, such as improved capacitance and wettability, it is important to note that an excess of nitrogen (presumably over 15%) aggravates the conducting properties, and in turn, the capacitance characteristics and the supercapacitor cyclability.

Apart from aqueous 1 M H_2SO_4, attention has been also devoted to other aqueous electrolytes, such as 6 M KOH or 1 M Na_2SO_4, and an organic electrolyte, for example 1 M TEA-BF_4 in AN. The best performance of Nt+2M+F (101 F/g) is observed in acidic solution, slightly exceeding the alkaline one (92 F/g). In organic solution (35 F/g) and in neutral aqueous Na_2SO_4 (26 F/g), the capacitance values are relatively low due to the absence of pseudo-faradaic reactions in these media and to the low SSA of the electrode material ($S_{BET} = 393$ m^2/g).[148]

The correlation between the nitrogen content in carbons with the electron density of states (DOS) has been studied with molecular quantum calculation. As a result, it was reported that the energy

gap between the conduction and valence bands affected by the nitrogen content was qualitatively correlated with the electronic conductivity and capacitance properties of the composite.[162]

Other routes were proposed to prepare nitrogenated carbons using N-rich precursors. With melamine polymerized in mica [150] followed by ammonia treatment,[151] the highest capacitance values have been obtained in KOH medium (280 F/cm^3 equal to 198 F/g), whereas values of 152 F/cm^3 equal to 115 F/g were measured in sulphuric acid. A very high capacitance (340 F/g) has been reached using templated carbons from acrylonitrile pyrolysis in NaY zeolite.[183] This high value results from the synergy between the highly developed surface area of the material and the pseudofaradaic reactions related to the presence of the nitrogenated functional groups. Another approach is based on the nitrogen plasma treatment of graphene and a high capacitance values of *circa* 280 F/g was reported which was 4-times higher than for the pristine graphene.[155]

4.5 Electrosorbed Hydrogen in Porous Carbons

Pseudocapacitive properties can also be observed for nanoporous carbons through the reversible electrosorption of hydrogen in aqueous media. In that case, during the negative polarization of an electrode, water is reduced and nascent hydrogen is adsorbed in the material and, finally, the adsorbed hydrogen is desorbed by anodic oxidation.[54, 155, 156, 157, 158, 159, 160]

Hydrogen sorption/desorption in a carbon electrode can proceed at high current loads, leading to interesting application for the negative electrode of ECs. However, while EDL charging takes place in a short time-scale of micro to milliseconds, hydrogen pseudocapacitance requires slightly longer time because of diffusion limitation typical for faradic reactions.

Hydrogen electrosorption can be performed on AC cloth or powder. The most important parameters of the carbon material controlling hydrogen storage are, among others, the volume of micropores and the PSD, a contribution of mesopores, surface functional groups, electrical conductivity, and the number of surface defects. Experiments on carbons with a controlled hierarchical micro/mesoporosity [54, 158, 159] have shown that hydrogen capacity expressed in H wt% can be increased. Presence of mesopores is profitable as the place for water decomposition (reduction) whereas micropores are suitable for hydrogen sorption.

Fig. 25 presents CVs which have been obtained with a microporous AC cloth (ACC) electrode in 6 M KOH.[184] The various loops have been recorded with a stepwise shift of the negative potential cut-off. For electrode potentials higher than the onset of the thermodynamic value corresponding to water decomposition (*i.e.*, -0.924 V *versus* Hg/HgO, in 6 M KOH), the box-like shape of the curves confirms the reversible charging of the electrical double-layer. The increase of negative current which is observed from the third loop, that is, when the potential cut-off is lower than the equilibrium potential, indicates that the faradaic water decomposition starts gradually to take place according to *Eq. (11)*:

$$H_2O + e^- \rightarrow H + OH^- \tag{11}$$

The nascent hydrogen formed in *Eq. (11)* is partly fixed on the nanopores surface as in *Eq. (12)*:

$$\langle C \rangle + xH \rightarrow \langle CH_x \rangle \tag{12}$$

whereas another part may recombine to form H_2 molecules.

Eq. (13) summarizes the overall process:

$$\langle C \rangle + xH_2O + xe^- \rightarrow \langle CH_x \rangle + xOH^- \tag{13}$$

where $<C>$ and $<CH_x>$ stand for the carbon substrate and for hydrogen inserted into this substrate, respectively. As a consequence, during the anodic scan, the positive current recorded above the equilibrium potential increases, being related with the electro-oxidation of hydrogen trapped in ACC pores. During the oxidation step, the *Eq. (13)* runs in opposite direction.

When the negative potential cut-off decreases, the positive current due to hydrogen oxidation increases, and the corresponding hump shifts towards more positive potential values (**Fig. 25**). The high over-potential for hydrogen oxidation reveals either strong hydrogen trapping in the carbon material or severe diffusional limitations.

Taking into account that electrochemical hydrogen trapping takes place essentially in micropores smaller than 0.7-0.8 nm [54, 155, 156, 157] and that the tortuous pore network may slow down the desorption process from these pores, this may explain the improved tendency to reversibility at low scan rate. A careful analysis of the CVs at various scan rates supplies information on the reversibility but also supports the assumption of weak $<C>$-H chemical bonding. Weak chemical bonding of hydrogen has been also indicated by thermoprogrammed desorption (TPD) analysis on ACC obtained after hydrogen insertion by galvanostatic charge.[151]

Since hydrogen seems to be stabilized in the carbon substrate by weak chemical bonds, the self-discharge is not important.[157, 159] Moreover, the capacity of carbon electrode increases at enhanced temperatures because the amount of hydrogen stored increases and the desorption potential is decreased. Therefore, reversible hydrogen electrosorption in porous carbon electrodes in aqueous medium is attractive for the construction of asymmetric capacitors which associate a negative carbon electrode storing hydrogen and a positive electrode in the form of carbon or composite based on MnO_2 or a conducting polymer.[7, 144] Such supercapacitors in aqueous medium can operate with a good cycle life at voltage values as high as 1.6 V. It has also been

demonstrated that even better performance (1.6 - 2.0 V) can be reached with symmetrical AC/AC capacitors using alkali sulfates as electrolyte.[8, 185] Taking into account the high electrical conductivity of the positive carbon electrode compared to any MnO_2-based composite, this new concept represents a great advantage for high power applications.

4.6 Faradaic Reactions originated from the Electrolyte

The enhancement of capacitance by pseudocapacitive charge storage can be also achieved by the application of redox-active electrolytes instead of using the electrode material as a source of redox reactions. In this case, the electrolyte is the main source of capacitance because of various oxidation states of the electrolytic species (*e.g.*, iodine, bromine, hydroquinones).[164-166, 167, 168] Taking into account that the faradaic reactions proceed at the electrode/electrolyte interface, the selection of an optimized carbon material is important.

The electrochemical behavior of the carbon/iodide interface has been demonstrated to yield beneficial performance in supercapacitor application.[164] Efficient charge storage is based on the specific sorption of iodide ions as well as stable reversible redox reactions connected with various possible oxidation states of iodine from -1 to +5. The solutions based on iodide ions play a dual role, that is, they show a good ionic conductivity as well as undergo faradaic reactions. It is important to note that the domain of iodide ions in the Pourbaix diagram is moderately stable in the range of water stability with a possibility of various oxidation states depending on the applied potential and pH value.

The 1 M KI solution applied in the experiments has a neutral pH value close to 7. In such a case, the following reactions, especially from **Eq. (14a-d)**, could be considered as source of pseudofaradaic effects.

$$3I^- \leftrightarrow I_3^- + 2e^- \tag{14a}$$

$$2I^- \leftrightarrow I_2 + 2e^- \tag{14b}$$

$$2I_3^- \leftrightarrow 3I_2 + 2e^- \tag{14c}$$

$$I_2 + 6H_2O \leftrightarrow 2IO_3^- + 12H^+ + 10e^- \tag{14d}$$
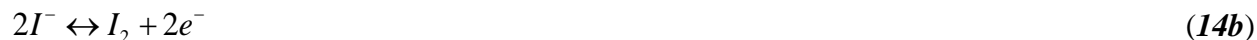
Iodine easily dissolves in the aqueous iodide solution forming the I_3^- complex. The potential range measured experimentally in the capacitor by CV and galvanostatic technique (**Fig. 26-27**) agrees with the thermodynamic values of the reactions presented before.[163] From both characteristics, it is well seen that this effect of iodide ions is observed for the positive electrode operating in a narrow range of potential and giving extremely high capacitance values exceeding 1840 F/g (estimated from integrated area of the voltammetry curve). As opposed to typical pseudocapacitive effects from electrode materials, for example oxides, which are often characterized by some diffusion limitations and observed only at moderate regimes, this two-electrode system can be loaded up to 50 A/g still supplying 125 F/g.

Very high capacitance values of the carbon/iodide interface have been proved during long-term cycling at a high current density of 1A/g and the cyclability is greatly affected by the type of metallic collector used for the cycling tests. In the case of gold collectors, a capacitive decrease of less than 20% was observed after 10000 cycles, whereas in the case of stainless steel, an increase occurs from 235 F/g during the first cycles up to 300 F/g after 10000 cycles. A shift of the operating potentials has been shown experimentally for both electrodes through additional

potential measurements after cycling and this process may explain this effect. The negative electrode with lower capacitance values operates in a more narrow range, while the operating potential range of the positive electrode, with high capacitance values, is extended to the negative direction.

The application of the carbon/iodide electrochemical system represents a new concept in supercapacitor development. This bi-functional iodide electrolyte, which ensures ionic conductivity and supplies pseudocapacitive effects, has advantages because it is inert, neutral in pH, and environmentally friendly. It gives an additional benefit concerning the choice of the current collectors and different metallic foils can be considered for this target but obviously stainless steel is the most suitable candidate.

Apart from iodides, interesting properties have been obtained when bromides are applied as electrolyte,[165] serving also as a source for pseudocapacitance. Among all halides, the iodide ions are the most environmentally friendly and because of its rich variety of oxidation states, iodine is probably the most suitable halide for this sort of energy storage.

In order to circumvent the disadvantage of low capacitance of the negative electrode in the halide-based systems, a new concept using two different electrolytes acting as conjugated redox couples has been developed.[167] Basically, the halide electrolyte is used for the positive electrode and another redox pair operates on the negative side (with a suitable separator between both electrodes).

Due to the high redox activity of vanadium-based aqueous electrolytes, these species were selected as candidates for pseudocapacitance source at the negative electrode. In the literature, a high activity of vanadium-based species is reported mainly in acidic solutions, which severely restrict their commercialization because of the prohibitive price of corrosion-resistant current

51

collectors (like gold or platinum). For this reason, neutral (pH = 7) aqueous electrolytes were applied, according to the pragmatic rule that supercapacitors will see growth only when the costs fall. Drawing on the experience of pure iodide-based electrolyte and the high redox activity of vanadium-based systems, 1 M potassium iodide (KI) has been applied as electrolyte for the positive electrode and 1 M vanadyl sulphate ($VOSO_4$) solution for the negative one (**Fig. 28,**).[187] Both electrolytes act as conjugated redox couples with AC electrodes ($S_{BET} \approx 2520$ m^2/g). In some cases, because of their mesoporosity and high electrical conductivity, CNTs (10 wt.%) have been added to improve the electrodes performance (**Fig. 29**). The two electrodes are soaked in the appropriate electrolytes and separated by a Nafion®-117 membrane, to avoid mixing of the electroactive electrolytic species. Comparable results were obtained by three different electrochemical techniques such as constant current charging/discharging, cyclic voltammetry and electrochemical impedance spectroscopy (EIS). The irregular shape of the galvanostatic charge/discharge dependence and well-defined peaks on the voltammetry curves, especially at slow scan rates, are indicative of pseudocapacitive phenomena. The improved performance when adding CNTs (**Fig. 29**) shows the importance of mesopores in the development of the interface between the redox species for both polarities of the system. Thus, high capacitance values (from 300 F/g to 1000 F/g depending on the current load) were obtained using AC + 10 wt% CNTs with two different electrolytic solutions separated by a Nafion® membrane. The two selected redox active electrolytes allow to reaching a high energy density, about 20 Wh/kg with a maximum power density of 2 kW/kg (calculated on the basis of the total mass of both electrodes).

A few papers describe also the effect of hydroquinone HQ dissolved in the electrolytic solution, being the source of pseudocapacitive effects.[166] It has been shown that OH functional groups in di-hydroxybenzenes as well as the pH-value of electrolytic solution have a significant effect on capacitive properties. Acidic medium seems to be optimal because of the proton source. Additive

of catechol, that is, 1,2-dihydroxybenzene (0.38 M) in 1 M sulfuric acid supplies moderate improvement of capacitance whereas the same amount of 1,4-dihydroxybenzene affects greatly the electrochemical performance (increase of capacitance from 123 F/g for pure acidic medium to 283 F/g with 1,4-dihydroxybenzene additive). It is assumed that grafting of the hydroquinone/quinone redox couple to carbon surface is at the origin of additional pseudocapacitance. Taking into account faradaic origin, these effects are certainly diffusion limited, hence, suitable micro/mesopores ratio of carbon is indispensable. The application of such redox active couple presents a new trend in capacitor development to increase the energy density.

5. High Voltage EDLCs

5.1 Electrolytes for high voltage EDLCs

Considering *Eq. (5)* and *Eq. (6)*, it is obvious that the enhancement of the operative voltage is the most effective way to increase both the energy and power of EDLCs. The operative voltage is normally limited by the electrochemical stability of the electrolyte. Therefore, the development of high performance EDLC cannot be realized without considering the electrolyte.

Commercially available EDLCs contain quaternary ammonium salts in PC or AN as electrolyte and generally operate up to 2.7 V - 2.8 V. AN-based electrolytes display higher conductivity and lower viscosity compared to the PC-based one. Therefore, EDLCs containing AN as solvent demonstrate normally higher power and better low temperature performance with respect to those containing PC. However, PC is less toxic and has a higher flash point than AN (AN was banned in Japan for many years because of safety concerns), and is usually considered as a safer electrolyte. In addition, the use of PC-based electrolytes allows the realization of devices having operative voltage slightly higher than that with AN.[76, 78, 91, 142, 186]

The possibility to increase the operative voltage of EDLC containing AN and PC-based electrolytes has been intensively investigated in the past years.[18, 187-189] These studies showed fundamental limitations to apply voltage beyond 3 V while maintaining stable performance when ACs are used in combination with the state-of-the-art electrolytes. In the case of AN, the electrolyte degradation seems to be the main obstacle for the increment of operative voltage, and the positive electrode seems to be the one that suffers the most in the case of such an increase.[76] In the case of PC, the formation of carbonates and the evolution of gaseous species (H_2 and CO_2) have been identified as the main reasons for the decrease of performance at high voltages.[76, 78, 142, 187] Considering this limitation, and with the aim to increase the operative voltage of EDLCs, several electrolytes have been proposed in the last years as alternative to the state-of-the-art. Generally, the alternative electrolytes proposed so far can be divided in two main categories: ionic liquids (ILs) and organic solvent based electrolytes (**Fig. 30**).

Ionic liquids generally include a bulky, unsymmetrical organic cation and a weakly coordinating inorganic/organic anion. The main advantages of ILs in organic solvents are the non-flammability, the negligible vapor pressure, the high chemical and thermal stability and hydrophobicity.[190] For these characteristics, ILs have attracted attention for use as "green" solvents and recently have been extensively investigated as electrolytes and/or electrolyte components in electrochemical devices.[191] The chemical-physical properties of ILs strongly depend on the water content present in these compounds.[192] Relatively small amounts of water can affect dramatically the conductivity, viscosity, electrochemical and chemical stability of ILs. For this reason, in order to be effectively used in EDLCs, ILs with water content lower than 10 - 20 ppm are needed, and hydrophobic ILs should be preferentially selected.[191, 193]

The use of IL electrolytes (often considered as solvent-free electrolytes) allows the realization of EDLC with operative voltage significantly higher than 3 V. So far, mainly two families of

(aprotic) IL have been considered, based respectively on the imidazolium cation [194, 195-198] and the pyrrolidinium cation.[131, 199, 200, 201-205] Since the chemical-physical properties, for example, ionic conductivity and viscosity, strongly depend on the ions present in these salts, it is not easy to make a general comment.[192] Nevertheless, considering the results so far reported, it is possible to assert that the imidazolium based-ILs normally display higher ionic conductivity and lower viscosity with respect to the pyrolidinium-based ones (see **Table 3**). On the other hand, the pyrolidinium-based ILs usually displays a larger electrochemical stability window than the imidazolium based-ones. EDLCs with imidazolium-based ILs operate up to 3.0 - 3.2V.[194, 195, 197, 198] while 3.5 - 3.7 V can be reached with the pyrrolidinium-based ILs.[198-200, 201-205] Consequently, the latter display a higher energy density compared to those containing imidazolium-based ILs, but a lower power density because of their lower ionic conductivity and higher viscosity. Due to the relatively high viscosity of these electrolytes and resulting high ESR of the ILs-based EDLCs, the power is often poor below room temperature. In order to overcome this limitation, mixtures of two different ILs have been proposed. This approach, which was already considered for the use of ILs in lithium-ion batteries,[206] leads to a solvent-free electrolyte with tunable properties. One important advantage related to the use of such mixtures is the possibility to lower the melting point of IL-based electrolytes,[195] and consequently to enlarge the operating temperature range of EDLCs. In a recent work, Lin *et al.* showed that the temperature range can be extended from -50 to 100 °C by using eutectic mixtures of ILs.[131] A second strategy becoming popular in lithium-ion batteries is based on the use of mixtures of IL and organic electrolyte.[193, 207] Frackowiak *et al.* (Ref. [208]) and later Lewandowski *et al.* (Ref. [197]) were the first to report the physical-chemical properties of several IL/organic electrolytes mixtures for EDLCs. Ruiz *et al.* studied a large number of mixtures and investigated their properties at different temperatures, showing that the ionic conductivity of these electrolytes is

much higher and the viscosity much lower than that of pure ILs.[205] Krause *et al.* demonstrated that a PC-PYR$_{14}$-TFSI mixture enables an operative voltage as high as 3.5 V with less than 5% capacitance loss after 100.000 cycles, resulting in high energy and high power density.[201]

In parallel, novel electrolytes containing organic solvents have been also investigated, either by implementing novel solvents, or by using solvent mixtures typically used in lithium-ion batteries. In the first case, Chiba *et al.* proposed the use of sulfone based electrolytes (*e.g.*, dimethylsulfone, DMSO), and showed that they enable an operative voltage higher than 3.0 V, along with high performance and high cycling stability.[188] Also, alkylated cyclic carbonates show a high electrochemical stability up to more than 3 V.[187] Adiponitrile (ADN) as a high flash point (163 °C) solvent has been proposed for EDLCs, demonstrating an operating voltage higher than as high 3.2 V at room temperature.[139, 209] The results of these study showed that the use of these alternative solvents make possible a significant increase of the operating voltage. Nevertheless, their moderate ionic conductivity and viscosity, especially at temperatures below room temperature, limit the power handling of such EDLCs. Lithium-ion battery (LIB) electrolytes have been also investigated in the last years for high voltage EDLCs.[210-212] They consist commonly of mixtures containing a high dielectric constant solvent (*e.g.*, ethylene carbonate, EC) and a low viscosity solvent (*e.g.*, dimethyl carbonate, DMC) in which a lithium salt (typically lithium hexafluorophosphate, LiPF$_6$) is dissolved. These mixtures display high ionic conductivity and rather large electrochemical stability, and when used in EDLCs allow operative voltages in the order of 3 V.[211] Nevertheless, they are very sensitive to moisture, and the presence of EC causes the formation of a passive layer (solid electrolyte interphase, SEI) on the carbon surface, limiting the EDLCs performance. Moreover, the flammability of the solvent and the limited chemical and thermal stability of LiPF$_6$ pose safety risks and reduce the operating temperature range.[191]

It is important to take into account that most of the ACs used in EDLC have not been developed for use in relative viscous electrolytes like those mentioned in the previous paragraph, and consequently they display non-optimized characteristics (*e.g.*, porous texture, wetting behavior). For this reason, a good matching between the intrinsic characteristics of the electrolyte and the carbonaceous materials needs to be considered for the development of high performance EDLCs. With this aim, carbon xerogel,[204] polypyrrole-derived AC,[213] microporous carbon,[202] CNTs and carbon onions[131] have been proposed as high affinity materials for ILs-based electrolyte. Another important aspect for the development of high voltage EDLCs is the electrodes mass balancing. When the electrochemical stability of the high voltage electrolytes is considered, one important aspect is the fact that the anodic and cathodic electrochemical stability limits are different; typically, the cathodic stability limit is higher than the anodic. When two electrodes of the same mass containing the same carbon are used, one of them may actually operate at a potential beyond the electrolyte stability limit, leading to a decreased cycle life of the EDLC. Such example is shown in **Fig. 31** (SYM $m_+/m_- = 1$) where, at voltage of 3.5 V, the potential of the positive electrode exceeds the anodic stability limit of the electrolyte. An improved utilization of the maximum electrochemical stability window can be accomplished *through* an asymmetric configuration [139, 204, 214] employing carbon electrodes with different masses, and the capacitance-voltage-relation can be expressed *via* **Eq. (15a-b)**:

$$C_{SP,+} \cdot m_+ \cdot \Delta U_+ = C_{SP,-} \cdot m_- \cdot \Delta U_- \qquad\qquad (15a)$$

$$\Delta U_+ + \Delta U_- = U_{max} \qquad\qquad (15b)$$

where ΔU_+ *and* ΔU_- is the working potential range of positive and negative electrodes, respectively. The sum of these two increments (**Eq. (15b)**) corresponds to the cell voltage (*i.e.*, the maximum width of the applied potential window U_{max}).[203, 210] Going back to the previous example in **Fig. 31**, the potential range ΔU_+ of the positive electrode must be reduced in order to

lower its maximum potential and to keeping it below the anodic stability limit of the electrolyte. This can be done by applying *Eq. (18)* and considering the different capacitance values of the two electrodes. **Fig. 31** shows an example of the influence of the electrode balancing on the performance of a high voltage ADN-based EDLC (U_{max} = 3.5 V).

In summary, for high voltage EDLCs with high performance three parameters appear crucial:

- electrolyte properties (ionic conductivity, viscosity, and electrochemical and chemical stability) to enable large U_{max}, low ESR and cycling stability;

- affinity (wetting) between carbon and electrolyte, in order to guarantee high capacitance and low ESR (which is a sensitive aspect for all EDLC systems);

- adjusting the mass ratio of the positively and negatively polarized electrode (balancing), in order to guarantee high cycling stability.

5.2 Lithium Ion Capacitors

In the last years, the demand of high energy, high power high cycling stability (in the order of several thousands of cycles) devices have increased consistently. Neither LIBs, nor EDLCs can satisfy these demands based on current technology.[91] Lithium ion batteries do not display a sufficiently long cycle life and have a limited power density, while EDLCs do not display sufficiently high energy density as required for many applications.[91, 215] A convenient strategy for the design of high voltage devices (*i.e.*, high power and energy density) is the creation of a hybrid system by combining a lithium-ion battery electrode with a supercapacitor electrode.[142, 216]

Among the hybrid devices proposed so far, the lithium-ion capacitor (LIC) is currently considered as one of the most interesting since it displays an operating voltage of about 3.8 - 4.0 V (**Fig. 32**), high energy (more than 20 Wh/kg) and cycle life in between those of LIBs and

58

EDLCs.[201, 215-225] LICs employ a combination of a graphite anode and a positive electrode composed of AC. During the charge-discharge of LICs, two processes simultaneously take place: Li^+ insertion/extraction at the graphite electrode and EDL formation/depletion on the porous AC electrode. As the negative electrode material does not contain any lithium initially, a key aspect is the pre-lithiation of the graphite anode. During this process, which takes place after the assembly and before cycling of the device, the graphite electrode is reduced in order to form the graphite intercalation compound and the Solid Electrolyte Intephase (SEI) on its surface - which is necessary for keeping a good stability of the material during further extraction/intercalation of lithium.[217, 219, 221-223, 225, 226] The initial amount of lithium intercalated into graphite affects the specific capacity, and the resulting specific energy of the LIC. The SEI formation is a prerequisite to efficient lithium intercalation-extraction during the charge-discharge process and it affects the cycle life of LICs.[217, 221, 222, 225] Usually, the anode is lithiated by using a sacrificial lithium electrode which simultaneously ensures a large source of lithium and does not alter the electrolyte composition.[216, 218, 220-224] However, it has the disadvantage to require metallic lithium, which might reduce the overall safety of the LIC (*e.g.*, because of thermal runaway) . Alternatively, pre-lithiation can be carried out by using the dissolved lithium salt as the lithium source.[215, 227] This approach has the advantage of removing the metallic lithium but complicates the electrolyte formulation. Since the lithium salt is acting partly as lithium source for the LIC, an unavoidable change (reduction) of lithium concentration occurs during the pre-lithiation that affects the physical-chemical characteristics (*e.g.*, ionic conductivity and viscosity) of the electrolyte.

Graphite is the most common anode material in LIBs, and for this reason has been also widely investigated for LICs. Graphite displays a Li intercalation potential between 0.2 and 0.1 V *versus* Li,[228] high capacity, and good cycling stability. Therefore, when used in combination with ACs,

it enables LICs with operating voltage as high as 4 V, high energy density, and good cycling stability.[218, 219, 221, 223, 224] The lithium ion loses its solvation shell through the SEI and it is fully desolvated before being intercalated into graphite.[223] The intercalation process into graphite is limited by lithium diffusion through the SEI; this limitation increases with the applied current density.[223] Therefore, the use of graphite, even if convenient, might limit the LICs performance during tests at high current densities. It is clear that the use of a material able to guarantee the same cell voltage as graphite with an improved behavior at high current density would be beneficial for high performance LICs.

With this aim, the use of hard carbon/stabilized lithium metal powder based anode has been proposed.[219] Very recently, soft carbon has been also considered for the realization of LIC.[222, 229] Although soft carbon has a higher initial irreversible capacity loss with respect to graphite, it has the advantage to better retain the capacity than graphite when high current densities are applied (**Fig. 33**). Moreover, it can display a higher capacity retention during prolonged cycling when compared to graphite, improving the performance of LIC during test at high current densities.[230]

ACs currently developed for EDLCs in non-aqueous electrolytes have been used in LIC, and no special development has been implemented for this kind of application. Recent work showed that some carbon blacks might display higher capacitance compared to AC, and for this reason it could be interesting for replacing ACs in LICs.[226] More recently, graphene has been also proposed as positive electrode material for LICs. However, even if the specific capacitance of this material is higher than that of ACs or carbon black, an effective introduction of graphene in LICs appear at the moment quite far.[225]

An important aspect related to the development of high performance LICs is the electrode mass balancing. In these devices, the two electrodes operate with two different mechanisms and they

60

display different capacities. Typically, the anode capacity is much larger than that of the positive electrode. While most of the anode capacity can be delivered in a rather small potential range (typically between 0 and 0.7 V *versus* Li/Li$^+$), the capacity of the AC is proportional to the potential excursion that the electrode is subjected to. Thus, for high voltage and high energy density LICs, it is very important to have an optimized electrode mass balancing which should consent the AC electrode to work in a wide potential window so that its capacity can be maximized, and the anode to work within a narrow potential range where its large capacity can be utilized. One of the main reasons for the loss of performance in LICs appears to be the shift of electrode (positive and negative) potential over cycles.[225] As soon as one of the two electrodes operates out of its optimal potential window the other electrode is affected as well. For example, as shown by Sivakkumar *et al.* [223], the self-discharge of the pre-lithiated graphite anode causes a shift of both electrodes towards higher potentials. The consequence of such a shift is a reduced capacity of both electrodes. The anode cannot operate in the potential range where most of the lithium is intercalated. At the same time, this shift forces the AC electrode to work at potentials where the electrolyte decomposition may occur.

As mentioned before, the SEI formed during pre-lithiation originates from the electrolyte decomposition. Moreover, the two different storage processes (chemical for the anode and physical for the positive electrode) occurring at the same during charge-discharge cycling imply different characteristics for the electrolyte. For these reasons, a careful selection of the electrolyte is necessary for the development of high performance LICs. Three aspects are of particular importance:

- high ionic conductivity and lithium mobility, necessary to guarantee high power;
- good film forming ability, necessary for the SEI formation;

- high overall electrochemical stability, necessary for the realization of high voltage devices.

So far, the electrolytes used in LICs were mainly LIBs electrolytes.[215, 216, 218-221, 223, 231] They were selected because of their high ionic conductivity, wide electrochemical stability window and ability for SEI formation (called film forming ability). However, because of their flammability and limited thermal stability, their use poses safety risks and might reduce the operative temperature range. Considering this point, the investigation of alternative electrolytes is important for high performance and safe LICs. Even so, a very limited number of studies considered alternative and safer electrolyte for these devices. Recently, the use of PC-based electrolytes [219] as well as the use methacrylate-based gel polymer electrolytes[232] has been proposed with the aim to improve the safety of soft-carbon based LICs. Nevertheless, a detailed investigation of alternative electrolytes is certainly necessary. New solvents (*e.g.*, based on IL) for lithium salts, or new types of electrolytes (*e.g.*, gel-polymer electrolytes or polymeric ionic liquids) may be developed, and their advantages and limits need to be understood and evaluated.

6. Conclusions

This review demonstrates that carbon is by far the best material for supercapacitor electrodes and this choice is independent of the kind of electrolyte and construction. Carbon is a highly versatile material, existing in almost infinite varieties of structures / textures and with adaptable morphology; additionally, the high electrical conductivity and low cost of carbon are determining criteria which make it the champion for supercapacitor application.

A lot of progress has been accomplished in understanding and optimizing the properties of carbon/carbon electrochemical capacitors within the last 10 years, allowing to designing materials capable to significantly enhance the energy density and / or power density, especially taking into account the industrial requirements for optimizing these parameters on a volumetric basis. It has been clearly established that developing the specific surface area of carbons is no longer the best solution to enhance the capacitance, particularly because the density of materials decreases and low volumetric performance is obtained. However, the capacitance can be optimized when the pore size of carbons fits with the size of desolvated/distorted ions from the electrolyte (or the bare ion in the case of ionic liquids). In other words, the materials should have essentially micropores in the range of around 1 nm for ion storage, but also some mesopores for optimized ion transportation within the carbon particles. There are now computational models and experimental works, for example, by nuclear magnetic resonance, demonstrating that the porosity of carbons in discharged capacitors is completely filled with ions and solvent molecules. When the capacitor is charged, there are only small movements of ions within the pores, with an increase of the number of ions of opposite charge to the electrode polarity and a decrease of the number of solvent molecules. Optimized carbons with additional mesopores or exohedral carbons with only external surface, like carbon nanotubes and onion like carbons, are the best solution to achieve very high power performance.

While organic electrolytes are almost exclusively used by industry until now, because they offer a large voltage stability of up to 2.7 / 2.8 V, new electrolytes appear very promising. Until very recently, aqueous electrolytes were considered not suitable because of the presumably small usable voltage window. The reason was that only traditional battery electrolytes based on H_2SO_4 and KOH were implemented for AC/AC capacitors, demonstrating a maximum voltage of 0.7 − 0.8 V. This is no longer the case, since it has been demonstrated that, in alkali sulfate media,

hydrogen can be electrochemically stored in the AC negative electrode with a high overpotential, leading to voltages up to 1.6 – 2.0 V. Besides, in aqueous media, the capacitance can be enhanced by carbon/redox species interfaces, for example by adding iodides or quinones to the electrolyte. Similarly, grafting functional surface groups and molecules that are capable to undergo fast redox reactions to carbon can also provide pseudocapacitive contributions.

Over the last decade, room temperature ionic liquids (RTILs) proved to be the most promising electrolyte to enhance the voltage of supercapacitors to values higher than 3.0V. However, their relatively high viscosity and low ionic conductivity reduce, at the present, the power performance of supercapacitors. Solutions have been proposed to compensate for these shortcomings: when RTILs are mixed with limited amounts of a solvent, such as propylene carbonate or acetonitrile, they seem to keep a high voltage stability window. Besides, it has been also demonstrated that eutectic mixtures of ionic liquids may allow reaching low operational temperatures, down to -50°C. Yet, such mixtures require the use of essentially mesoporous carbons which are obviously not optimal for high volumetric performance. It means that still some optimization remains necessary to better adapt the compatibility of the RTIL/carbon couple.

Finally, in the last years, the family of electrochemical capacitors has been enriched by the hybrid systems, where only one of the electrodes is dominated by double-layer related energy storage. The most popular system is the lithium ion capacitor, made of a graphite (or other kinds of carbons) intercalation negative electrode and a positive electrical double-layer activated carbon electrode. Recent developments by industrial companies demonstrate that such systems can operate up to 3.7 V with a very high cycle life and excellent power performance that classifies them as a true electrochemical capacitor.

To summarize, extremely important progress has been accomplished in the recent years for understanding the mechanisms of carbon/carbon capacitor operation, but also for developing and

optimizing new materials, new electrolytes and new concepts. In most of these researches, enhancing the energy density was the main guideline. It must nevertheless be mentioned that the winner will never be the system with the highest energy density. There are other factors, such as cost, environmental issues, and kind of applications that have to be taken into account, meaning that there are niches for many propositions of materials and electrolyte developments. For these reasons, at the end of this review, we are confident that there is still plenty of room for a plethora of future research in the field of carbons and electrolytes for electrochemical capacitors.

Table 1. Sizes (in nm) of solvated and desolvated TEA and BF_4-ions [233].

	TEA^+	BF_4^-
Solvated in AN	1.30	1.16
Solvated in PC	1.35	1.40
Desolvated	0.67	0.48

Table 2. Physicochemical and electrochemical characteristics of the nitrogen rich nanocomposites. C_{sp} stands for the capacitance estimated at 5 A/g current load, that is, 50 mA/cm^2. Two-electrode cell in 1 M H_2SO_4.[154]

Sample	S_{BET} (m^2/g)	V_{total} (cm^3/g)	V_{micro} (cm^3/g)	C_{sp} (F/g)	Nitrogen content (wt.%)
M+F*	329	0.162	0.152	4	21.7
Nt+3M+F*	403	0.291	0.174	100	14.0
Nt+2M+F*	393	0.321	0.167	126	11.7
Nt+M+F*	381	0.424	0.156	83	7.4

* M+F (composite from melamine and formaldehyde without carbon nanotubes), Nt+M+F (composite with carbon nanotubes, melamine and formaldehyde), Nt+2M+F (similar composite with twofold melamine proportion in the blend), and Nt+3M+F (threefold melamine proportion).

Table 3. Ionic conductivity and viscosity of some electrolytes for high voltage EDLCs at 20 °C.

AN (acetonitrile), **PC** (propylene carbonate), **TEA-BF$_4$** (tetraethylammonium tetrafluoroborate), **EiPS** (ethyl isopropyl sulfone), **2,3 BC** (2,3-butylene carbonate), **ADN** (adiponitrile), EC (ethylene carbonate), DMC (dimethyl carbonate), LiPF$_6$ (lithium hexafluorophosphate), **EMIM-PF$_6$** (1-ethyl-3-methylimidazolium hexafluorophosphate), **EMIM-BF$_4$** (1-ethyl-3-methylimidazolium tetrafluoroborate), **EMIM-TFSI** (1-ethyl-3-methylimidazolium bis(trifluoromethanesulfonyl)imide), **EMIM-FSI** (1-ethyl-3-methyl imidazolium bis(fluorosulfonyl)imide), **PYR$_{14}$-TFSI** (N-butyl-Nmethylpyrrolidinium bis(trifluoromethanesulfonyl)imide), **PYR$_{1(201)}$-TFSI** (N-methoxyethyl-N-methylpyrrolidinium bis(trifuoromethanesulfonyl)imide), **PYR$_{14}$-FSI** (N-butyl-N-methylpyrrolidinium bis(fluorosulfonyl)imide), **PIP$_{13}$-FSI** (N-methyl-N-propylpiperidinium bis(fluorosulfonyl)imide), **n.a.** (not available), [*] from BASF website (52012BF-9822_US_SelectilyteLP_Datasheet-051512)

Electrolyte	Reference	Conductivity (mS/cm)	Viscosity (mPa·s)
Organic solvents			
Conventional			
AN-TEA-BF$_4$	[139]	55.0	0.6
PC-TEA-BF$_4$	[201]	13.0	2.6
Alternative Organic			
EiPS	[187]	n.a.	5.6
2.3 BC	[187]	n.a.	2.8
ADN-0.7M TEA-BF$_4$	[139]	4.3	6.6
Lithium-ion batteries			
EC-DMC (3:7) 1M Li-PF$_6$ [*]		11.8	2.7
Ionic Liquids			
Solvent-free			
EMIM-PF$_6$	[205]	10	18.0
EMIM-BF$_4$	[197]	12	34.0
EMIM-TFSI	[196]	8.4	28.0
EMIM-FS	[196]	15.5	17.9
PYR$_{14}$-TFSI	[201]	2.6	62.0
PYR$_{1(201)}$ -TFSI	[199]	3.8	57.0
PYR$_{14}$FSI-PIP$_{13}$FSI	[131]	4.9	n.a.
ILs co-solvents			
PC-PYR$_{14}$-TFSI (1:1 wt%.)	[201]	10.3	5.6
AN-PYR$_{14}$-TFSI (1:1 wt.%)	[205]	57	n.a.
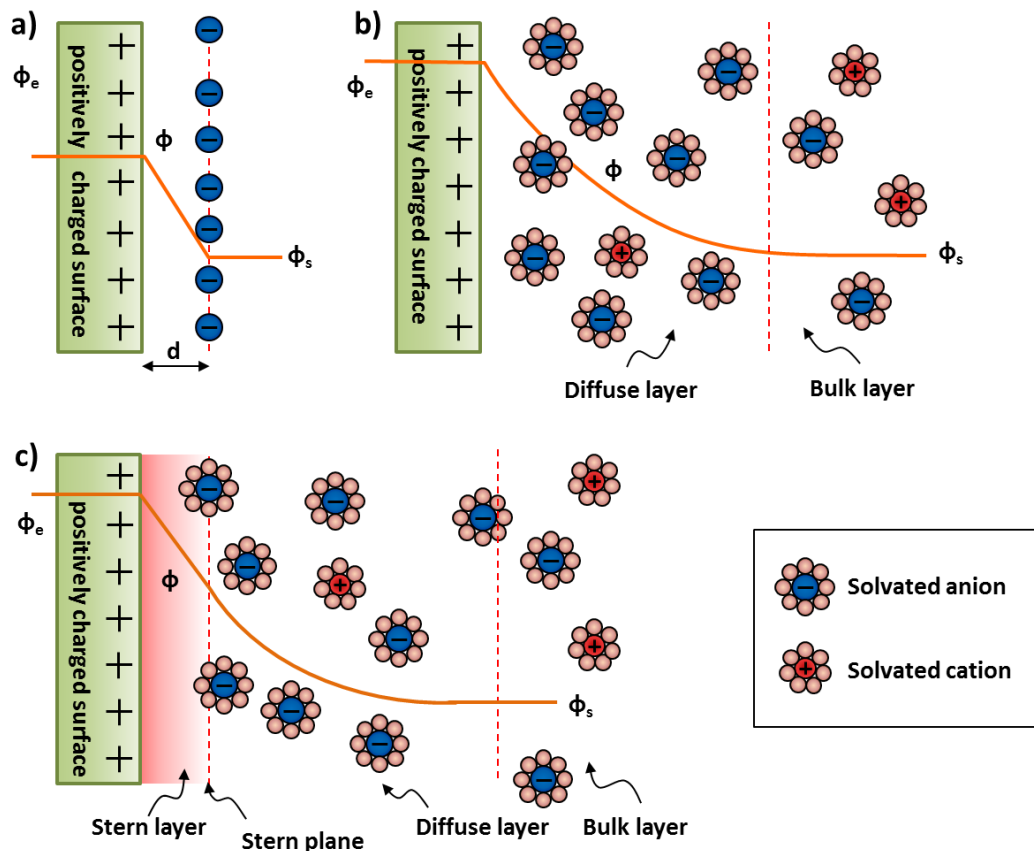
Fig. 1. (**a**) Helmholtz, (**b**) Gouy-Chapman, and (**c**) Stern model of the electrical double-layer formed at a positively charged electrode in an aqueous electrolyte. The electrical potential, φ, decreases when transitioning from the electrode, φ_e, to the bulk electrolyte infinite away from the electrode surface, φ_s. The Stern plane marks the distance of closest approach of the ions to the charged surface. Note the absence of charges / ions in the Stern layer. The diffuse layer starts in the range of $10 - 100$ nm from the electrode surface.
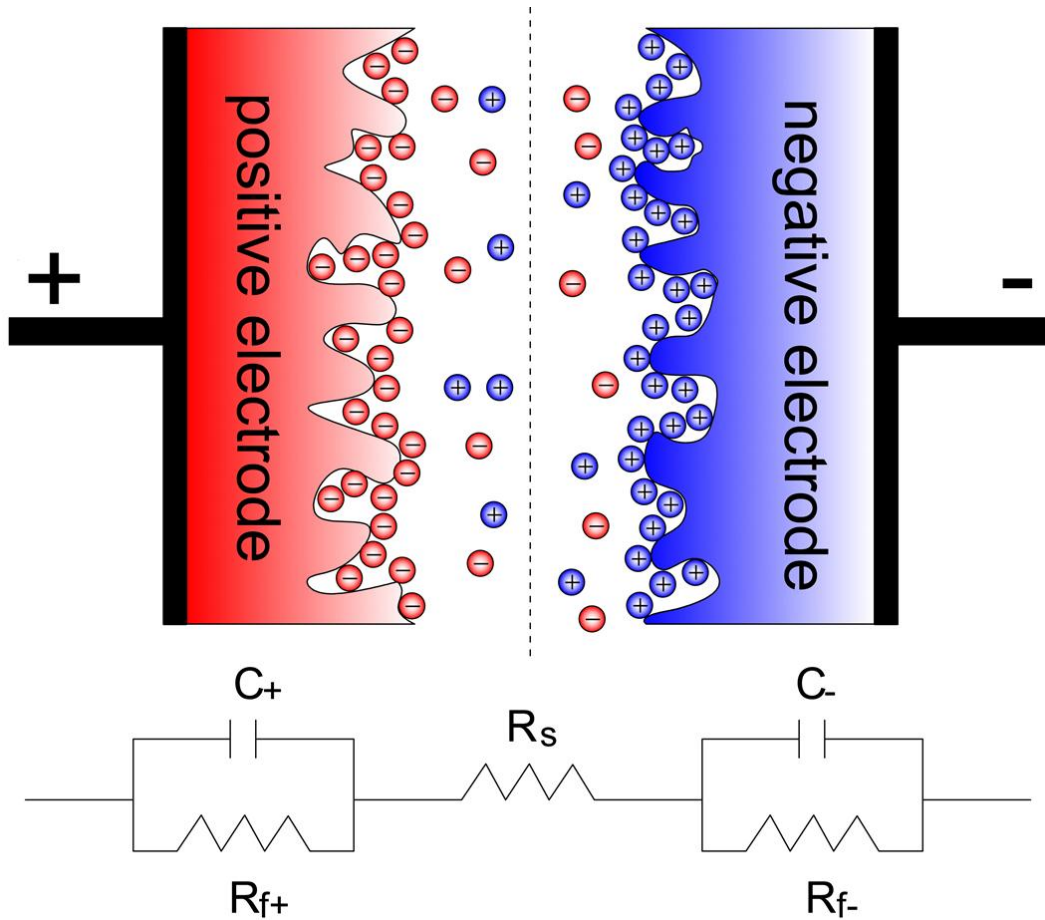
Fig. 2 : Representation of the charged state of a symmetric electrical double-layer capacitor using porous electrodes and of the corresponding equivalent circuit (adapted from Ref. [16]). R denotes resistors, C denotes capacitors.
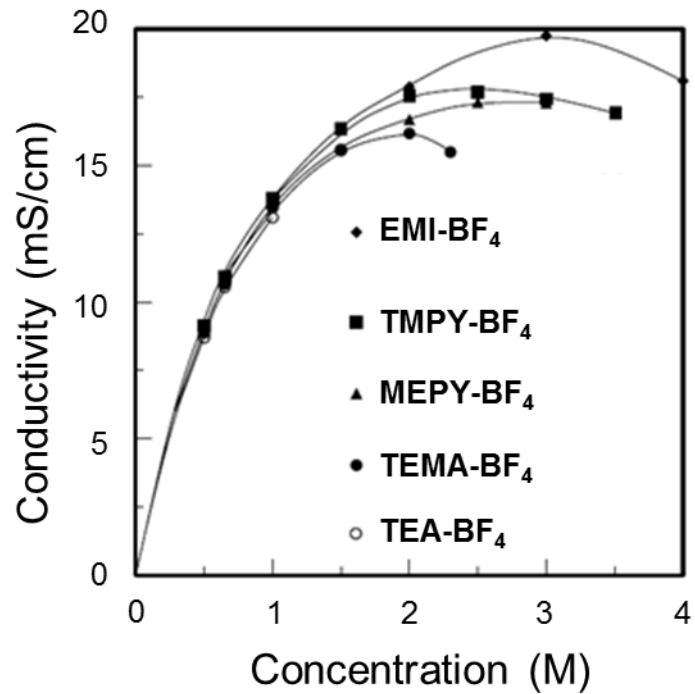
Fig. 3 : Conductivity *versus* concentration of quaternary ammonium salts in propylene carbonate (PC) at 25 °C (adapted from Ref. [16]). EMI-BF$_4$: 1-ethyl-3-methylimidazolium tetrafluoroborate; TMPY-BF$_4$: tetramethylene-pyrrolidinium tetrafluoroborate; MEPY-BF$_4$: 1-ethyl-1-methylpyrrolidinium tetrafluoroborate; TEMA-BF$_4$: triethylmethylpyrrolidinium tetrafluoroborate; TEA-BF$_4$: tetraethylammonium tetrafluoroborate.
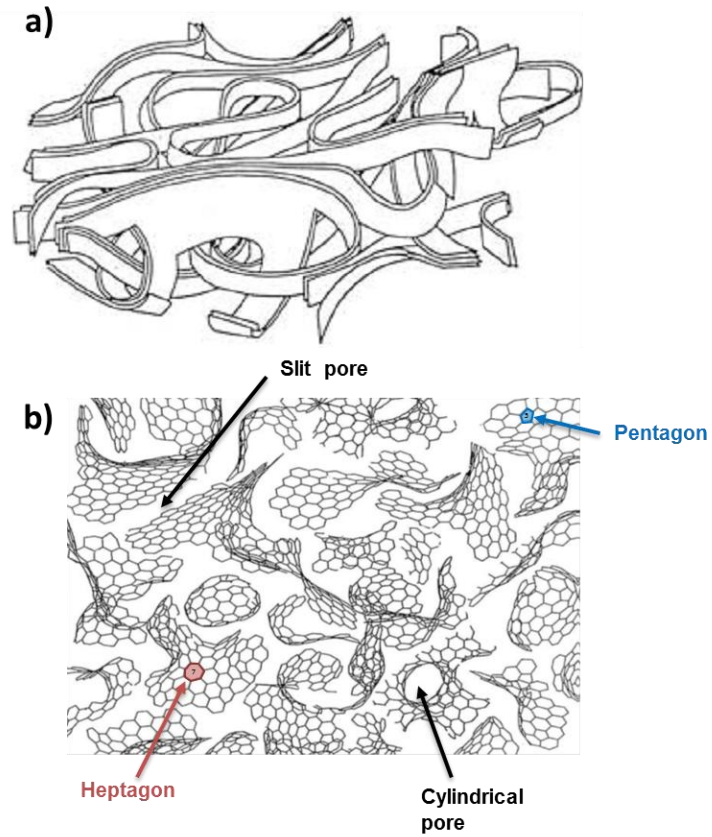
Fig. 4 : (**a**) Nanotextural model of a non-graphitizable carbon from PVDC according to Ban *et al*. [36]. (**b**) Schematic nanotextural and structural model of a non-graphitizable carbon showing fullerene-like elements. The arrows show pentagonal and heptagonal defects in the graphene structure.[38]
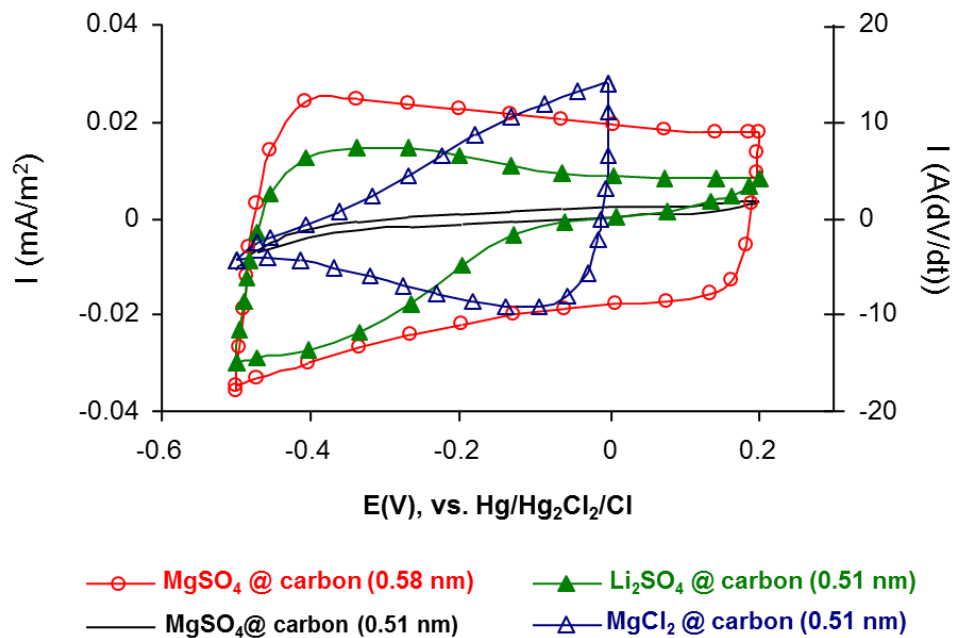
Fig. 5: Voltammograms of activated carbon electrodes with average pore size of 0.58 nm and 0.51 nm obtained in 0.1 M $MgSO_4$ solution. For comparison, curves are also given for pores of 0.51 nm in 0.1 M Li_2SO_4 and $MgCl_2$ solutions. The current is normalized per unit of BET SSA (adapted from Ref. [49]).
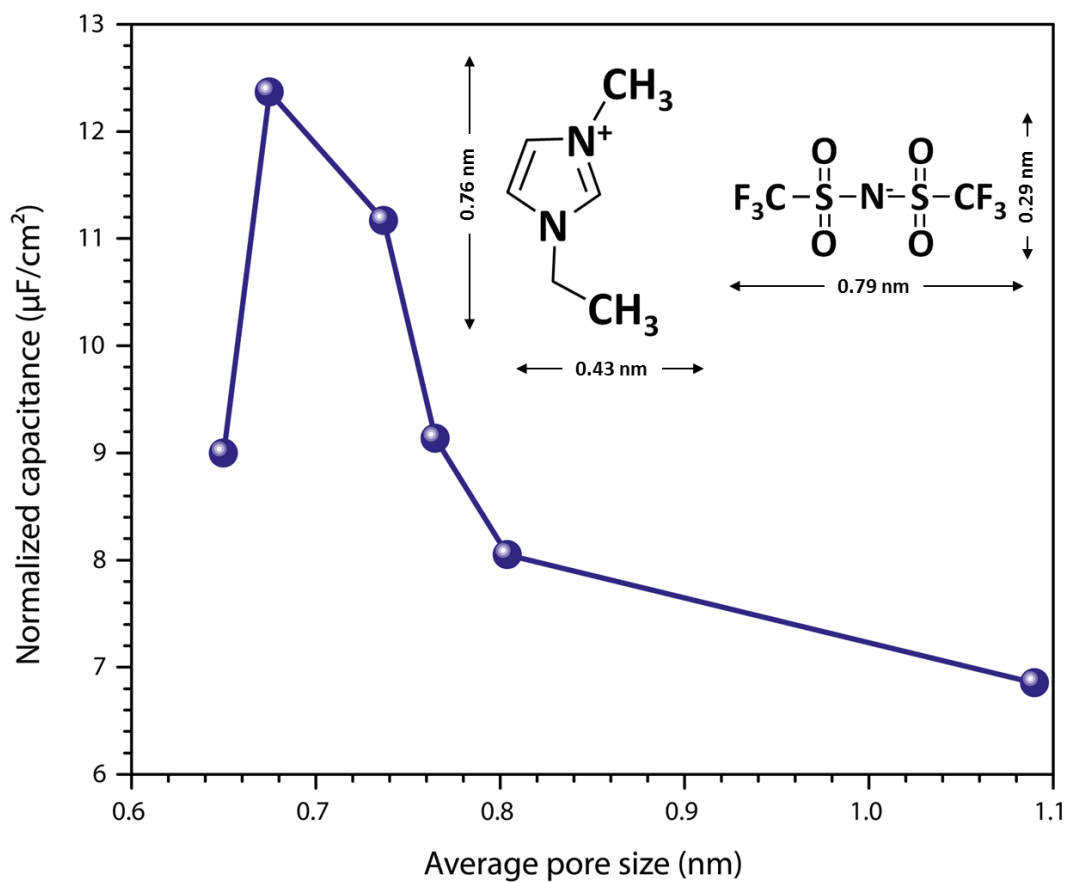
Fig. 6: Normalized capacitance (gravimetric capacitance divided by S_{BET}) *versus* average pore size of a series of carbide derived carbons, and models of the structure of EMI and TFSI ions (adapted from Ref. [53]).
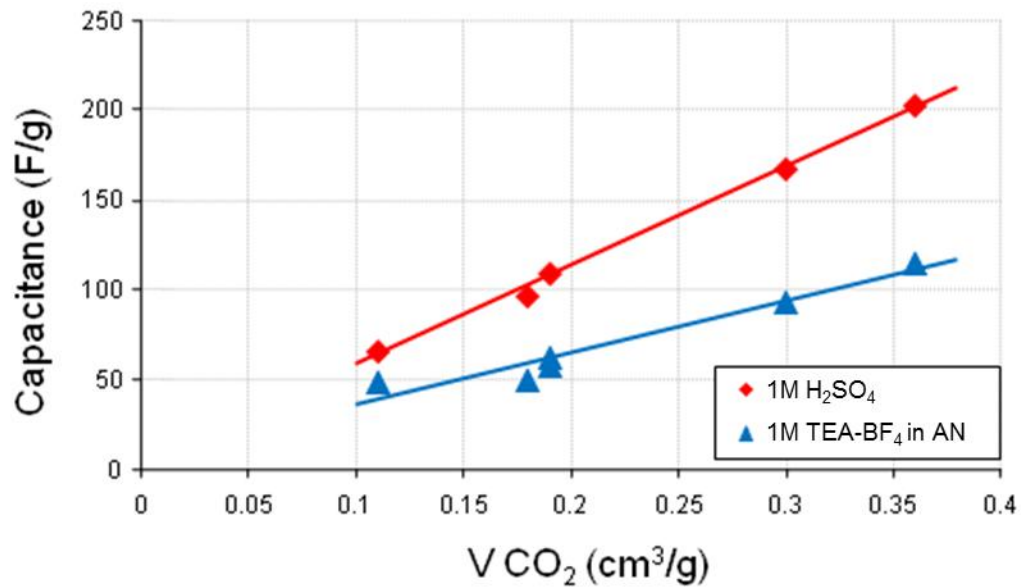
Fig. 7: Capacitance in two electrolytic media *versus* the volume of micropores smaller than 0.7 - 0.8 nm for various templated carbons (adapted from Ref. [54]).
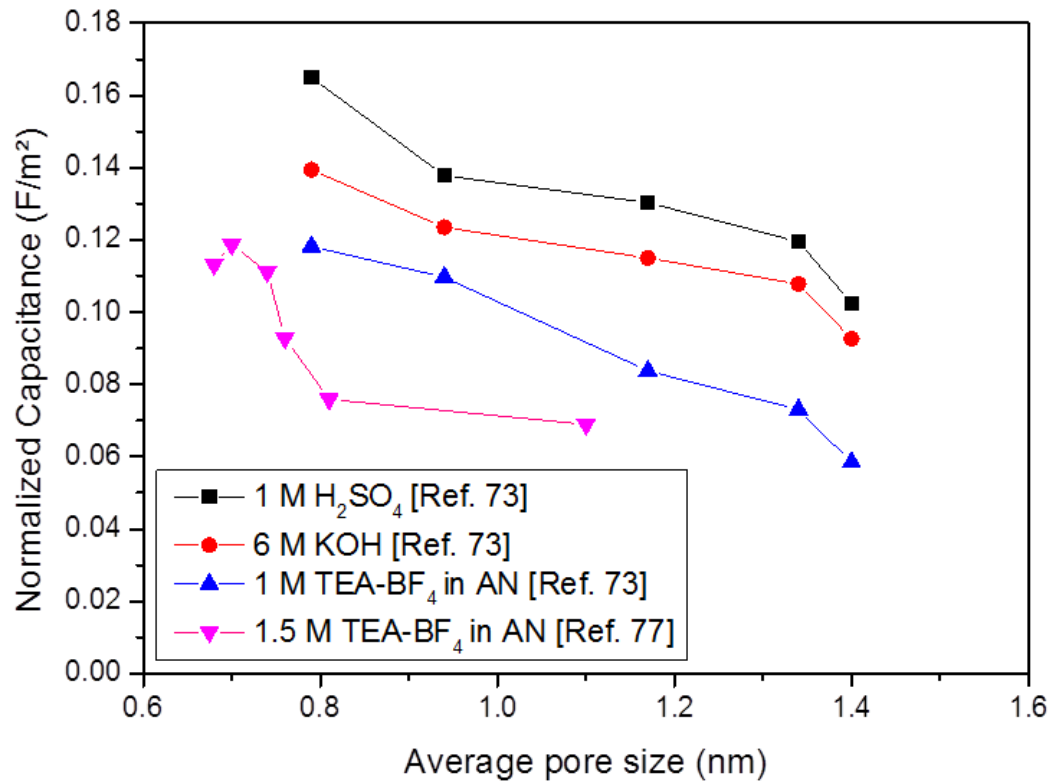
Fig. 8: Capacitance normalized to S_{BET} *versus* the average pore size (data adapted from Ref. [55, 60]).
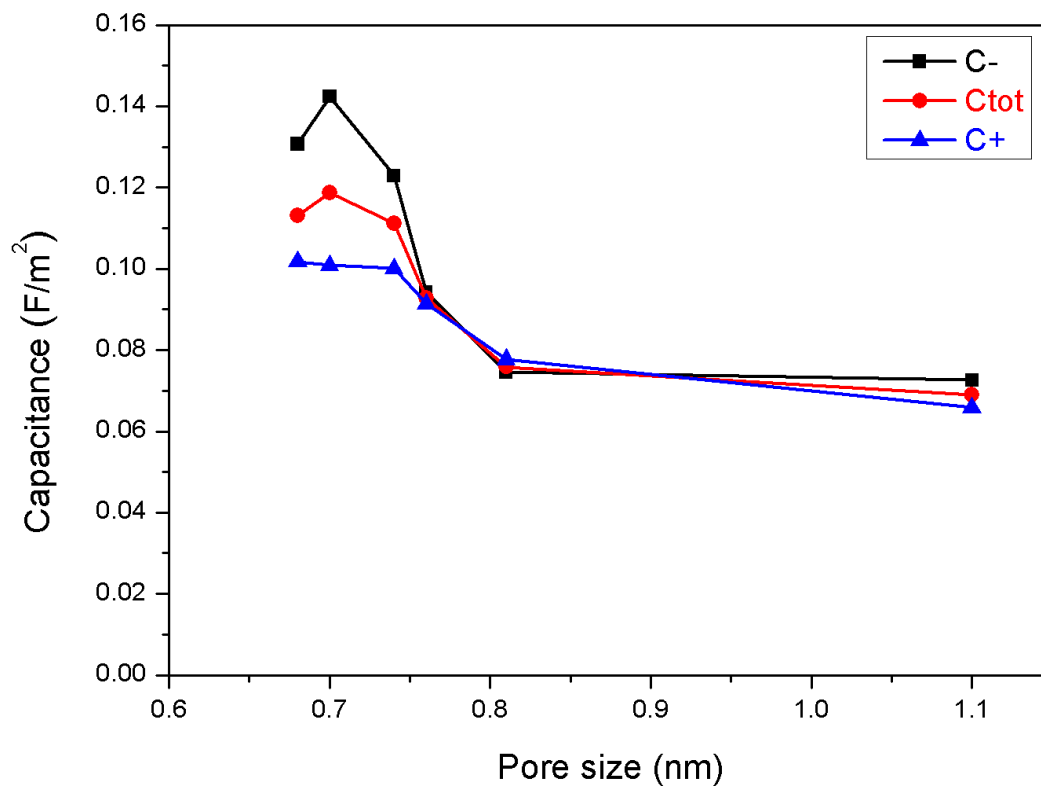
Fig. 9: Specific capacitance calculated from a constant current discharge of 5 mA/cm^2 for the electrodes (C_- and C_+) and for the system (C_{total}) *versus* the average pore size of the carbons in 1.5 TEA-BF$_4$ in AN (adapted from Ref. [60]).
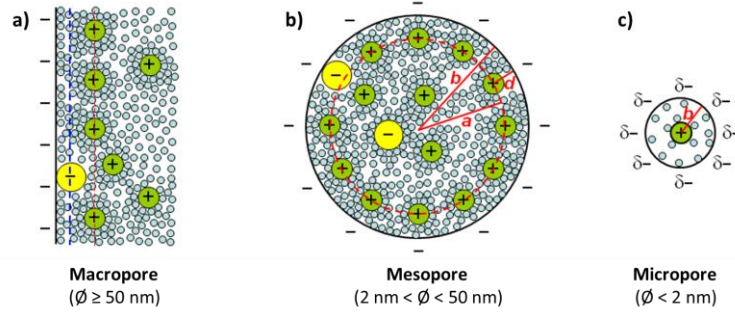
Fig. 10: Models of ions electrosorption in the different kinds of pores: (**a**) macropore; (**b**) negatively charged mesopore with cations approaching the pore wall to form an electrical double-cylinder capacitor with radii b and a for the outer and inner cylinders, respectively, separated by a distance d; (**c**) negatively charged micropore of radius b with solvated cations of radius a_0 lining up to form an electrical wire-in-cylinder capacitor (from Ref. [69]).
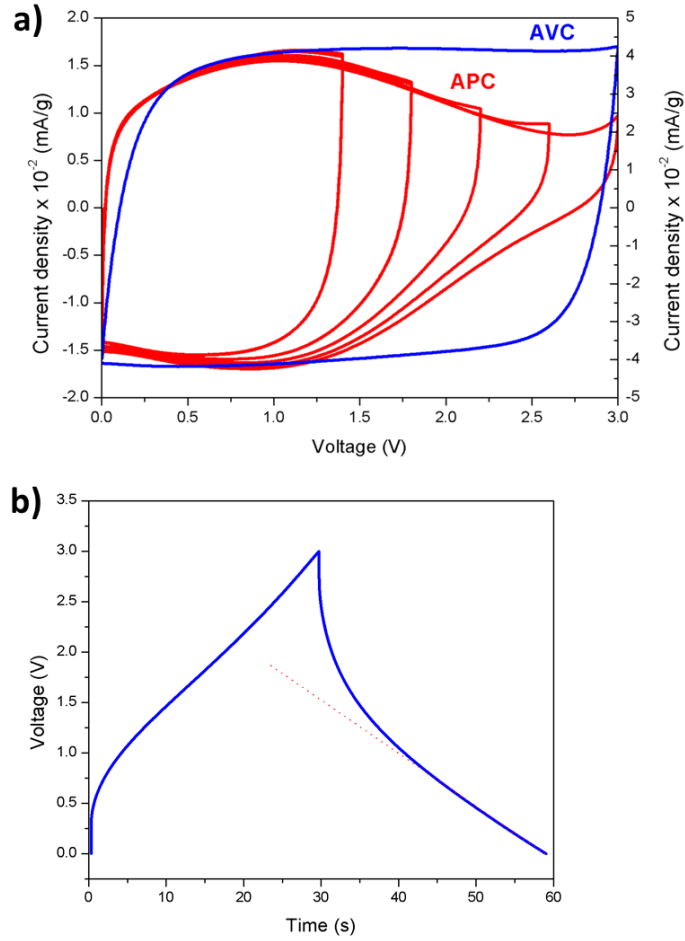
Fig. 11: (**a**) Cyclic voltammograms for EDLCs based on APC carbon (left-hand side *y*-axis for current) and AVC carbon (right-hand side *y*-axis for current); (**b**) Galvanostatic charge-discharge of the EDL capacitor based on the microporous carbon APC at a current density of 960 mA/g. The straight part of the discharging line is extrapolated in order to discriminate the point of porosity saturation (adapted from Ref. [70]).
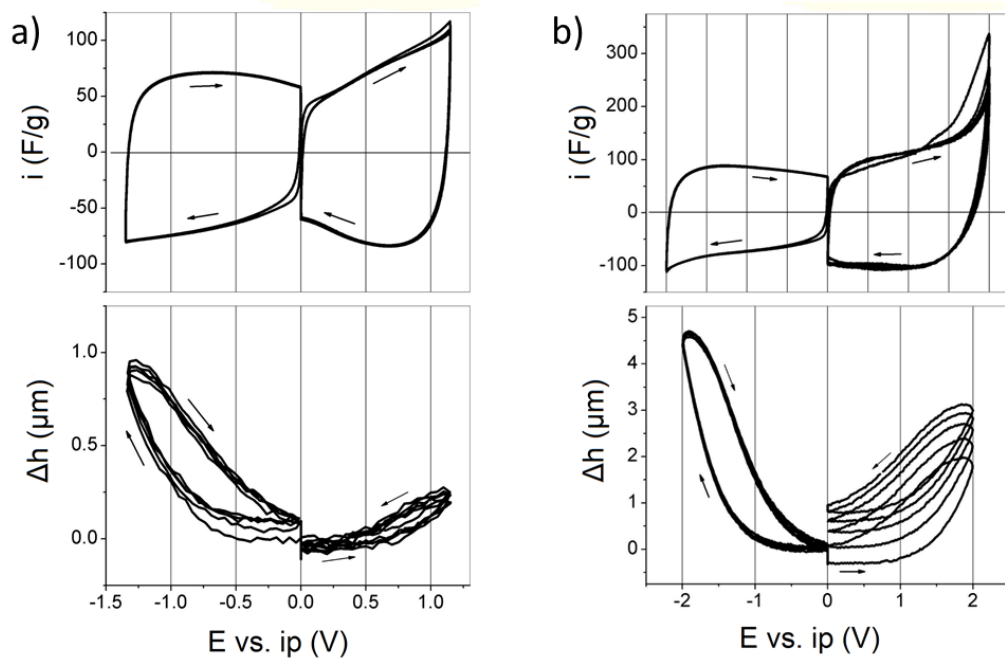
Fig. 12: Three-electrode voltammograms obtained for different potential ranges (top) and simultaneous measurement of the expansion of each electrode (bottom; all adapted from Ref. [73]).

(**a**) negative electrode from 0 to -1.35 V *versus* ip, positive electrode from 0 to 1.15 V *versus* ip.

(**b**) negative electrode from 0 to -2 V *versus* ip, positive electrode from 0 to 2 V *versus* ip.
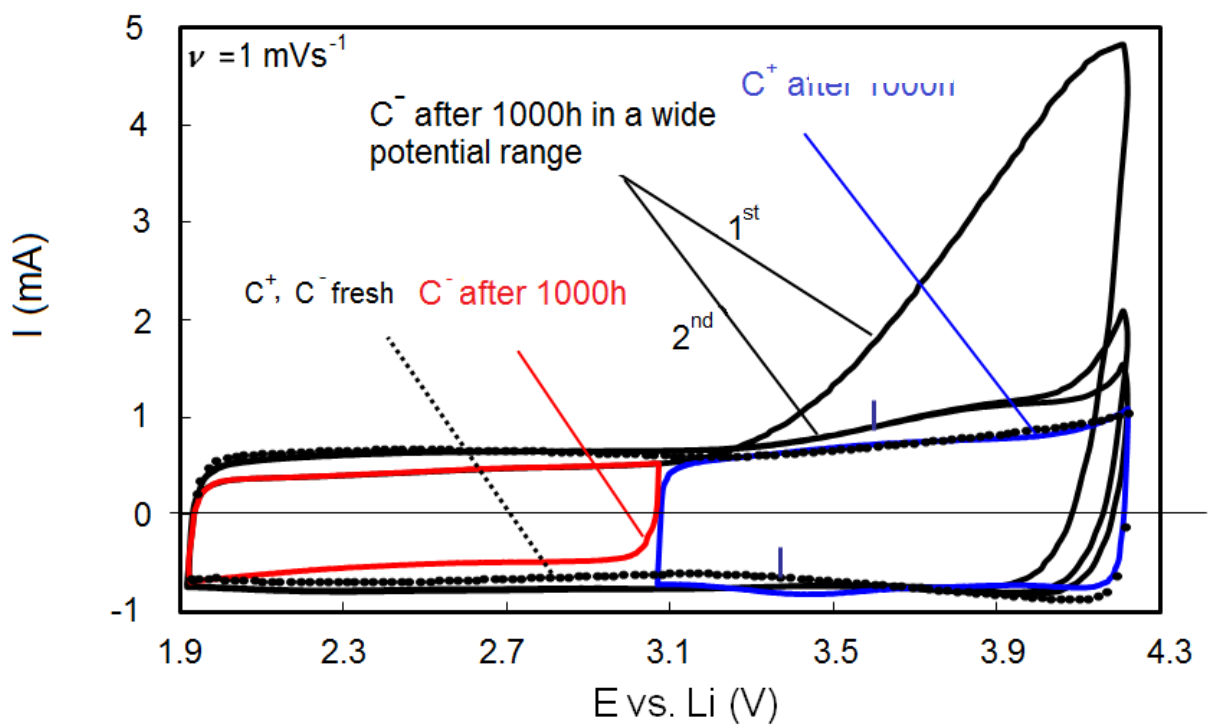
Fig. 13: Cyclic voltammograms (1 mV/s) in 1 M TEA-BF$_4$/AN of each electrode of a symmetric cell before and after 1000 hours floating at 50 °C (adapted from Ref. [74]).
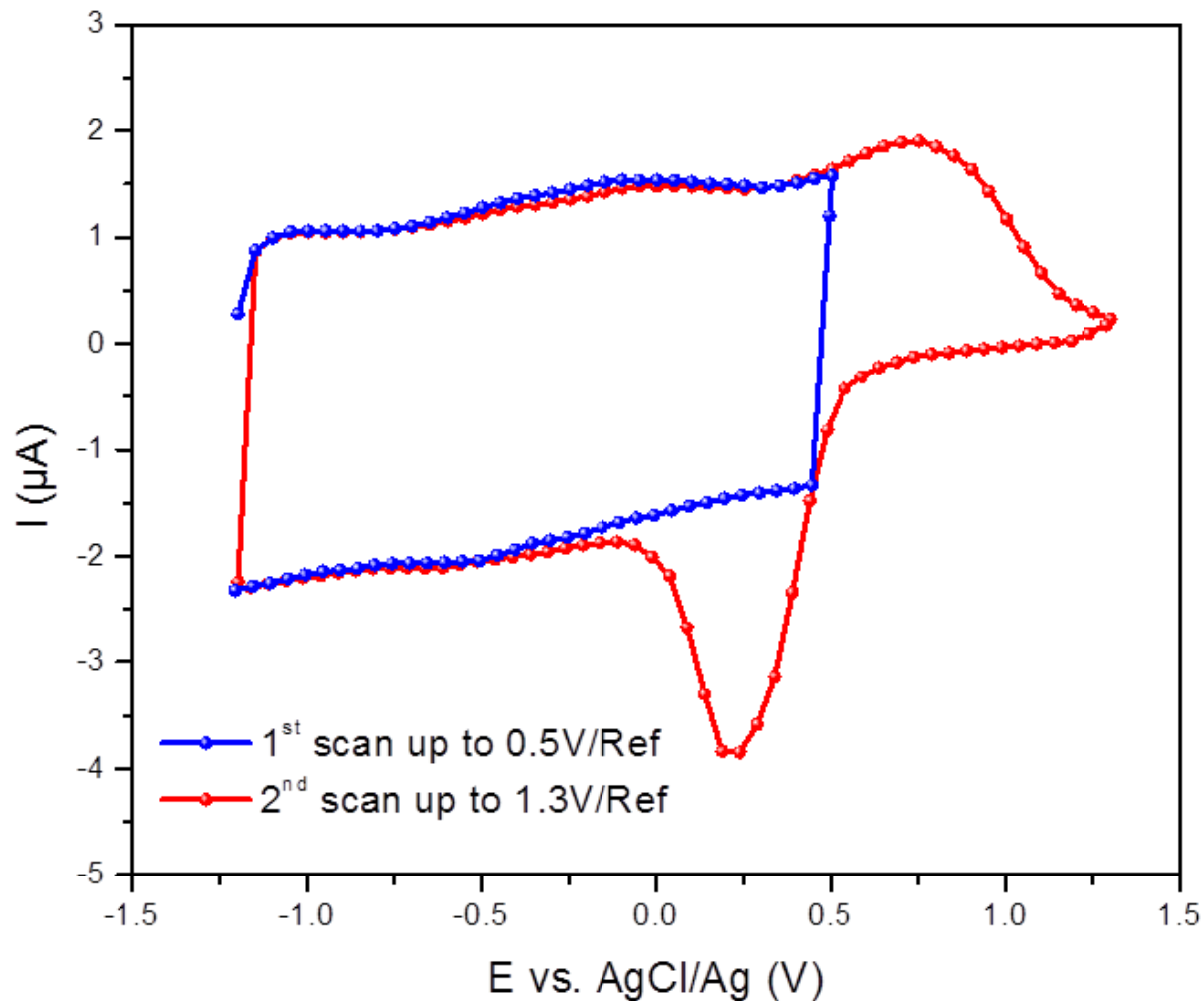
Fig. 14: Three-electrode voltammograms of a CDC with 0.68 nm average pore size in 2 M EMI-TFSI/AN at 10 mV/s: first scan (blue curve) from -1.2 V up to 0.5 V *versus* Ag reference potential range and second scan (red curve) from -1.2 V *versus* Ag reference up to 1.3 V *versus* Ag reference potential range (from Ref. [79]).
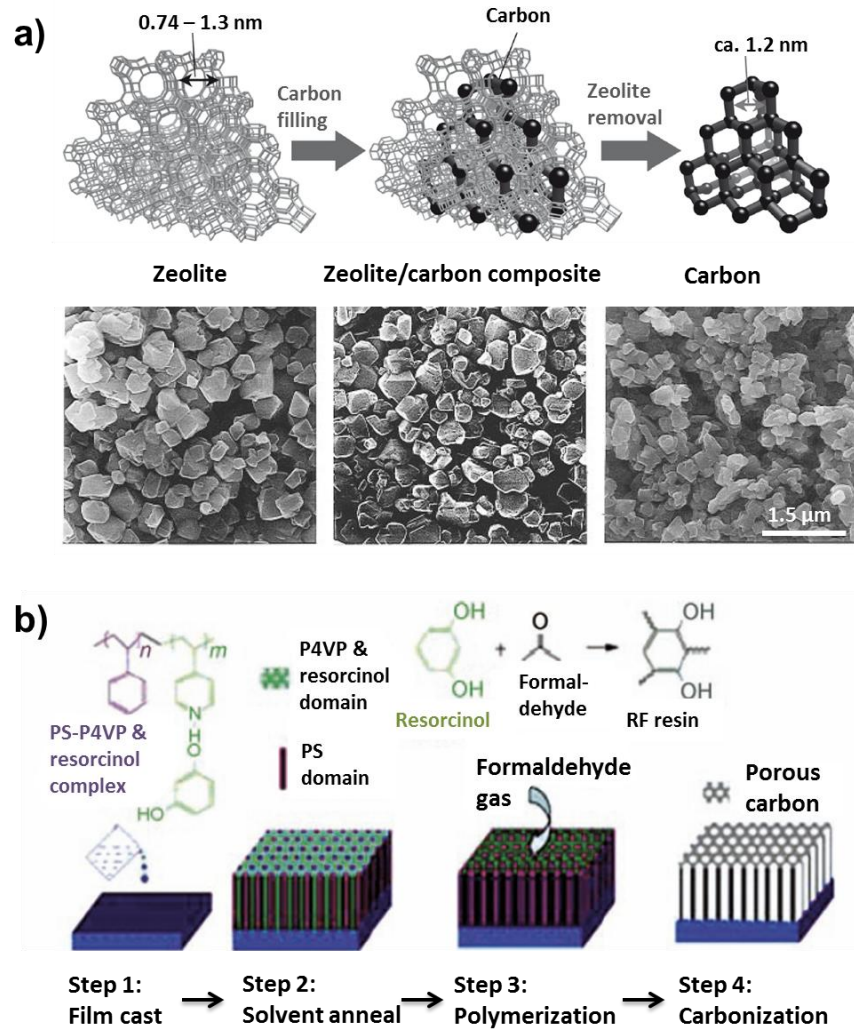
Fig. 15: Schematic drawing of templating processes and resulting carbon particles: (**a**) Zeolite-templated carbons (ZTC) - modified after Ref. [234]; (**b**) Soft-templated, ordered mesoporous carbon (Ref. [235])
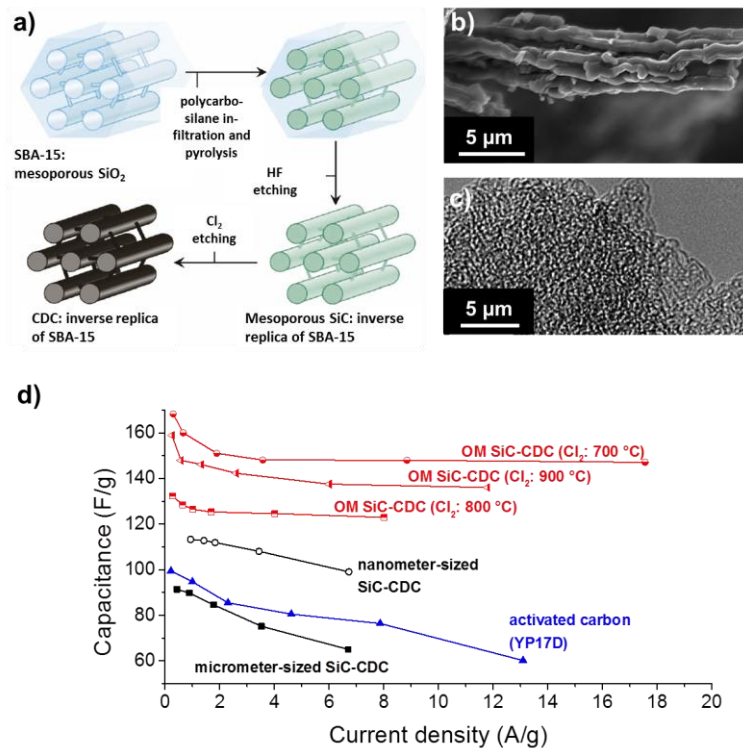
Fig. 16: (**a**) Schematic synthesis of ordered mesoporous (OM) carbide-derived carbon (CDC) employing SBA-15 hard templating of mesoporous SiC and subsequent chlorination (*i.e.*, removal of silicon). (**b-c**) Electron micrographs (b: SEM; c: TEM) of OM-CDC obtained from OM-SiC. (**d**) Power handling ability and specific capacitance of OM-CDC in comparison with conventional activated carbon AC (YP17D) and conventional micro- and nanoparticulate CDC tested in 1 M TEA-BF$_4$/AN. (**a-c**: from Ref. [67]; **d**: data extracted from Ref. [67])
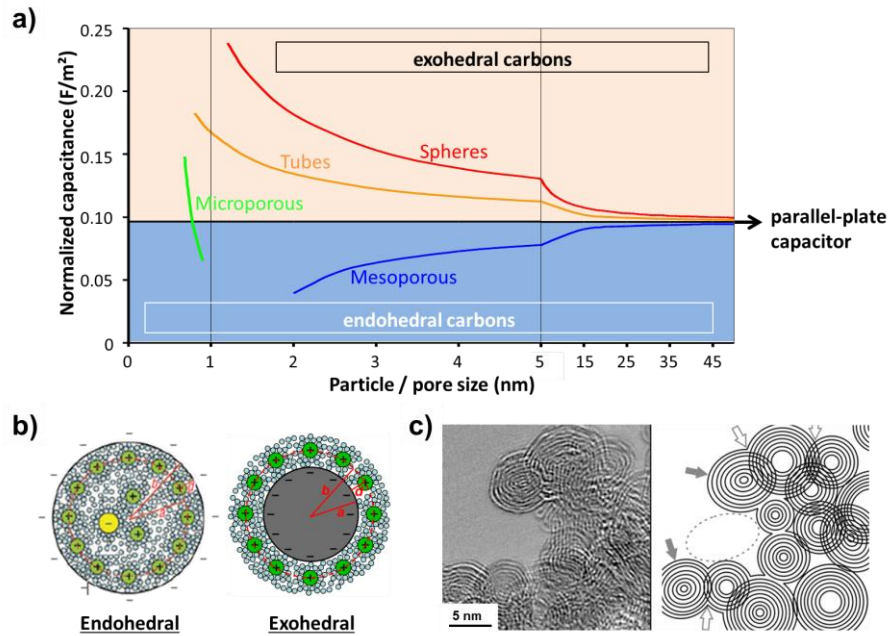
Fig. 17: (**a**) Normalized capacitance *versus* particle / pore size comparing endohedral (*i.e.*, carbons with an internal porosity and negative pore surface curvature) with exohedral carbons (*i.e.*, external, positively curved surfaces). (**b**) Schematic concept of electrical double-layer (DL) formation in micro- and mesopores and for exohedral carbons. (**c**) Transmission electron microscopy (TEM) image and schematic drawing of carbon onion films exhibiting positive (grey arrows) and negative (white arrows) surface curvature. (from Ref. [109])
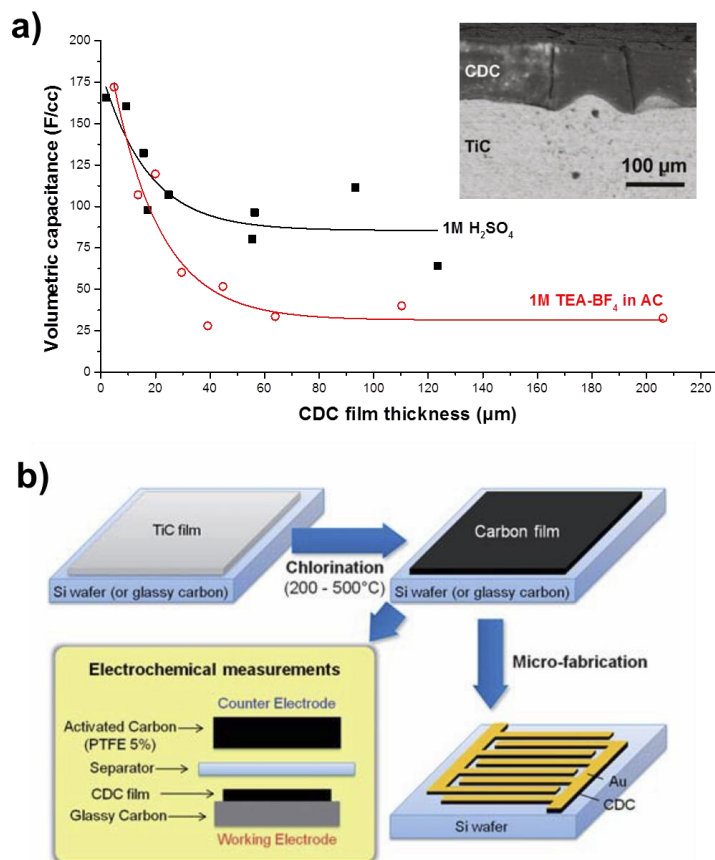
Fig. 18: (**a**) Rate performance and capacitance fade as a function of the thickness of a carbide-derived carbon (CDC) thin film (1 M TEA-BF$_4$/AN and 1 M H$_2$SO$_4$; data from Ref. [124]). The inset shows an approximately 100 μm thick CDC film in a scanning electron microscopy (SEM) cross-section. (**b**) Schematic drawing of patterned TiC-CDC thin film supercapacitors (from Ref. [126]).
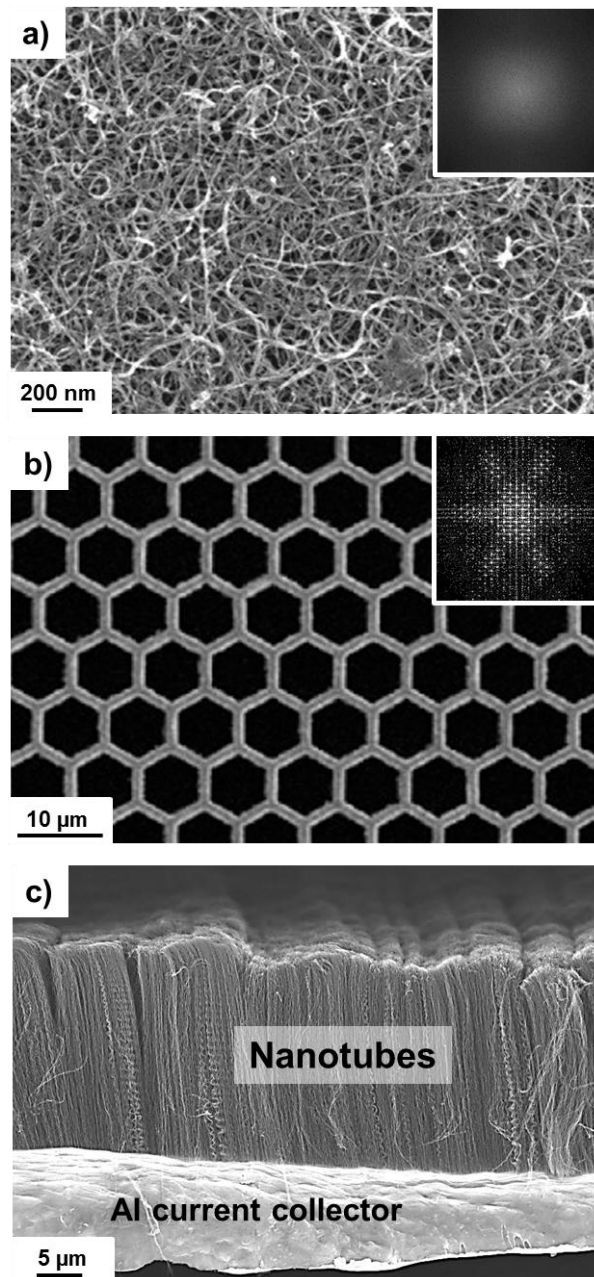
Fig. 19:   (**a**) Scanning electron microscopy (SEM) image of a CNT film obtained by electrophoretic deposition of multi-wall carbon nanotubes (MWCNT; from Ref. [236]); the inset shows a Fourier Transform (FT) of the CNT orientation and documents the random alignment. (**b**) SEM image of a CNT film (from Ref. [130]) with a high level of pattern periodicity (see FT inset). (**c**) SEM image of a vertically aligned CNT film grown on an Al current (from Ref. [131]).
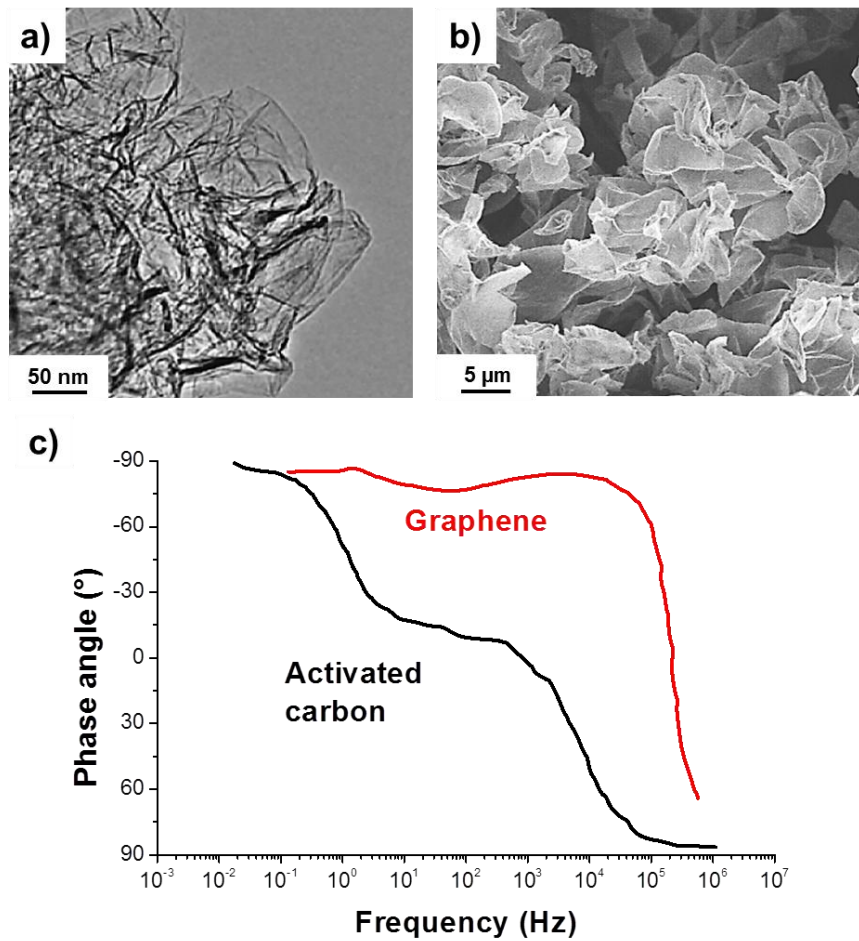
Fig. 20: (**a**) Chemically modified graphene (CMG; from Ref. [133]) and (**b**) graphene powder (from Ref. [135]). (**c**) Phase angle of activated carbon and graphene evidencing the high power handling ability of graphene (data from Ref. [136]).

CNT electrode
porous conducting array
good cycle life
low capacitance

Depositing pseudocapacitive materials on CNT
electrodes for novel composite electrodes with
superior capacitive properties

Pseudocapacitive materials
high theoretical capacitance
low utilization ratio
poor rate and cycle life

Conducting polymer/CNT composite

Metal oxide/CNT composite

Fig. 21:   A schematic diagram illustrating how pseudocapacitive materials can be deposited

on CNTs. The different representation for both coatings traduces different physico-chemical and

electrochemical   properties   for   polymers   and   metal   oxides
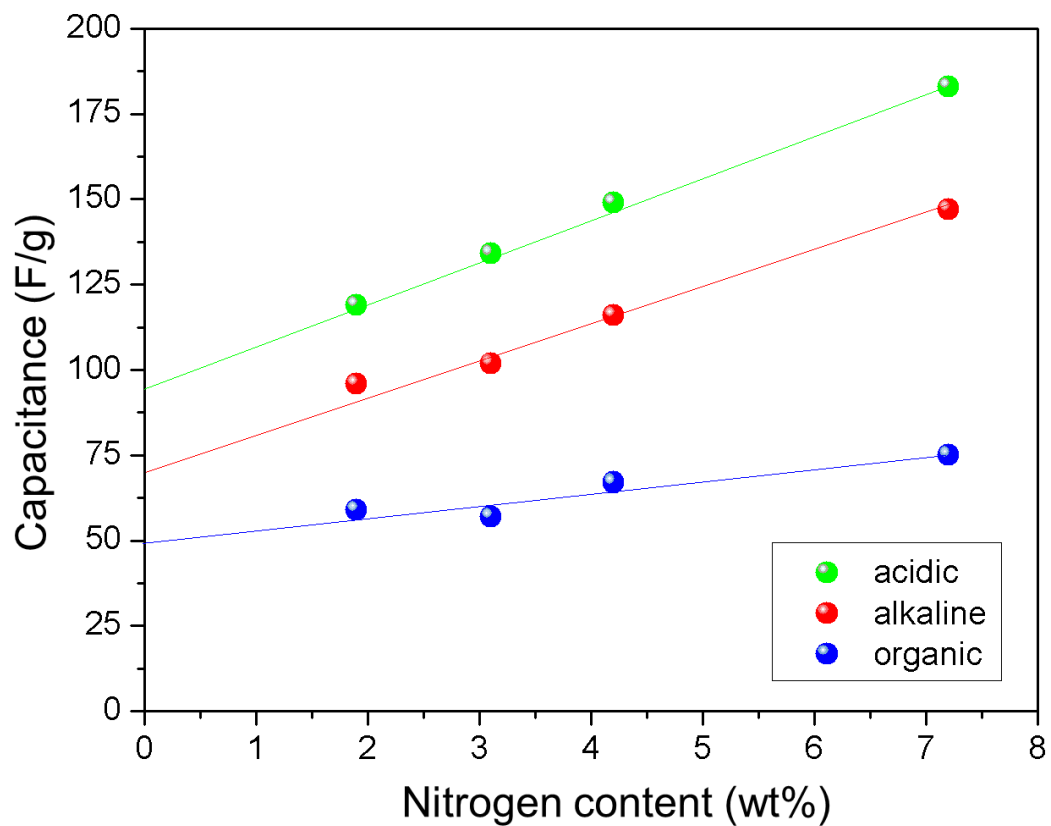
Fig. 22:   Capacitance values *versus* nitrogen content of N-enriched PAN-derived carbons in

1 M H_2SO_4, 6 M KOH, 1 M TEA-BF$_4$ in AN.[149]
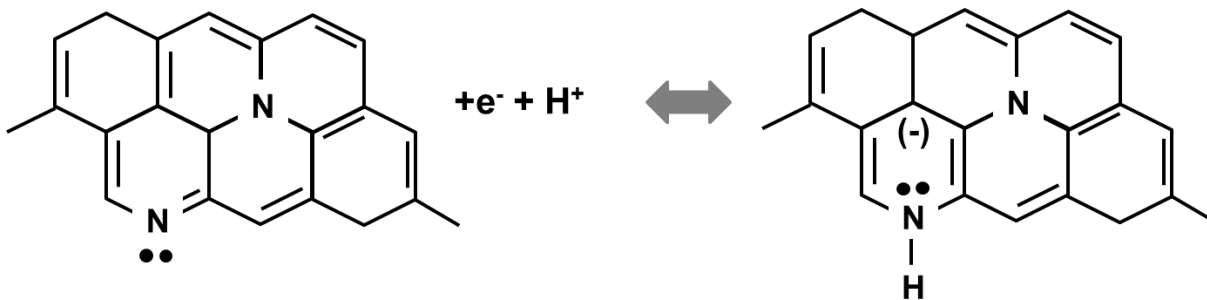
Fig. 23:   Scheme of a possible redox reaction with pyridinic nitrogen.
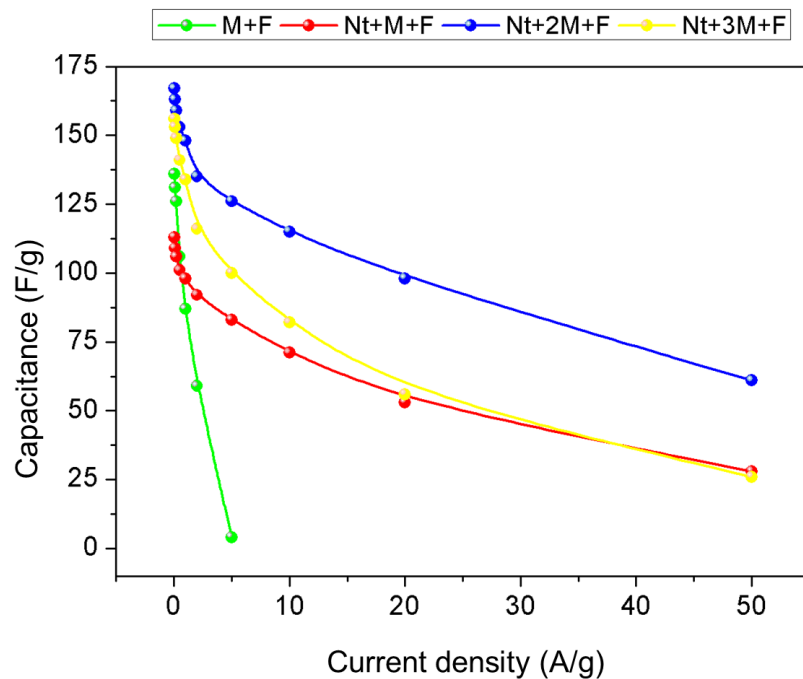
Fig. 24: Capacitance *versus* current load for the composites investigated in sulfuric acid(1M) electrolytic solution. M+F (composite from melamine and formaldehyde without carbon nanotubes), Nt+M+F (composite with carbon nanotubes, melamine and formaldehyde), Nt+2M+F (similar composite with twofold melamine proportion in the blend), and Nt+3M+F (threefold melamine proportion).Two-electrode cell.[162]
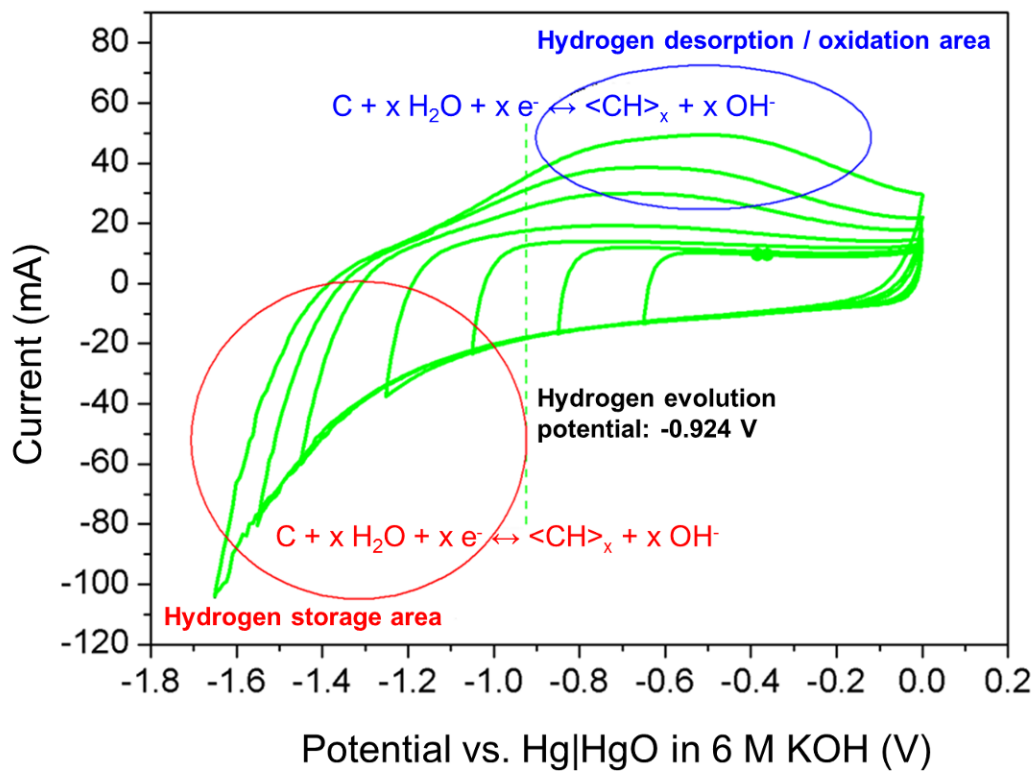
Fig. 25: Cyclic voltammograms of an activated carbon tissue electrode in 6 M KOH at 5 mV/s scan rate with a gradual shift to negative values of potential.[184]
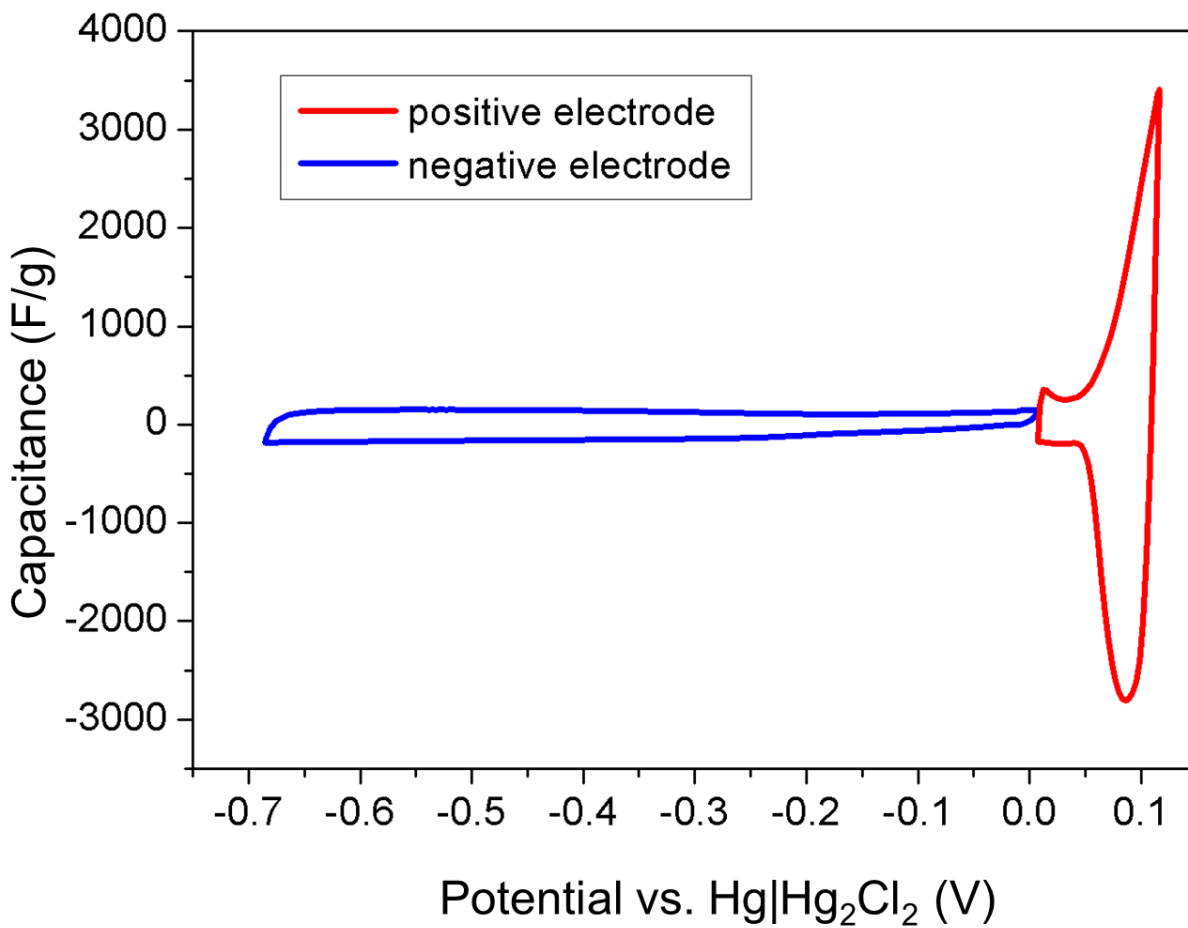
Fig. 26: Cyclic voltammograms at 5 mV/s scan rate for AC in 1 M KI solution. Potentials of both electrodes are measured separately *versus* the saturated calomel electrode.[163]
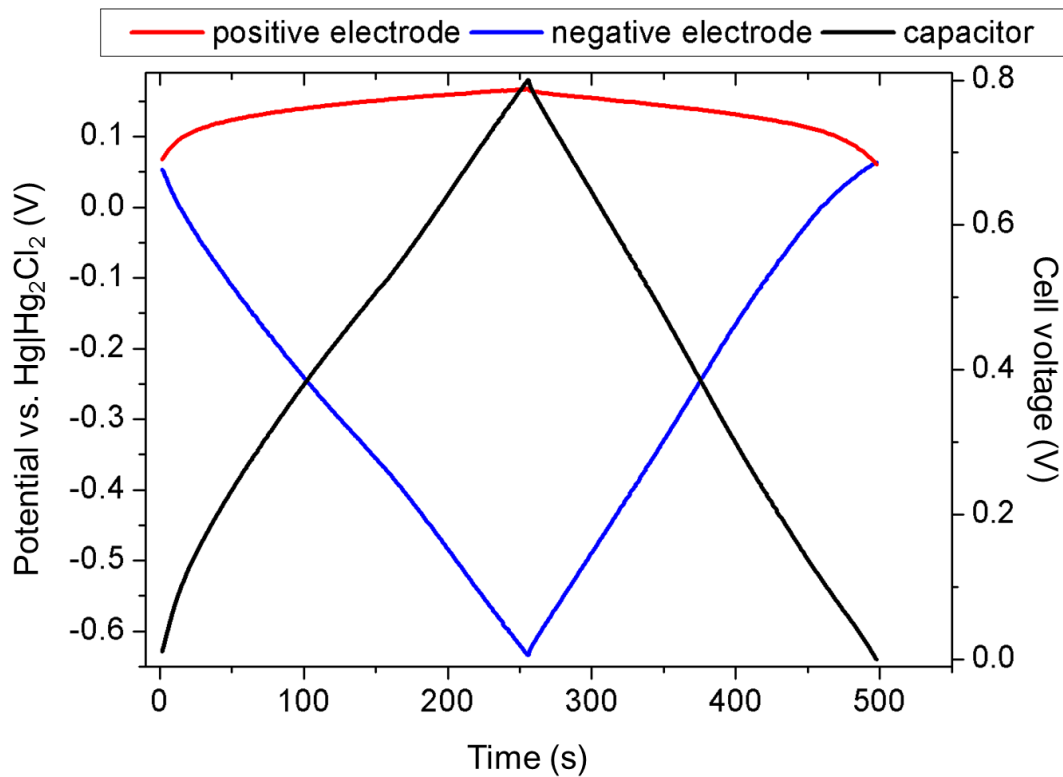
Fig. 27: Galvanostatic charge/discharge of a capacitor built from AC in 1 M KI solution at a current load of 500 mA/g. The voltage of the two-electrode cell (black) as well as the potential of the positive (red) and negative (blue) electrodes *versus* SCE are shown separately.[163]
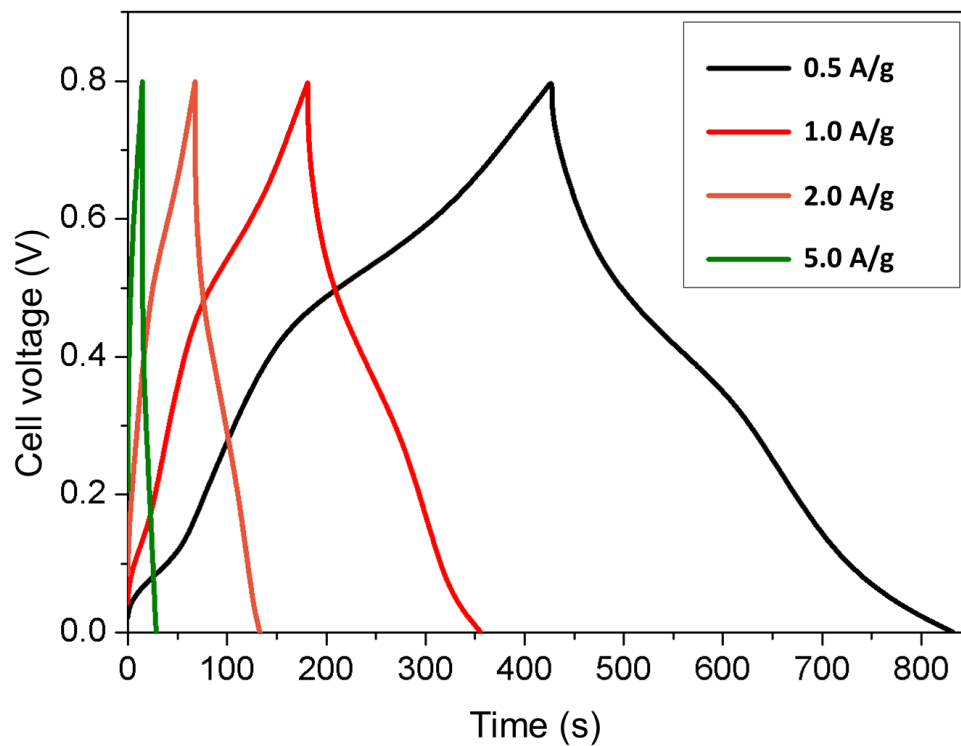
Fig. 28: Galvanostatic charge/discharge characteristics at different current loads for a capacitor operating in KI/VOSO₄ conjugated redox couples as 1 M aqueous electrolyte solutions.[167]
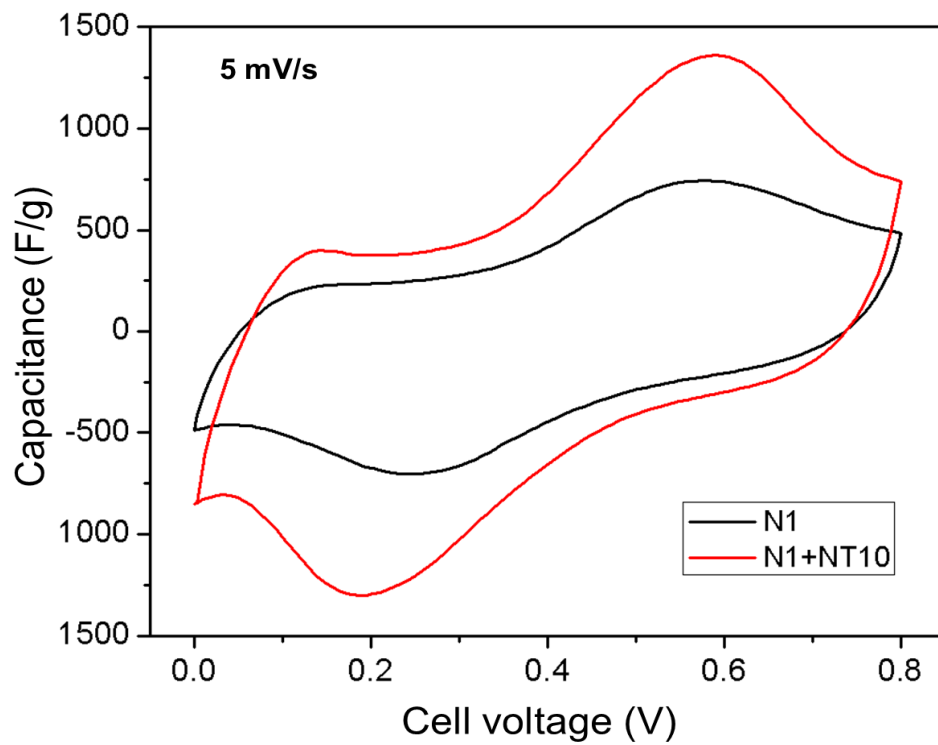
Fig. 29: Effect of adding CNTs to activated carbon on the cyclic voltammetry performance of cells constituted of two redox couples KI/VOSO$_4$ aqueous solutions (1 M) at a 5mV/s scan rate. NT10: 10 wt.% addition of CNTs.[161]
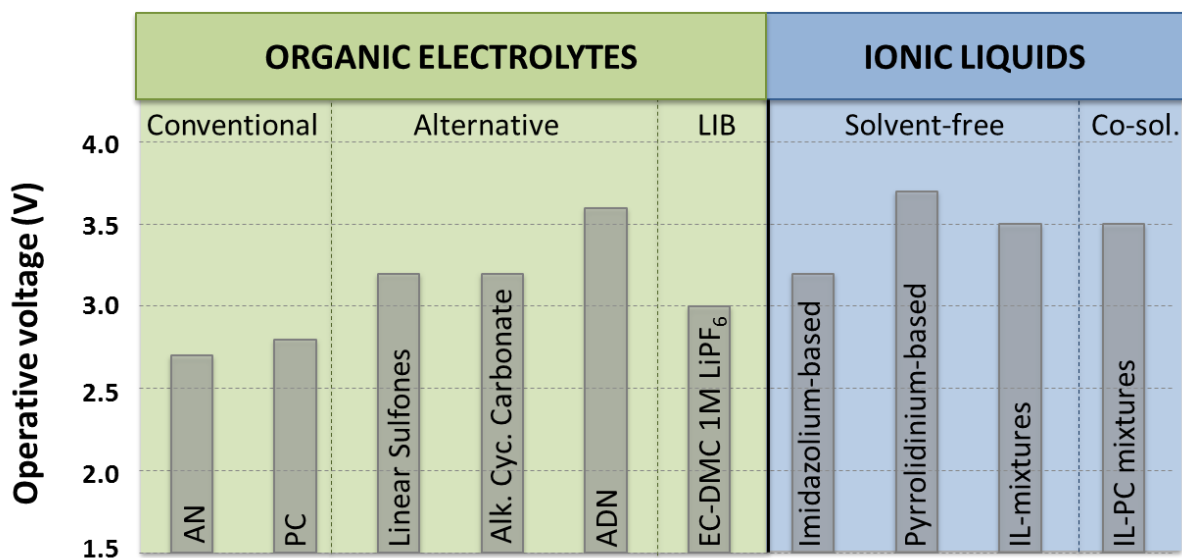
Fig. 30: Comparison of the EDLCs operating voltage achievable with organic electrolyte and ionic liquids based electrolytes. **AN** (acetonitrile), **PC** (propylene carbonate), **ADN** (adiponitrile), **Alkylat. Cyc. Carb.** (alkylated cyclic carbonate), **EC** (ethylene carbonate), **DMC** (dimethyl carbonate), **LiPF$_6$** (lithium hexafluorophosphate), **IL** (ionic liquids)
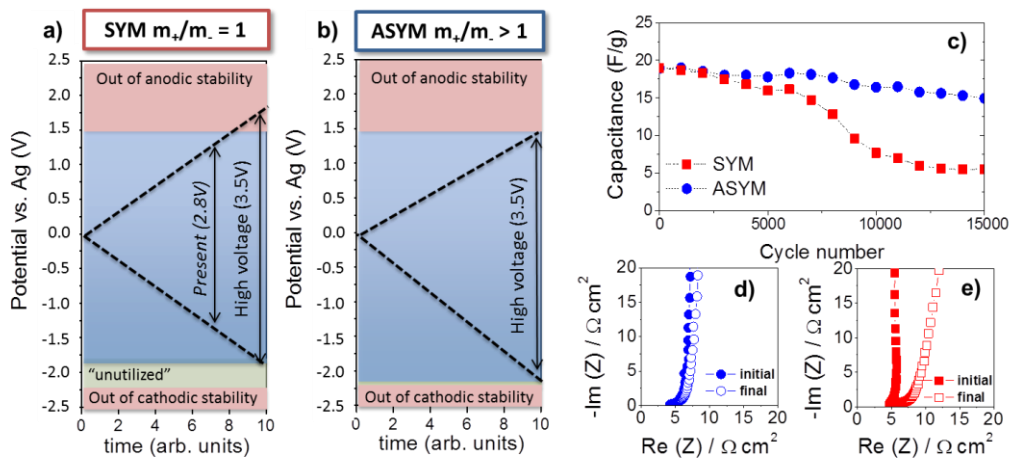
Fig. 31: Influence of the electrode balancing (**a** and **b**) on the cycling stability of EDLCs operating at 3.5 V and containing 0.7 M TEA-BF$_4$ in ADN as electrolyte (**c**). In panel **d** and **e** is clearly visible the beneficial effect of the balancing on the resistance and capacitance of the EDLCs
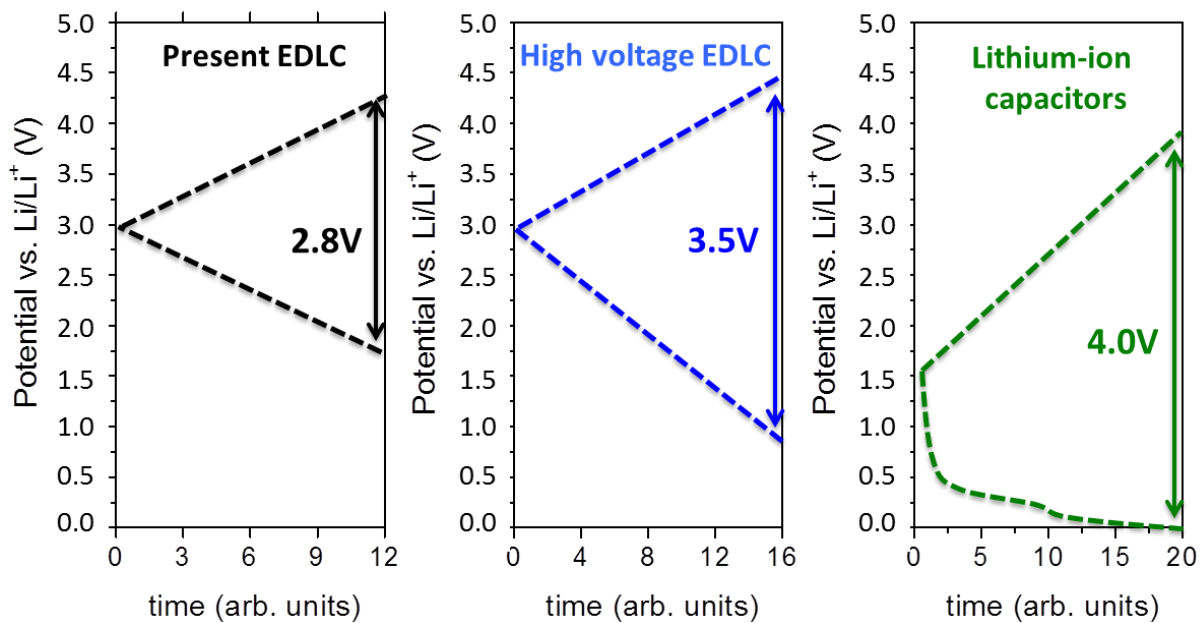
Fig. 32: Comparison of the operating voltage and electrode potential profiles of EDLCs (currently available and high voltage) and lithium-ion capacitors subjected to an identical current density.
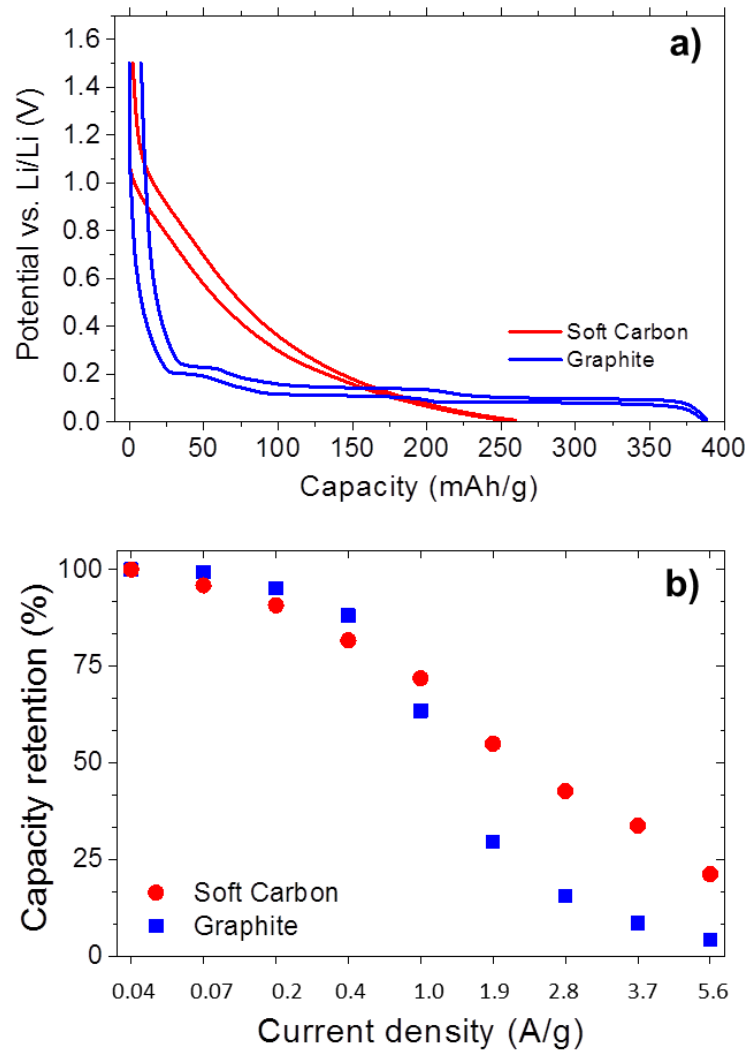
Fig. 33: Comparison of voltage profile (**a**) and capacity retention under increased current densities (**b**) of a graphite electrode (SFG 6L, Timcal, initial capacity 370 mAh/g) and a soft carbon electrode (PeC Timcal, initial capacity 250 mAh/g). The values reported in the figure refer to the capacity of the materials in half-cell tests.

Acknowledgements

102

Prof. François Béguin

Until 2012, François Béguin was Professor of materials science in Orléans University (France), and he was Director of national programmes on Energy Storage (Stock-E), Hydrogen and Fuel Cells (H-PAC) and electricity management (PROGELEC) in the French Agency for Research (ANR). Since 2011, he is Professor in Poznan University of Technology (Poland), where he has been recently awarded the WELCOME stipend from the Foundation for Polish Science. His research activities are devoted to chemical and electrochemical applications of carbon materials, with a special attention to the development of nano-carbons with controlled porosity and surface functionality for applications to lithium batteries, supercapacitors, electrochemical hydrogen storage, and reversible electrosorption of water contaminants.

Jun.-Prof. Volker Presser

Volker Presser obtained his PhD in Applied Mineralogy in 2006 from the Eberhard Karls University in Tübingen, Germany. As a Humboldt Research Fellow and Research Assistant Professor, he worked between 2010 and 2012 at the A.J. Drexel Nanotechnology Institute at Drexel University, Philadelphia, USA, on tunable nanoporous carbons for energy & gas storage and biomedical applications. As leader of the Energy Materials Group at the INM – Leibniz Institute for New Materials and Junior-Professor at the Saarland University, Saarbrücken, Germany, he investigates carbon and carbide-based supercapacitors, hybrid devices, and solutions for capacitive deionization.

Dr. Andrea Balducci

Andrea Balducci received his PhD in Materials Science in 2006 at the Paul Sabatier University of Toulouse, France. Since October 2009, he is the scientific leader of the supercapacitors group at MEET Battery Research Center of the University of Münster, Germany. He is working on the development of safe and high performance supercapacitors and lithium-ion batteries. He is also interested on the development of new high power hybrid devices.

Prof. Elzbieta Frackowiak

Elzbieta Frackowiak is Professor in the Institute of Chemistry and Technical Electrochemistry at Poznan University of Technology, Poland. Her research interests are especially devoted to storage/conversion of energy in electrochemical capacitors, Li-ion batteries, fuel cells. Main topics: application of activated carbon materials for supercapacitors and hydrogen storage, use of composite electrodes from nanotubes, conducting polymers, doped carbons and transition metal oxides for supercapacitors. She serves as Chair of Division 3 "Electrochemical Energy Conversion and Storage" of the International Society of Electrochemistry (2009-2014) and is the winner of the Foundation for Polish Science Prize (2011).

By F. Béguin, V. Presser, A. Balducci, and E. Frackowiak
Carbons and Electrolytes for Advanced Supercapacitors

Electrochemical capacitors, also known as supercapacitors, are devices for highly efficient energy storage and recovery. This review summarizes the science and technology of carbon supercapacitors, especially regarding the relation between ion size / ion desolvation and the pore size of electrically charged porous carbon materials. Using pseudocapacitive materials and employing electrolytes that allow applying very high cell voltages is presented as two strategies to improve the energy density.
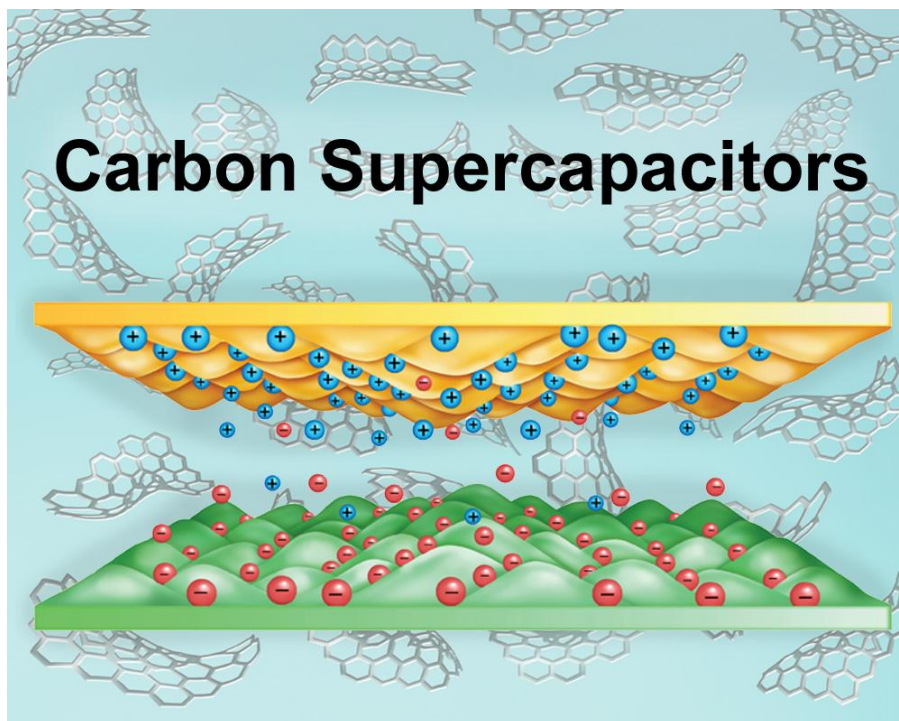
References

[1]   H. Helmholtz, Annalen der Physik 1853, 89, 211.
[2]   L. G. Gouy, J. Phys. Theor. Appl. 1910, 9, 457.
[3]   O. Stern, Zeitschrift für Elektrochemie and angewandte physikalische Chemie 1924, 30, 508.
[4]   J. R. Miller, A. F. Burke, Electrochem. Soc. Interface 2010, 17, 53
[5]   J. B. Goodenough, Y. Kim, Chemistry of Materials 2009, 22, 587.
[6]   V. Ruiz, C. Blanco, E. Raymundo-Piñero, V. Khomenko, F. Béguin, R. Santamaría, Electrochimica Acta 2007, 52, 4969.
[7]   V. Khomenko, E. Raymundo-Piñero, E. Frackowiak, F. Béguin, Applied Physics A 2006, 82, 567.
[8]   L. Demarconnay, E. Raymundo-Piñero, F. Béguin, Electrochemistry Communications 2010, 12, 1275; K. Fic, G. Lota, M. Meller, E. Frackowiak, Energy & Environmental Science 2012, 5, 5842.
[9]   Q. Gao, L. Demarconnay, E. Raymundo-Pinero, F. Béguin, Energy & Environmental Science 2012, 5, 9611.
[10]   T. Brousse, D. Bélanger , D. Guay, in *Supercapacitors: materials, systems and applications*, (Eds: F. Béguin, E. Frackowiak), Wiley, Weinheim 2013, 257
[11]   A. Burke, Journal of Power Sources 2000, 91, 37.
[12]   J. Gamby, P. L. Taberna, P. Simon, J. F. Fauvarque, M. Chesneau, Journal of Power Sources 2001, 101, 109.
[13]   M. Ue, Journal of The Electrochemical Society 1994, 141, 3336.
[14]   M. Arulepp, L. Permann, J. Leis, A. Perkson, K. Rumma, A. Jänes, E. Lust, Journal of Power Sources 2004, 133, 320; P. Liu, M. Verbrugge, S. Soukiazian, Journal of Power Sources 2006, 156, 712.
[15]   M. Ue, M. Takeda, M. Takehara, S. Mori, Journal of The Electrochemical Society 1997, 144, 2684; K. Xu, M. S. Ding, T. R. Jow, Journal of The Electrochemical Society 2001, 148, A267.
[16]   M. Ue, Electrochemistry 2007, 75, 565.
[17]   S. Mori, K. Ida, M. Ue, Process for producing quaternary salts. 1988, European Patent Office, EP 0291074 ; M. Ue, M. Takehara, Y. Oura, A. Toriumi, M. Takeda, Denki Kagaku Electrochemistry 2001, 69, 458; M. Ue, M. Takehara, M. Takeda, Denki Kagaku Electrochemistry 1997, 65, 969.
[18]   K. Chiba, Electrolytic solution for electric double layer capacitor and electric double layer capacitor 2008, US Patent Office, US 20060274475 A1.
[19]   M. Galiński, A. Lewandowski, I. Stępniak, Electrochimica Acta 2006, 51, 5567.
[20]   M. Mastragostino, F. Soavi, Journal of Power Sources 2007, 174, 89; R. D. Rogers, K. R. Seddon, Science 2003, 302, 792; K. R. Seddon, Nature Materials 2003, 2, 363; D. Weingarth, H. Noh, A. Foelske-Schmitz, A. Wokaun, R. Kötz, Electrochimica Acta 2013, 103, 119; D. Weingarth, A. Foelske-Schmitz, R. Kötz, Journal of Power Sources 2013, 225, 84.
[21]   N. Nanbu, T. Ebina, H. Uno, S. Ishizawa, Y. Sasaki, Electrochimica Acta 2006, 52, 1763.
[22]   T. E. Rufford, D. Hulicova-Jurcakova, Z. Zhu, G. Q. Lu, Electrochemistry Communications 2008, 10, 1594.
[23]   K. Kierzek, E. Frackowiak, G. Lota, G. Gryglewicz, J. Machnikowski, Electrochimica Acta 2004, 49, 1169.
[24]   L. Wei, M. Sevilla, A. B. Fuertes, R. Mokaya, G. Yushin, Advanced Energy Materials 2011, 1, 356.

[25]   C. Portet, M. A. Lillo-Rodenas, A. Linares-Solano, Y. Gogotsi, Physical Chemistry Chemical Physics 2009, 11, 4943.

[26]   E. Frackowiak, S. Delpeux, K. Jurewicz, K. Szostak, D. Cazorla-Amoros, F. Béguin, Chemical Physics Letters 2002, 361, 35.

[27]   M. Noked, A. Soffer, D. Aurbach, Journal of Solid State Electrochemistry 2011, 15, 1563.

[28]   V. Presser, L. Zhang, J. J. Niu, J. McDonough, C. Perez, H. Fong, Y. Gogotsi, Advanced Energy Materials 2011, 1, 423.

[29]   K. S. W. Sing, D. H. Everett, R. A. V. Haul, L. Moscou, R. A. Pierotti, J. Rouquerol, T. Siemieniewska, Pure and Applied Chemistry 1985, 57, 603

[30]   X. Py, A. Guillot, B. Cagnon, Carbon 2003, 41, 1533; R. Mysyk, Q. Gao, E. Raymundo-Piñero, F. Béguin, Carbon 2012, 50, 3367.

[31]   J. Jagiello, J. P. Olivier, The Journal of Physical Chemistry C 2009, 113, 19382; A. V. Neimark, Y. Lin, P. I. Ravikovitch, M. Thommes, Carbon 2009, 47, 1617; P. I. Ravikovitch, A. V. Neimark, Langmuir 2006, 22, 11171.

[32]   D. D. Do, HD Adsorption Science & Technology 2003, 21, 389.

[33]   L. He, S. M. Chathoth, Y. B. Melnichenko, V. Presser, J. McDonough, Y. Gogotsi, Microporous and Mesoporous Materials 2012, 149, 46.

[34]   G. Yushin, R. Dash, J. Jagiello, J. E. Fischer, Y. Gogotsi, Advanced Functional Materials 2006, 16, 2288.

[35]   R. E. Franklin, Proceedings of the Royal Society of London. Series A. Mathematical and Physical Sciences 1951, 209, 196.

[36]   L. L. Ban, D. Crawford, H. Marsh, Journal of Applied Crystallography 1975, 8, 415.

[37]   S. Ergun, L. E. Alexander, Nature 1962, 195, 765; S. Ergun, V. Tiensuu, Acta Crystallographica 1959, 12, 1050.

[38]   P. J. F. Harris, International Materials Reviews 1997, 42, 206.

[39]   P. J. F. Harris, Critical Reviews in Solid State and Materials Sciences 2005, 30, 235; P. J. F. Harris, S. C. Tsang, Philosophical Magazine A 1997, 76, 667.

[40]   J. F. H. Peter, L. Zheng, S. Kazu, Journal of Physics: Condensed Matter 2008, 20, 362201.

[41]   S. K. Jain, R. J. M. Pellenq, J. P. Pikunic, K. E. Gubbins, Langmuir 2006, 22, 9942.

[42]   D. Lozano-Castelló, D. Cazorla-Amorós, A. Linares-Solano, S. Shiraishi, H. Kurihara, A. Oya, Carbon 2003, 41, 1765; T. Morimoto, K. Hiratsuka, Y. Sanada, K. Kurihara, Journal of Power Sources 1996, 60, 239.

[43]   S. Brunauer, P. H. Emmett, E. Teller, Journal of the American Chemical Society 1938, 60, 309

[44]   O. Barbieri, M. Hahn, A. Herzog, R. Kötz, Carbon 2005, 43, 1303.

[45]   M. D. Stoller, C. W. Magnuson, Y. Zhu, S. Murali, J. W. Suk, R. Piner, R. S. Ruoff, Energy & Environmental Science 2011, 4, 4685.

[46]   E. Avraham, B. Yaniv, A. Soffer, D. Aurbach, The Journal of Physical Chemistry C 2008, 112, 7385.

[47]   L. Eliad, E. Pollak, N. Levy, G. Salitra, A. Soffer, D. Aurbach, Applied Physics A 2006, 82, 607.

[48]   M. Noked, E. Avraham, Y. Bohadana, A. Soffer, D. Aurbach, The Journal of Physical Chemistry C 2009, 113, 7316.

[49]   L. Eliad, G. Salitra, A. Soffer, D. Aurbach, The Journal of Physical Chemistry B 2001, 105, 6880.

[50]   M. M. Hantel, V. Presser, R. Kötz, Y. Gogotsi, Electrochemistry Communications 2011, 13, 1221

[51]   T. M. Arruda, M. Heon, V. Presser, P. C. Hillesheim, S. Dai, Y. Gogotsi, S. V. Kalinin, N. Balke, Energy and Environmental Science 2013, 6, 225

[52]   C. O. Ania, J. Pernak, F. Stefaniak, E. Raymundo-Piñero, F. Béguin, Carbon 2006, 44, 3126.

[53]   C. Largeot, C. Portet, J. Chmiola, P.-L. Taberna, Y. Gogotsi, P. Simon, Journal of the American Chemical Society 2008, 130, 2730.

[54]   C. Vix-Guterl, E. Frackowiak, K. Jurewicz, M. Friebe, J. Parmentier, F. Béguin, Carbon 2005, 43, 1293.

[55]   E. Raymundo-Piñero, K. Kierzek, J. Machnikowski, F. Béguin, Carbon 2006, 44, 2498.

[56]   J. Chmiola, G. Yushin, Y. Gogotsi, C. Portet, P. Simon, P. L. Taberna, Science 2006, 313, 1760.

[57]   Y. Gogotsi, A. Nikitin, H. Ye, W. Zhou, J. E. Fischer, B. Yi, H. C. Foley, M. W. Barsoum, Nature Materials 2003, 2, 591

[58]   M. Deschamps, E. Gilbert, P. Azais, E. Raymundo-Piñero, M. R. Ammar, P. Simon, D. Massiot, F. Béguin, Nature Materials 2013, 12, 351.

[59]   T. A. Centeno, O. Sereda, F. Stoeckli, Physical Chemistry Chemical Physics 2011; T. A. Centeno, M. Sevilla, A. B. Fuertes, F. Stoeckli, Carbon 2005, 43, 3012

[60]   J. Chmiola, C. Largeot, P.-L. Taberna, P. Simon, Y. Gogotsi, Angewandte Chemie International Edition 2008, 47, 3392.

[61]   V. Presser, M. Heon, Y. Gogotsi, Advanced Functional Materials 2011, 21, 810.

[62]   R. Lin, P. L. Taberna, J. Chmiola, D. Guay, Y. Gogotsi, P. Simon, Journal of The Electrochemical Society 2009, 156, A7.

[63]   D.-e. Jiang, Z. Jin, D. Henderson, J. Wu, The Journal of Physical Chemistry Letters 2012, 3, 1727.

[64]   S. Boukhalfa, L. He, Y. B. Melnichenko, G. Yushin, Angewandte Chemie 2013, 125, 4716.

[65]   K. Murakami, Y. Mogi, K. Tabayashi, T. Shimoyama, K. Yamada, Y. Shinozaki, Carbonaceous material, its production process and electric double layer capacitor employing it. 2005, US Patent Office, US 6865068.

[66]   J. Segalini, B. Daffos, P. L. Taberna, Y. Gogotsi, P. Simon, Electrochimica Acta 2010, 55, 7489.

[67]   Y. Korenblit, M. Rose, E. Kockrick, L. Borchardt, A. Kvit, S. Kaskel, G. Yushin, ACS Nano 2010, 4, 1337.

[68]   Y. Korenblit, A. Kajdos, W. C. West, M. C. Smart, E. J. Brandon, A. Kvit, J. Jagiello, G. Yushin, Advanced Functional Materials 2012, 22, 1655.

[69]   J. Huang, B. G. Sumpter, V. Meunier, Chemistry – A European Journal 2008, 14, 6614; J. Huang, B. G. Sumpter, V. Meunier, Angewandte Chemie International Edition 2008, 47, 520.

[70]   R. Mysyk, E. Raymundo-Piñero, F. Béguin, Electrochemistry Communications 2009, 11, 554.

[71]   R. Mysyk, E. Raymundo-Piñero, J. Pernak, F. Béguin, The Journal of Physical Chemistry C 2009, 113, 13443.

[72]   C. O. Ania, J. Pernak, F. Stefaniak, E. Raymundo-Piñero, F. Béguin, Carbon 2009, 47, 3158.

[73]   M. Hahn, O. Barbieri, F. P. Campana, R. Kötz, R. Gallay, Applied Physics A 2006, 82, 633.

[74]   D. Aurbach, M. D. Levi, G. Salitra, N. Levy, E. Pollak, J. Muthu, Journal of The Electrochemical Society 2008, 155, A745.

[75]   L. J. Hardwick, M. Hahn, P. Ruch, M. Holzapfel, W. Scheifele, H. Buqa, F. Krumeich, P. Novák, R. Kötz, Electrochimica Acta 2006, 52, 675; L. J. Hardwick, P. W. Ruch, M. Hahn, W. Scheifele, R. Kötz, P. Novák, Journal of Physics and Chemistry of Solids 2008, 69, 1232.

[76]   P. W. Ruch, D. Cericola, A. Foelske, R. Kötz, A. Wokaun, Electrochimica Acta 2010, 55, 2352.

[77]   P. Azaïs, L. Duclaux, P. Florian, D. Massiot, M.-A. Lillo-Rodenas, A. Linares-Solano, J.-P. Peres, C. Jehoulet, F. Béguin, Journal of Power Sources 2007, 171, 1046.

[78]   P. W. Ruch, D. Cericola, A. Foelske-Schmitz, R. Kötz, A. Wokaun, Electrochimica Acta 2010, 55, 4412.

[79]   R. Lin, P. Huang, J. Ségalini, C. Largeot, P. L. Taberna, J. Chmiola, Y. Gogotsi, P. Simon, Electrochimica Acta 2009, 54, 7025.

[80]   O. Kimizuka, O. Tanaike, J. Yamashita, T. Hiraoka, D. N. Futaba, K. Hata, K. Machida, S. Suematsu, K. Tamamitsu, S. Saeki, Y. Yamada, H. Hatori, Carbon 2008, 46, 1999.

[81]   P. W. Ruch, R. Kötz, A. Wokaun, Electrochimica Acta 2009, 54, 4451.

[82]   J. Chmiola, G. Yushin, R. Dash, Y. Gogotsi, Journal of Power Sources 2006, 158, 765.

[83]   Y. Zhai, Y. Dou, D. Zhao, P. F. Fulvio, R. T. Mayes, S. Dai, Advanced Materials 2011, 23, 4828.

[84]   T. Kyotani, Z. Ma, A. Tomita, Carbon 2003, 41, 1451.

[85]   K. Matsuoka, Y. Yamagishi, T. Yamazaki, N. Setoyama, A. Tomita, T. Kyotani, Carbon 2005, 43, 876.

[86]   H. Nishihara, H. Itoi, T. Kogure, P.-X. Hou, H. Touhara, F. Okino, T. Kyotani, Chemistry – A European Journal 2009, 15, 5355.

[87]   P. Krawiec, E. Kockrick, L. Borchardt, D. Geiger, A. Corma, S. Kaskel, The Journal of Physical Chemistry C 2009, 113, 7755.

[88]   Y. Gogotsi, *Carbon nanomaterials*, CRC Taylor & Francis, Boca Raton 2006.

[89]   L. Borchardt, M. Oschatz, M. Lohe, V. Presser, Y. Gogotsi, S. Kaskel, Carbon 2012, 50, 3987; M. Oschatz, L. Borchardt, M. Thommes, K. A. Cychosz, I. Senkovska, N. Klein, R. Frind, M. Leistner, V. Presser, Y. Gogotsi, S. Kaskel, Angewandte Chemie International Edition 2012, 51, 7577.

[90]   C. Liang, Z. Li, S. Dai, Angewandte Chemie International Edition 2008, 47, 3696.

[91]   P. Simon, Y. Gogotsi, Nature Materials 2008, 7, 845.

[92]   D. Pech, M. Brunet, H. Durou, P. Huang, V. Mochalin, Y. Gogotsi, P.-L. Taberna, P. Simon, Nature Nanotechnology 2010, 5, 651.

[93]   C. Portet, G. Yushin, Y. Gogotsi, Journal of The Electrochemical Society 2008, 155, A531.

[94]   C. R. Pérez, S.-H. Yeon, J. Ségalini, V. Presser, P.-L. Taberna, P. Simon, Y. Gogotsi, Advanced Functional Materials 2013, 23, 1081

[95]   F. J. Keil, C. Rieckmann, Hungarian Journal of Industrial Chemistry 1993, 21, 277; F. J. Keil, C. Rieckmann, Chemical Engineering Science 1994, 49, 4811.

[96]   Z.-Y. Yuan, B.-L. Su, Journal of Materials Chemistry 2006, 16, 663.

[97]   P. Krawiec, D. Geiger, S. Kaskel, Chemical Communications 2006, 0, 2469.

[98]   Z. Wu, Y. Yang, D. Gu, Q. Li, D. Feng, Z. Chen, B. Tu, P. A. Webley, D. Zhao, Small 2009, 5, 2738.

[99]   D.-W. Wang, F. Li, M. Liu, G. Q. Lu, H.-M. Cheng, Angewandte Chemie International Edition 2008, 47, 373.

[100]   A. Yoshida, I. Tanahashi, Y. Takeuchi, A. Nishino, IEEE Transactions on Components, Hybrids, and Manufacturing Technology 1987, 10, 100.

[101] I. Tanahashi, A. Yoshida, A. Nishino, Journal of The Electrochemical Society 1990, 137, 3052.

[102] K. Leitner, A. Lerf, M. Winter, J. O. Besenhard, S. Villar-Rodil, F. Suárez-García, A. Martínez-Alonso, J. M. D. Tascón, Journal of Power Sources 2006, 153, 419.

[103] S.-H. Yoon, S. Lim, Y. Song, Y. Ota, W. Qiao, A. Tanaka, I. Mochida, Carbon 2004, 42, 1723.

[104] Y. Gao, V. Presser, L. Zhang, J. J. Niu, J. K. McDonough, C. R. Pérez, H. Lin, H. Fong, Y. Gogotsi, Journal of Power Sources 2012, 201, 368.

[105] E. Frackowiak, K. Metenier, V. Bertagna, F. Béguin, Applied Physics Letters 2000, 77, 2421.

[106] E. Frackowiak, F. Béguin, Carbon 2001, 39, 937.

[107] J. K. McDonough, A. I. Frolov, V. Presser, J. Niu, C. H. Miller, T. Ubieto, M. V. Fedorov, Y. Gogotsi, Carbon 2012, 50, 3298.

[108] G. Feng, R. Qiao, J. Huang, S. Dai, B. G. Sumpter, V. Meunier, Physical Chemistry Chemical Physics 2011, 13, 1152.

[109] J. Huang, B. G. Sumpter, V. Meuniera, G. Yushina, C. Portet, Y. Gogotsia, Journal of Materials Research 2010, 25, 1525.

[110] T. Kim, S. Lim, K. Kwon, S.-H. Hong, W. Qiao, C. K. Rhee, S.-H. Yoon, I. Mochida, Langmuir 2006, 22, 9086.

[111] L. Xing, J. Vatamanu, G. D. Smith, D. Bedrov, The Journal of Physical Chemistry Letters 2012, 3, 1124.

[112] C. Niu, E. K. Sichel, R. Hoch, D. Moy, H. Tennent, Applied Physics Letters 1997, 70, 1480.

[113] E. Frackowiak, K. Jurewicz, S. Delpeux, F. Béguin, Journal of Power Sources 2001, 97 - 98, 822

[114] K. Jurewicz, K. Babeł, R. Pietrzak, S. Delpeux, H. Wachowska, Carbon 2006, 44, 2368.

[115] C. Du, N. Pan, Journal of Power Sources 2006, 160, 1487.

[116] A. Izadi-Najafabadi, S. Yasuda, K. Kobashi, T. Yamada, D. N. Futaba, H. Hatori, M. Yumura, S. Iijima, K. Hata, Advanced Materials 2010, 22, E235.

[117] M. E. Plonska-Brzezinska, L. Echegoyen, Journal of Materials Chemistry A 2013.

[118] C. Portet, J. Chmiola, Y. Gogotsi, S. Park, K. Lian, Electrochimica Acta 2008, 53, 7675.

[119] C. Portet, G. Yushin, Y. Gogotsi, Carbon 2007, 45, 2511.

[120] W. Guixin, S. Zongping, Y. Zuolong, Nanotechnology 2007, 18, 205705.

[121] P.-L. Taberna, G. Chevallier, P. Simon, D. Plée, T. Aubert, Materials Research Bulletin 2006, 41, 478.

[122] P. F. Fulvio, R. T. Mayes, X. Wang, S. M. Mahurin, J. C. Bauer, V. Presser, J. McDonough, Y. Gogotsi, S. Dai, Advanced Functional Materials 2011, 21, 2208.

[123] K. Jost, C. R. Perez, J. K. McDonough, V. Presser, M. Heon, G. Dion, Y. Gogotsi, Energy & Environmental Science 2011, 4, 5060.

[124] J. Chmiola, C. Largeot, P.-L. Taberna, P. Simon, Y. Gogotsi, Science 2010, 328, 480.

[125] M. Kaempgen, C. K. Chan, J. Ma, Y. Cui, G. Gruner, Nano Letters 2009, 9, 1872.

[126] M. Heon, S. Lofland, J. Applegate, R. Nolte, E. Cortes, J. D. Hettinger, P.-L. Taberna, P. Simon, P. Huang, M. Brunet, Y. Gogotsi, Energy & Environmental Science 2011, 4, 135.

[127] F. Liu, A. Gutes, I. Laboriante, C. Carraro, R. Maboudian, Applied Physics Letters 2011, 99, 112104.

[128] W. Gao, N. Singh, L. Song, Z. Liu, A. L. M. Reddy, L. Ci, R. Vajtai, Q. Zhang, B. Wei, P. M. Ajayan, Nature Nanotechnology 2011, 6, 496.

[129] M. F. El-Kady, R. B. Kaner, Nature Communications 2013, 4, 1475.

111

[130]   C. Li, Y. Zhang, M. Mann, D. Hasko, W. Lei, B. Wang, D. Chu, D. Pribat, G. A. J. Amaratunga, W. I. Milne, Applied Physics Letters 2010, 97, 113107.

[131]   R. Lin, P.-L. Taberna, S. Fantini, V. Presser, C. R. Pérez, F. Malbosc, N. L. Rupesinghe, K. B. K. Teo, Y. Gogotsi, P. Simon, The Journal of Physical Chemistry Letters 2011, 2, 2396.

[132]   B. Kim, H. Chung, W. Kim, The Journal of Physical Chemistry C 2010, 114, 15223.

[133]   M. D. Stoller, S. Park, Y. Zhu, J. An, R. S. Ruoff, Nano Letters 2008, 8, 3498.

[134]   A. Yu, I. Roes, A. Davies, Z. Chen, Applied Physics Letters 2010, 96, 253105.

[135]   C. Liu, Z. Yu, D. Neff, A. Zhamu, B. Z. Jang, Nano Letters 2010, 10, 4863.

[136]   J. R. Miller, R. A. Outlaw, B. C. Holloway, Science 2010, 329, 1637.

[137]   M. M. Hantel, T. Kaspar, R. Nesper, A. Wokaun, R. Kötz, Electrochemistry Communications 2011, 13, 90.

[138]   C. Arbizzani, M. Mastragostino, F. Soavi, Journal of Power Sources 2001, 100, 164; R. Campomanes, S. E. Bittencourt, J. S. C. Campos, Synthetic Metals 1999, 102, 1230; V. Gupta, N. Miura, Materials Letters 2006, 60, 1466; J.-H. Kim, Y.-S. Lee, A. K. Sharma, C. G. Liu, Electrochimica Acta 2006, 52, 1727; A. Laforgue, P. Simon, J. F. Fauvarque, J. F. Sarrau, P. Lailler, Journal of The Electrochemical Society 2001, 148, A1130; A. Laforgue, P. Simon, C. Sarrazin, J.-F. Fauvarque, Journal of Power Sources 1999, 80, 142; H. Li, J. Wang, Q. Chu, Z. Wang, F. Zhang, S. Wang, Journal of Power Sources 2009, 190, 578; M. Mastragostino, C. Arbizzani, F. Soavi, Solid State Ionics 2002, 148, 493; B. Muthulakshmi, D. Kalpana, S. Pitchumani, N. G. Renganathan, Journal of Power Sources 2006, 158, 1533; K. S. Ryu, X. Wu, Y.-G. Lee, S. H. Chang, Journal of Applied Polymer Science 2003, 89, 1300; J. Sandler, M. S. P. Shaffer, T. Prasse, W. Bauhofer, K. Schulte, A. H. Windle, Polymer 1999, 40, 5967; S. R. Sivakkumar, W. J. Kim, J.-A. Choi, D. R. MacFarlane, M. Forsyth, D.-W. Kim, Journal of Power Sources 2007, 171, 1062.

[139]   A. Brandt, P. Isken, A. Lex-Balducci, A. Balducci, Journal of Power Sources 2012, 204, 213.

[140]   K. Jurewicz, S. Delpeux, V. Bertagna, F. Béguin, E. Frackowiak, Chemical Physics Letters 2001, 347, 36; C. Peng, J. Jin, G. Z. Chen, Electrochimica Acta 2007, 53, 525; H. Zhang, G. Cao, W. Wang, K. Yuan, B. Xu, W. Zhang, J. Cheng, Y. Yang, Electrochimica Acta 2009, 54, 1153.

[141]   V. Khomenko, E. Frackowiak, F. Béguin, Electrochimica Acta 2005, 50, 2499.

[142]   K. Naoi, P. Simon, Journal of The Electrochemical Society Interface 2008, 17, 34.

[143]   M. S. Hong, S. H. Lee, S. W. Kim Electrochemical and Solid-State Letters 2002, 5, A227.

[144]   T. Brousse, M. Toupin, D. Bélanger, Journal of The Electrochemical Society 2004, 151, A614; V. Khomenko, E. Raymundo-Piñero, F. Béguin, Journal of Power Sources 2006, 153, 183.

[145]   J. M. Miller, B. Dunn, Langmuir 1999, 15, 799; M. Toupin, T. Brousse, D. Bélanger, Chemistry of Materials 2002, 14, 3946; N.-L. Wu, Materials Chemistry and Physics 2002, 75, 6; K.-W. Nam, C.-W. Lee, X.-Q. Yang, B. W. Cho, W.-S. Yoon, K.-B. Kim, Journal of Power Sources 2009, 188, 323.

[146]   E. Raymundo-Piñero, V. Khomenko, E. Frackowiak, F. Béguin, Journal of The Electrochemical Society 2005, 152, A229.

[147]   X.-H. Yang, Y.-G. Wang, H.-M. Xiong, Y.-Y. Xia, Electrochimica Acta 2007, 53, 752.

[148]   A. Malak, K. Fic, G. Lota, C. Vix-Guterl, E. Frackowiak, Journal of Solid State Electrochemistry 2010, 14, 811.

[149]   E. Frackowiak, G. Lota, J. Machnikowski, C. Vix-Guterl, F. Béguin, Electrochimica Acta 2006, 51, 2209.

[150]   D. Hulicova, J. Yamashita, Y. Soneda, H. Hatori, M. Kodama, Chemistry of Materials 2005, 17, 1241.

[151]   D. Hulicova-Jurcakova, M. Kodama, S. Shiraishi, H. Hatori, Z. H. Zhu, G. Q. Lu, Advanced Functional Materials 2009, 19, 1800.

[152]   H. M. Jeong, J. W. Lee, W. H. Shin, Y. J. Choi, H. J. Shin, J. K. Kang, J. W. Choi, Nano Letters 2011, 11, 2472; Y.-H. Lee, Y.-F. Lee, K.-H. Chang, C.-C. Hu, Electrochemistry Communications 2011, 13, 50; C. Qin, X. Lu, G. Yin, Z. Jin, Q. Tan, X. Bai, Materials Chemistry and Physics 2011, 126, 453; B. Xu, H. Duan, M. Chu, G. Cao, Y. Yang, Journal of Materials Chemistry A 2013, 1, 4565.

[153]   G. Lota, B. Grzyb, H. Machnikowska, J. Machnikowski, E. Frackowiak, Chemical Physics Letters 2005, 404, 53.

[154]   G. Lota, K. Lota, E. Frackowiak, Electrochemistry Communications 2007, 9, 1828.

[155]   K. Jurewicz, E. Frackowiak, F. Béguin, Electrochemical and Solid-State Letters 2001, 4, A27.

[156]   E. Frackowiak, K. Jurewicz, K. Szostak, S. Delpeux, F. Béguin, Fuel Processing Technology 2002, 77–78, 213; K. Jurewicz, E. Frackowiak, F. Béguin, Applied Physics A 2004, 78, 981.

[157]   F. Béguin, M. Friebe, K. Jurewicz, C. Vix-Guterl, J. Dentzer, E. Frackowiak, Carbon 2006, 44, 2392.

[158]   D. Qu, Journal of Power Sources 2008, 179, 310; B. Fang, M. Kim, J. H. Kim, J.-S. Yu, Langmuir 2008, 24, 12068; K. Babeł, K. Jurewicz, Carbon 2008, 46, 1948.

[159]   F. Béguin, K. Kierzek, M. Friebe, A. Jankowska, J. Machnikowski, K. Jurewicz, E. Frackowiak, Electrochimica Acta 2006, 51, 2161.

[160]   M. J. Bleda-Martínez, J. M. Pérez, A. Linares-Solano, E. Morallón, D. Cazorla-Amorós, Carbon 2008, 46, 1053; B. Fang, H. Zhou, I. Honma, The Journal of Physical Chemistry B 2006, 110, 4875.

[161]   B. E. Conway, B. V. Tilak, Electrochimica Acta 2002, 47, 3571.

[162]   G. Lota, K. Fic, E. Frackowiak, Energy & Environmental Science 2011, 4, 1592.

[163]   G. Lota, E. Frackowiak, Electrochemistry Communications 2009, 11, 87.

[164]   G. Lota, K. Fic, E. Frackowiak, Electrochemistry Communications 2011, 13, 38.

[165]   S. Yamazaki, T. Ito, M. Yamagata, M. Ishikawa, Electrochimica Acta 2012, 86, 294.

[166]   S. Roldán, C. Blanco, M. Granda, R. Menéndez, R. Santamaría, Angewandte Chemie 2011, 123, 1737; S. Roldán, M. Granda, R. Menéndez, R. Santamaría, C. Blanco, The Journal of Physical Chemistry C 2011, 115, 17606.

[167]   E. Frackowiak, K. Fic, M. Meller, G. Lota, ChemSusChem 2012, 5, 1181.

[168]   K. H. An, K. K. Jeon, J. K. Heo, S. C. Lim, D. J. Bae, Y. H. Lee, Journal of the Electrochemical Society 2002, 149, A1058.

[169]   K. Lota, V. Khomenko, E. Frackowiak, Journal of Physics and Chemistry of Solids 2004, 65, 295; G. Z. Chen, M. S. P. Shaffer, D. Coleby, G. Dixon, W. Zhou, D. J. Fray, A. H. Windle, Advanced Materials 2000, 12, 522; M. Hughes, M. S. P. Shaffer, A. C. Renouf, C. Singh, G. Z. Chen, D. J. Fray, A. H. Windle, Advanced Materials 2002, 14, 382; W. Hong, Y. Xu, G. Lu, C. Li, G. Shi, Electrochemistry Communications 2008, 10, 1555; Q. Wu, Y. Xu, Z. Yao, A. Liu, G. Shi, ACS Nano 2010, 4, 1963; H. Wang, Q. Hao, X. Yang, L. Lu, X. Wang, Electrochemistry Communications 2009, 11, 1158; E. Frackowiak, in *Encyclopedia of Nanoscience and Nanotechnology*, (Eds: J. A. Schwarz, C. I. Contescu, K. Putyera), Marcel Dekker, New York 2004, 537.

[170]   V. V. N. Obreja, Physica E: Low-dimensional Systems and Nanostructures 2008, 40, 2596.

[171]   W.-D. Zhang, B. Xu, L.-C. Jiang, Journal of Materials Chemistry 2010, 20, 6383.

[172]   J. P. Zheng, Journal of The Electrochemical Society 2003, 150, A484; V. Ganesh, S. Pitchumani, V. Lakshminarayanan, Journal of Power Sources 2006, 158, 1523; E. Frackowiak, Physical Chemistry Chemical Physics 2007, 9, 1774.

[173]   Y. J. Kang, B. Kim, H. Chung, W. Kim, Synthetic Metals 2010, 160, 2510; H. Kawaoka, M. Hibino, H. Zhou, I. Honma, Solid State Ionics 2005, 176, 621; X. Jin, W. Zhou, S. Zhang, G. Z. Chen, Small 2007, 3, 1513; H. Zhang, G. Cao, Z. Wang, Y. Yang, Z. Shi, Z. Gu, Nano Letters 2008, 8, 2664; H. Zheng, W. Kang, Z. Fengming, F. Tang, T. E. Rufford, L. Wang, C. Ma, Solid State Ionics 2010, 181, 1690; A. L. M. Reddy, M. M. Shaijumon, S. R. Gowda, P. M. Ajayan, The Journal of Physical Chemistry C 2009, 114, 658; T. Bordjiba, D. Bélanger, Electrochimica Acta 2010, 55, 3428; H. Zhang, G. Cao, Y. Yang, Energy & Environmental Science 2009, 2, 932.

[174]   H. Pan, J. Li, Y. Feng, Nanoscale Research Letters 2010, 5, 654

[175]   M. Pourbaix, *Atlas of Electrochemical Equilibria in Aqueous Solutions* NACE International, Houston 1974.

[176]   S. R. Sivakkumar, J. M. Ko, D. Y. Kim, B. C. Kim, G. G. Wallace, Electrochimica Acta 2007, 52, 7377; Q. Li, J. Liu, J. Zou, A. Chunder, Y. Chen, L. Zhai, Journal of Power Sources 2011, 196, 565; Y. Hou, Y. Cheng, T. Hobson, J. Liu, Nano Letters 2010, 10, 2727.

[177]   E. Raymundo-Piñero, F. Leroux, F. Béguin, Advanced Materials 2006, 18, 1877.

[178]   E. Raymundo-Piñero, M. Cadek, F. Béguin, Advanced Functional Materials 2009, 19, 1032.

[179]   M. A. Montes-Morán, D. Suárez, J. A. Menéndez, E. Fuente, Carbon 2004, 42, 1219.

[180]   E. Raymundo-Piñero, M. Cadek, M. Wachtler, F. Béguin, ChemSusChem 2011, 4, 943.

[181]   K. Jurewicz, K. Babeł, A. Ziółkowski, H. Wachowska, Electrochimica Acta 2003, 48, 1491.

[182]   F. Béguin, K. Szostak, G. Lota, E. Frackowiak, Advanced Materials 2005, 17, 2380.

[183]   C. O. Ania, V. Khomenko, E. Raymundo-Piñero, J. B. Parra, F. Béguin, Advanced Functional Materials 2007, 17, 1828.

[184]   G. Lota, K. Fic, K. Jurewicz, E. Frackowiak, Central European Journal of Chemistry 2011, 9, 20.

[185]   M. P. Bichat, E. Raymundo-Piñero, F. Béguin, Carbon 2010, 48, 4351.

[186]   A. G. Pandolfo, A. F. Hollenkamp, Journal of Power Sources 2006, 157, 11.

[187]   K. Chiba, T. Ueda, Y. Yamaguchi, Y. Oki, F. Saiki, K. Naoi, Journal of The Electrochemical Society 2011, 158, A1320.

[188]   K. Chiba, T. Ueda, Y. Yamaguchi, Y. Oki, F. Shimodate, K. Naoi, Journal of The Electrochemical Society 2011, 158, A872.

[189]   K. Naoi, Fuel Cells 2010, 10, 825.

[190]   K. E. Johnson, The Electrochemical Society Interface 2007, 16, 38; S. Randström, G. B. Appetecchi, C. Lagergren, A. Moreno, S. Passerini, Electrochimica Acta 2007, 53, 1837; S. Randström, M. Montanino, G. B. Appetecchi, C. Lagergren, A. Moreno, S. Passerini, Electrochimica Acta 2008, 53, 6397; Q. Zhou, W. A. Henderson, G. B. Appetecchi, M. Montanino, S. Passerini, The Journal of Physical Chemistry B 2008, 112, 13577.

[191]   A. Balducci, S. S. Jeong, G. T. Kim, S. Passerini, M. Winter, M. Schmuck, G. B. Appetecchi, R. Marcilla, D. Mecerreyes, V. Barsukov, V. Khomenko, I. Cantero, I. De Meatza, M. Holzapfel, N. Tran, Journal of Power Sources 2011, 196, 9719.

[192]   M. Armand, F. Endres, D. R. MacFarlane, H. Ohno, B. Scrosati, Nature Materials 2009, 8, 621.

[193]   R. S. Kühnel, N. Böckenfeld, S. Passerini, M. Winter, A. Balducci, Electrochimica Acta 2011, 56, 4092.

[194]   M. Giovanni, M. Pumera, Electrochemistry Communications 2011, 13, 203; H. Kurig, M. Vestli, A. Jänes, E. Lust, Electrochemical and Solid-State Letters 2011, 14, A120; Y. Shim, H. J. Kim, Y. Jung, Faraday Discussions 2012, 154, 249; L. Wei, G. Yushin, Journal of Power Sources 2011, 196, 4072; M. Yamagata, K. Soeda, S. Ikebe, S. Yamazaki, M. Ishikawa, Electrochimica Acta.
[195]   R. Palm, H. Kurig, K. Tõnurist, A. Jänes, E. Lust, Electrochemistry Communications 2012, 22, 203.
[196]   N. Handa, T. Sugimoto, M. Yamagata, M. Kikuta, M. Kono, M. Ishikawa, Journal of Power Sources 2008, 185, 1585.
[197]   A. Lewandowski, A. Olejniczak, M. Galinski, I. Stepniak, Journal of Power Sources 2010, 195, 5814.
[198]   W. Liu, X. Yan, J. Lang, Q. Xue, Journal of Materials Chemistry 2012, 22, 8853.
[199]   C. Arbizzani, M. Biso, D. Cericola, M. Lazzari, F. Soavi, M. Mastragostino, Journal of Power Sources 2008, 185, 1575.
[200]   A. Balducci, R. Dugas, P. L. Taberna, P. Simon, D. Plée, M. Mastragostino, S. Passerini, Journal of Power Sources 2007, 165, 922; M. Lazzari, M. Mastragostino, F. Soavi, Electrochemistry Communications 2007, 9, 1567.
[201]   A. Krause, A. Balducci, Electrochemistry Communications 2011, 13, 814.
[202]   C. Largeot, P. L. Taberna, Y. Gogotsi, P. Simon, Electrochemical and Solid-State Letters 2011, 14, A174.
[203]   M. Lazzari, M. Mastragostino, A. G. Pandolfo, V. Ruiz, F. Soavi, Journal of The Electrochemical Society 2011, 158, A22.
[204]   M. Lazzari, F. Soavi, M. Mastragostino, Journal of Power Sources 2008, 178, 490.
[205]   V. Ruiz, T. Huynh, S. R. Sivakkumar, A. G. Pandolfo, RSC Advances 2012, 2, 5591.
[206]   G. B. Appetecchi, M. Montanino, A. Balducci, S. F. Lux, M. Winterb, S. Passerini, Journal of Power Sources 2009, 192, 599; M. Kunze, S. Jeong, E. Paillard, M. Winter, S. Passerini, The Journal of Physical Chemistry C 2010, 114, 12364; S. F. Lux, M. Schmuck, G. B. Appetecchi, S. Passerini, M. Winter, A. Balducci, Journal of Power Sources 2009, 192, 606.
[207]   A. Guerfi, M. Dontigny, P. Charest, M. Petitclerc, M. Lagacé, A. Vijh, K. Zaghib, Journal of Power Sources 2010, 195, 845; B. S. Lalia, N. Yoshimoto, M. Egashira, M. Morita, Journal of Power Sources 2010, 195, 7426.
[208]   E. Frackowiak, G. Lota, J. Pernak, Applied Physics Letters 2005, 86, 164104.
[209]   A. Brandt, A. Balducci, Journal of The Electrochemical Society 2012, 159, A2053.
[210]   A. Laheäär, A. Jänes, E. Lust, Electrochimica Acta 2011, 56, 9048.
[211]   A. Laheäär, A. Jänes, E. Lust, Journal of Electroanalytical Chemistry 2012, 669, 67.
[212]   A. Laheäär, A. Jänes, E. Lust, Electrochimica Acta 2012, 82, 309; A. Laheäär, H. Kurig, A. Jänes, E. Lust, Electrochimica Acta 2009, 54, 4587.
[213]   L. Wei, M. Sevilla, A. B. Fuertes, R. Mokaya, G. Yushin, Advanced Functional Materials 2012, 22, 827.
[214]   D. Cericola, R. Kötz, A. Wokaun, Journal of Power Sources 2011, 196, 3114.
[215]   V. Khomenko, E. Raymundo-Piñero, F. Béguin, Journal of Power Sources 2008, 177, 643.
[216]   D. Cericola, R. Kötz, Electrochimica Acta 2012, 72, 1.
[217]   T. Aida, I. Murayama, K. Yamada, M. Morita, Journal of The Electrochemical Society 2007, 154, A798.
[218]   T. Aida, K. Yamada, M. Morita, Electrochemical and Solid-State Letters 2006, 9, A534.
[219]   W. J. Cao, J. P. Zheng, Journal of Power Sources 2012, 213, 180.
[220]   H. Konno, T. Kasashima, K. Azumi, Journal of Power Sources 2009, 191, 623.

[221]   N. Ogihara, Y. Igarashi, A. Kamakura, K. Naoi, Y. Kusachi, K. Utsugi, Electrochimica Acta 2006, 52, 1713.
[222]   M. Schroeder, M. Winter, S. Passerini, A. Balducci, Journal of The Electrochemical Society 2012, 159, A1240.
[223]   S. R. Sivakkumar, J. Y. Nerkar, A. G. Pandolfo, Electrochimica Acta 2010, 55, 3330.
[224]   S. R. Sivakkumar, A. G. Pandolfo, Electrochimica Acta 2012, 65, 280.
[225]   M. D. Stoller, S. Murali, N. Quarles, Y. Zhu, J. R. Potts, X. Zhu, H.-W. Ha, R. S. Ruoff, Physical Chemistry Chemical Physics 2012, 14, 3388.
[226]   A. Krause, P. Kossyrev, M. Oljaca, S. Passerini, M. Winter, A. Balducci, Journal of Power Sources 2011, 196, 8836.
[227]   C. Decaux, G. Lota, E. Raymundo-Piñero, E. Frackowiak, F. Béguin, Electrochimica Acta 2012, 86, 282.
[228]   M. Winter, J. O. Besenhard, M. E. Spahr, P. Novák, Advanced Materials 1998, 10, 725.
[229]   M. Schroeder, M. Winter, S. Passerini, A. Balducci, Journal of Power Sources 2013, 238, 388.
[230]   J.-H. Kim, J.-S. Kim, Y.-G. Lim, J.-G. Lee, Y.-J. Kim, Journal of Power Sources 2011, 196, 10490.
[231]   S. R. Sivakkumar, A. S. Milev, A. G. Pandolfo, Electrochimica Acta 2011, 56, 9700.
[232]   M. Schroeder, P. W. Isken, M., S. Passerini, A. Lex-Balducci, A. Balducci, Journal of Electrochemical Society 2013, in press.
[233]   C.-M. Yang, Y.-J. Kim, M. Endo, H. Kanoh, M. Yudasaka, S. Iijima, K. Kaneko, Journal of the American Chemical Society 2007, 129, 20.
[234]   T. Kyotani, T. Nagai, S. Inoue, A. Tomita, Chemistry of Materials 1997, 9, 609.
[235]   C. Liang, K. Hong, G. A. Guiochon, J. W. Mays, S. Dai, Angewandte Chemie International Edition 2004, 43, 5785.
[236]   D. Chunsheng, P. Ning, Nanotechnology 2006, 17, 5314.